



UNIVERSITY OF BRITISH COLUMBIA



Andrea Damascelli

UBC-MPI Quantum Matter Institute

ARPES on Correlated Electron Systems

CUSO Lecture – Lausanne 02/2011



Outline

- Introduction: Transition metal oxides
- ARPES: Fundamentals and spectral function
- ARPES: Technique and developments
- Sr_2RuO_4 : A Fermi liquid with SO coupling
- Polarons and sudden approximation
- HTSC: The fate of quasiparticle strength



ARPES ON COMPLEX SYSTEMS

Electronic and Magnetic Interactions in Novel Complex Systems

Angle-resolved photoemission spectroscopy (ARPES) is one of the most direct methods of studying the electronic structure of solids and is the only truly momentum-resolved probe, which is essential for the investigation of low dimensional and strongly anisotropic systems. By measuring momentum and kinetic energy of the electrons photoemitted from a sample illuminated with radiation of energy larger than the material work function, it is possible to gain information on both energy and the momentum of the electronic excitations inside the solid.

As the intensity measured in photoemission experiments is proportional to the single-particle spectral function $A(\mathbf{k},\omega)=-(1/\pi)\text{Im}G(\mathbf{k},\omega)$, ARPES provides direct insights on the Green's function $G(\mathbf{k},\omega)$ which describes the propagation of an electron in a many-body system. This is of vital importance in elucidating the connection between electronic, magnetic, and chemical structure of solids, in particular for those complex systems which cannot be described within the independent-particle picture.

The last decade witnessed significant progress in this technique and its applications, thus ushering in a new era in photoelectron spectroscopy. Today, ARPES experiments with 2 meV energy resolution and 0.2 degree angular resolution are a reality even for photoemission on solids, providing detailed information on band dispersion and Fermi surface, as well as on the strength and nature of those many-body correlations which may profoundly affect the one-electron excitation spectrum and, in turn, determine the macroscopic physical properties.

The Photoelectric Effect

ARPES: Introduction

ARPES on HTSC's

ARPES: Viewgraphs

Physica Scripta. Vol. T109, 61–74, 2004

Probing the Electronic Structure of Complex Systems by ARPES

Andrea Damascelli

Department of Physics & Astronomy, University of British Columbia, 6224 Agricultural Road, Vancouver, British Columbia V6T 1Z1, Canada

Received June 18, 2003; accepted June 30, 2003

PACS Ref: 79.60.i, 71.18.+y; 71.20.-b

Abstract

Angle-resolved photoemission spectroscopy (ARPES) is one of the most direct methods of studying the electronic structure of solids. By measuring the kinetic energy and angular distribution of the electrons photoemitted from a sample illuminated with sufficiently high-energy radiation, one can gain information on both the energy and momentum of the electrons propagating inside a material. This is of vital importance in elucidating the connection between electronic, magnetic, and chemical structure of solids, in particular for those complex systems which cannot be appropriately described within the independent-particle picture. The last decade witnessed significant progress in this technique and its applications, thus ushering in a new era in photoelectron spectroscopy; today, ARPES experiments with 2 meV energy resolution and 0.2° angular resolution are a reality even for photoemission on solids. In this paper we will review the fundamentals of the technique and present some illustrative experimental results; we will show how ARPES can probe the momentum-dependent electronic structure of solids providing detailed information on band dispersion and Fermi surface as well as on the strength and nature of many-body correlations, which may profoundly affect the one-electron excitation spectrum and in turn the macroscopic physical properties.

photoemission event is decomposed in three independent steps: optical excitation between the initial and final *bulk* Bloch eigenstates, *travel* of the excited electron to the surface, and escape of the photoelectron into vacuum after transmission through the *surface* potential barrier. This is the most common approach, in particular when photoemission spectroscopy is used as a tool to map the electronic band structure of solids. However, from the quantum-mechanical point of view photoemission should not be described in terms of several independent events but rather as a *one-step* process (Fig. 1(b)): in terms of an optical transition (with probability given by Eq. (12)) between initial and final states consisting of many-body wave functions that obey appropriate boundary conditions at the surface of the solid. In particular (see Fig. 2), the initial state should be one of the possible *N*-electron eigenstates of the semi-infinite crystal, and the final state must be one of the



UNIVERSITY OF BRITISH COLUMBIA



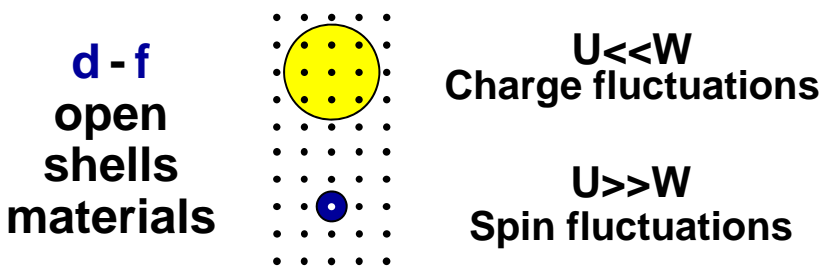
Outline Part I

Introduction:

Transition metal oxides

CUSO Lecture – Lausanne 02/2011

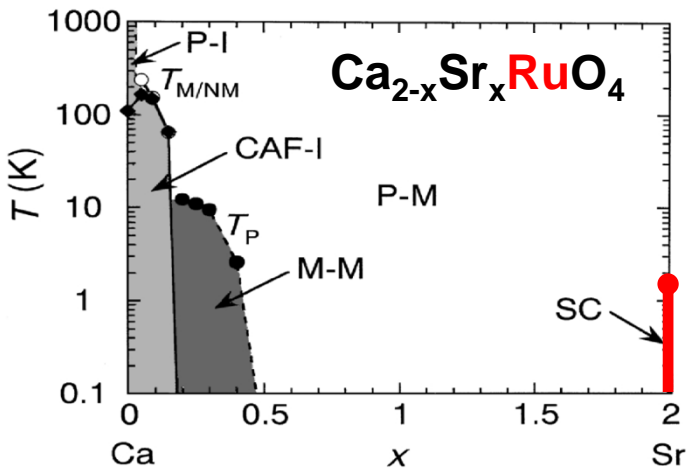
Strongly Correlated Electron Systems



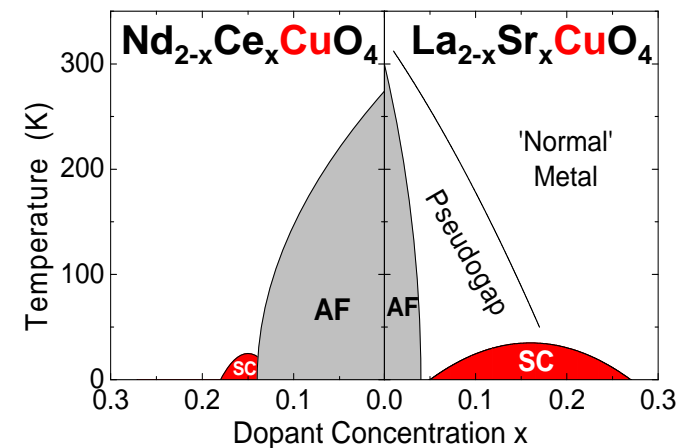
Control parameters
Bandwidth (U/W)
Band filling
Dimensionality

I	II	IIIb	IVb	Vb	VIb	VIIb	VIIIb	Ib	IIb	III	IV	V	VI	VII	0		
H															He		
Li	Be																
Na	Mg																
K	Ca	Sc	Ti	V	Cr	Mn	Fe	Co	Ni	Cu	Zn	Ga	Ge	As	Se	Br	Kr
Rb	Sr	Y	Zr	Nb	Mo	Tc	Ru	Rh	Pd	Ag	Cd	In	Sn	Sb	Te	I	Xe
Cs	Ba	La*	Hf	Ta	W	Re	Os	Ir	Pt	Au	Hg	Tl	Pb	Bi	Po	At	Rn
Fr	Ra	Ac**	Rf	Db	Sg	Bh	Hs	Mt									
Lanthanides	*	Ce	Pr	Nd	Pm	Sm	Eu	Gd	Tb	Dy	Ho	Er	Tm	Yb	Lu		
Actinides	**	Th	Pa	U	Np	Pu	Am	Cm	Bk	Cf	Es	Fm	Md	No	Lr		

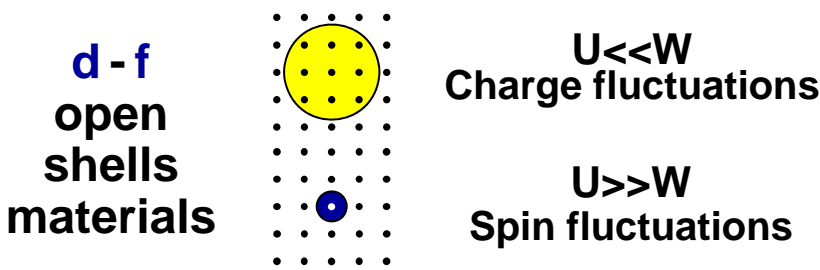
Degrees of freedom
Charge / Spin
Orbital
Lattice



- Kondo
- Mott-Hubbard
- Heavy Fermions
- Unconventional SC
- Spin-charge order
- Colossal MR



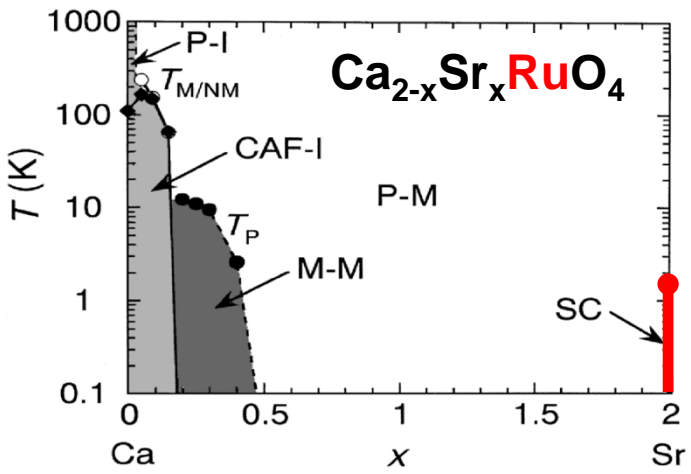
Strongly Correlated Electron Systems



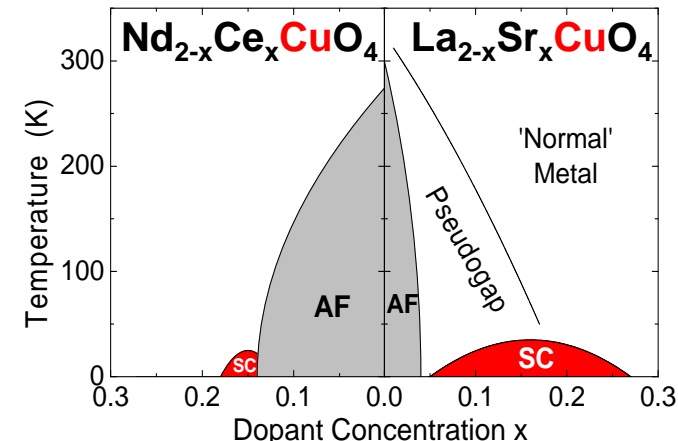
Control parameters
Bandwidth (U/W)
Band filling
Dimensionality

I	II	IIIb	IVb	Vb	VIb	VIIb	VIIIb	Ib	IIb	III	IV	V	VI	VII	0		
H															He		
Li	Be														Ne		
Na	Mg														Ar		
K	Ca	Sc	Ti	V	Cr	Mn	Fe	Co	Ni	Cu	Zn	Ga	Ge	As	Se	Br	Kr
Rb	Sr	Y	Zr	Nb	Mo	Tc	Ru	Rh	Pd	Ag	Cd	In	Sn	Sb	Te	I	Xe
Cs	Ba	La*	Hf	Ta	W	Re	Os	Ir	Pt	Au	Hg	Tl	Pb	Bi	Po	At	Rn
Fr	Ra	Ac**	Rf	Db	Sg	Bh	Hs	Mt									
Lanthanides		*Ce	Pr	Nd	Pm	Sm	Eu	Gd	Tb	Dy	Ho	Er	Tm	Yb	Lu		
Actinides	**	Th	Pa	U	Np	Pu	Am	Cm	Bk	Cf	Es	Fm	Md	No	Lr		

Degrees of freedom
Charge / Spin
Orbital
Lattice



d-orbitals radial extent
Spin-orbit coupling

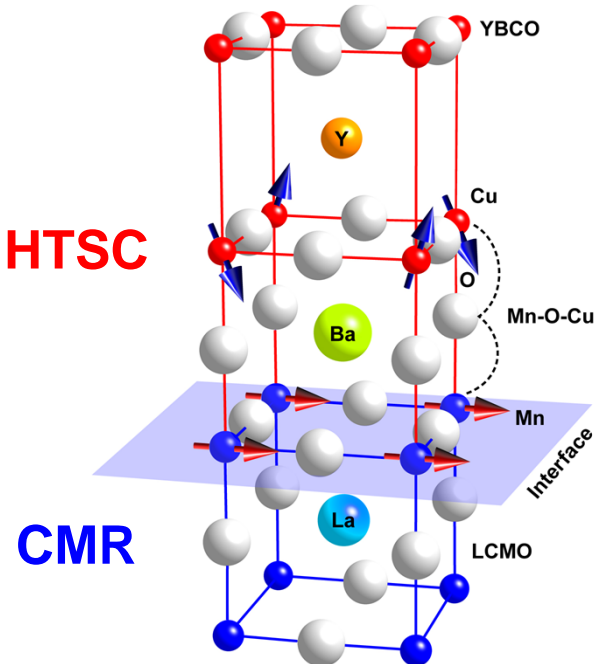


Novel Complex Materials and Functionalities



Tune the physical properties

Chakhalian et al., Nature Physics 2006



- Modern synthesis methods
Single crystals, multilayers, nanostructures
- Sophisticated structural tools
Physical, chemical, and magnetic structures
- Novel probes of intrinsic susceptibilities
Lattice, magnetic, and electronic excitations

$$\begin{array}{ll} \varepsilon(q, q', \omega) & \chi(q, q', \omega) \\ N(\vec{r}, E) & A(\vec{k}, E) \end{array}$$

Interface-tuned magnetism
in oxide multilayers



Understand interplay of
lattice, spin, charge, orbital
degrees of freedom



UNIVERSITY OF BRITISH COLUMBIA



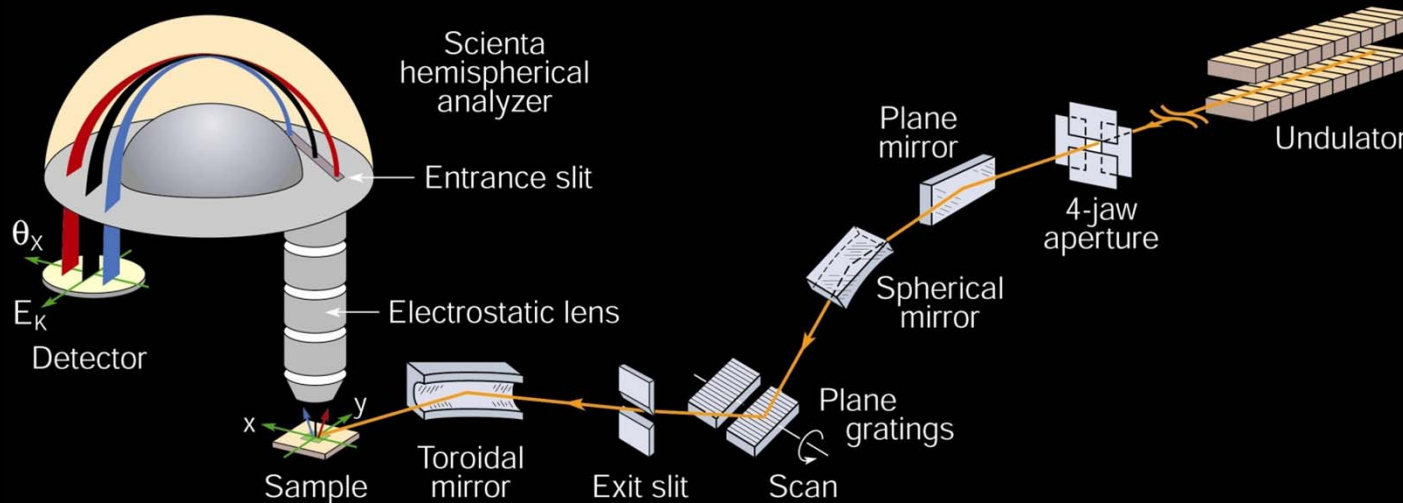
Outline Part I

ARPES: Fundamentals and spectral function

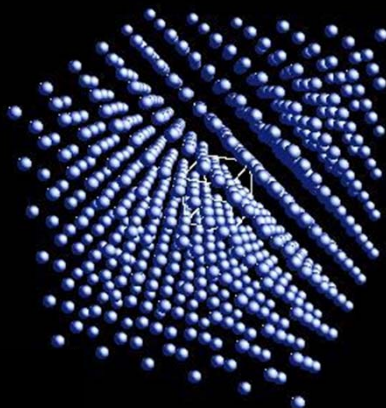
CUSO Lecture – Lausanne 02/2011



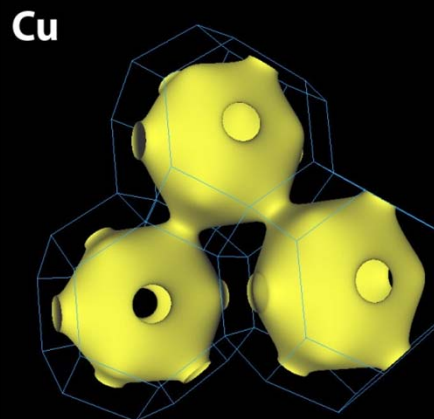
Scientific application: Spectroscopy



Angle-Resolved Photoelectron Spectroscopy (ARPES)

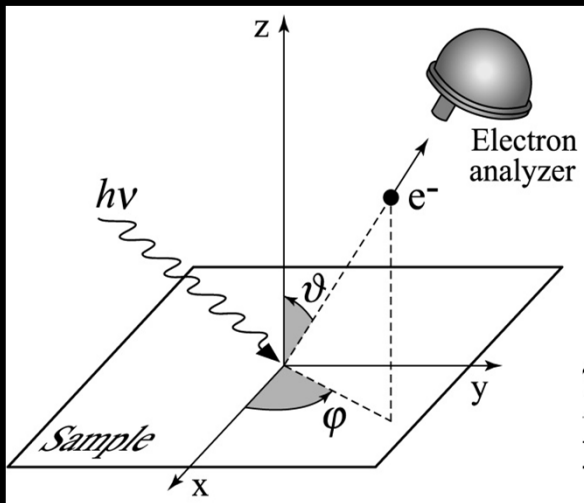


Crystal
Structure?
X-ray
diffraction



Cu
Electronic
Structure?
Photoelectron
spectroscopy

Scientific application: Spectroscopy



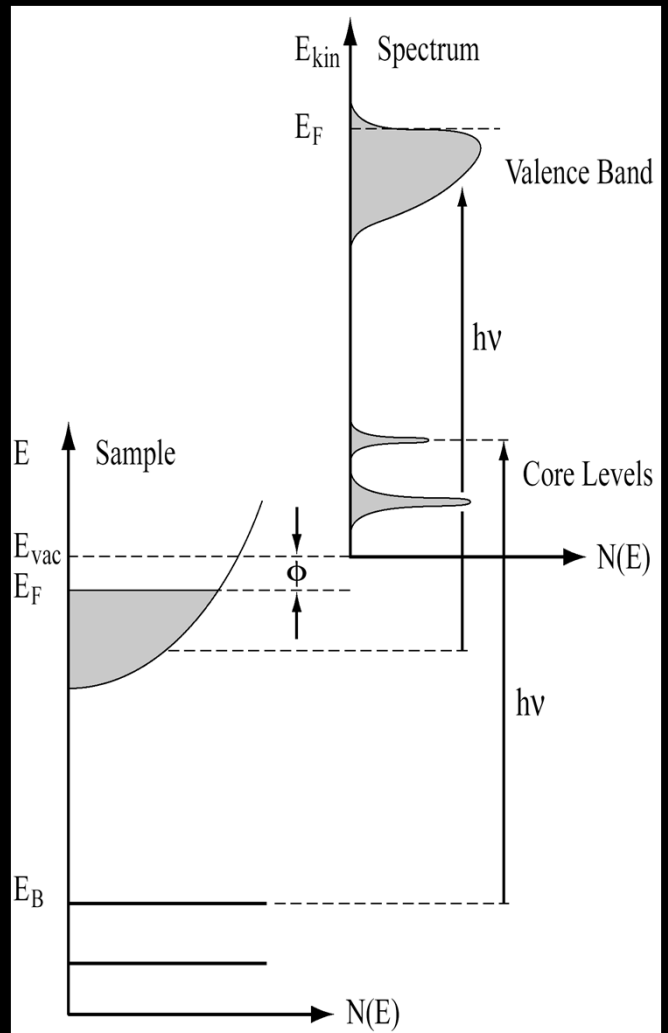
Electron Spectroscopy for Chemical Analysis (ESCA)

Kai Siegbahn:



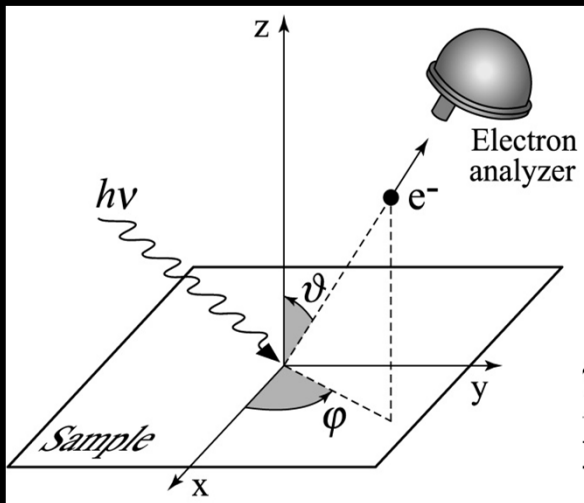
1981

“for his contribution to the development of high-resolution electron spectroscopy”



$$E_{kin} = h\nu - \phi - |E_B|$$

Scientific application: Spectroscopy



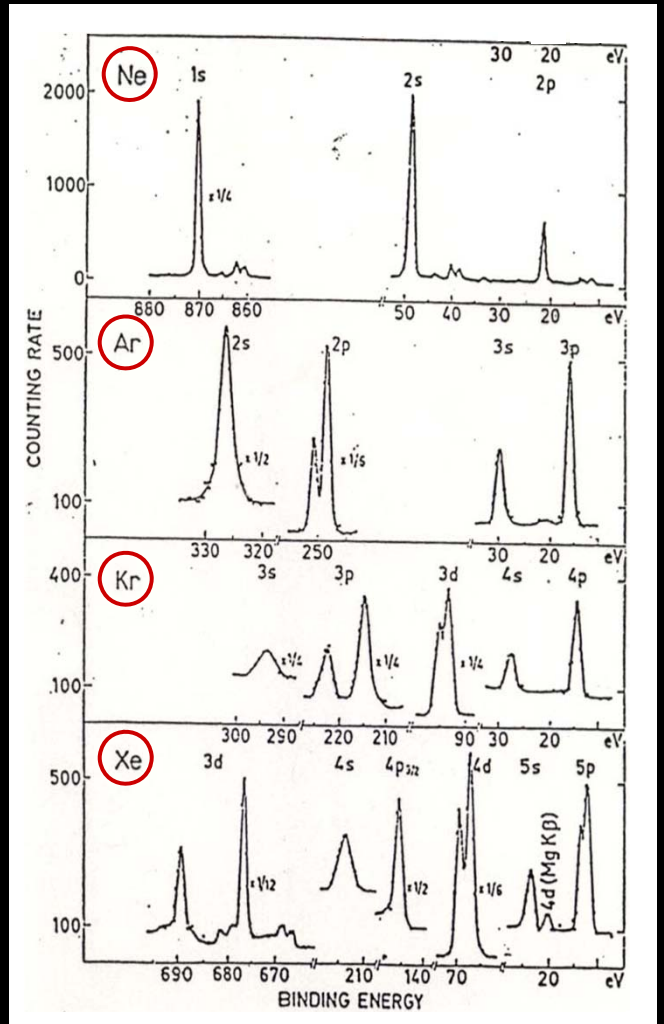
Electron Spectroscopy for Chemical Analysis (ESCA)

Kai Siegbahn:



1981

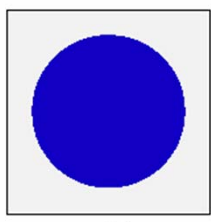
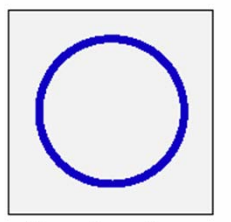
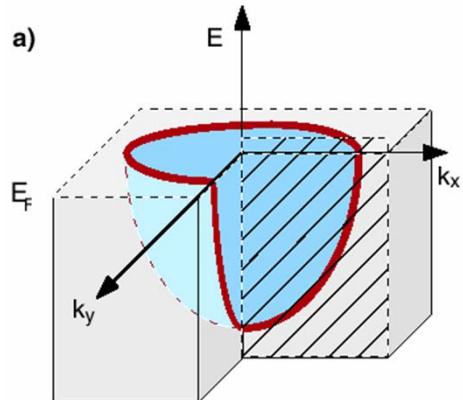
"for his contribution to the development of high-resolution electron spectroscopy"



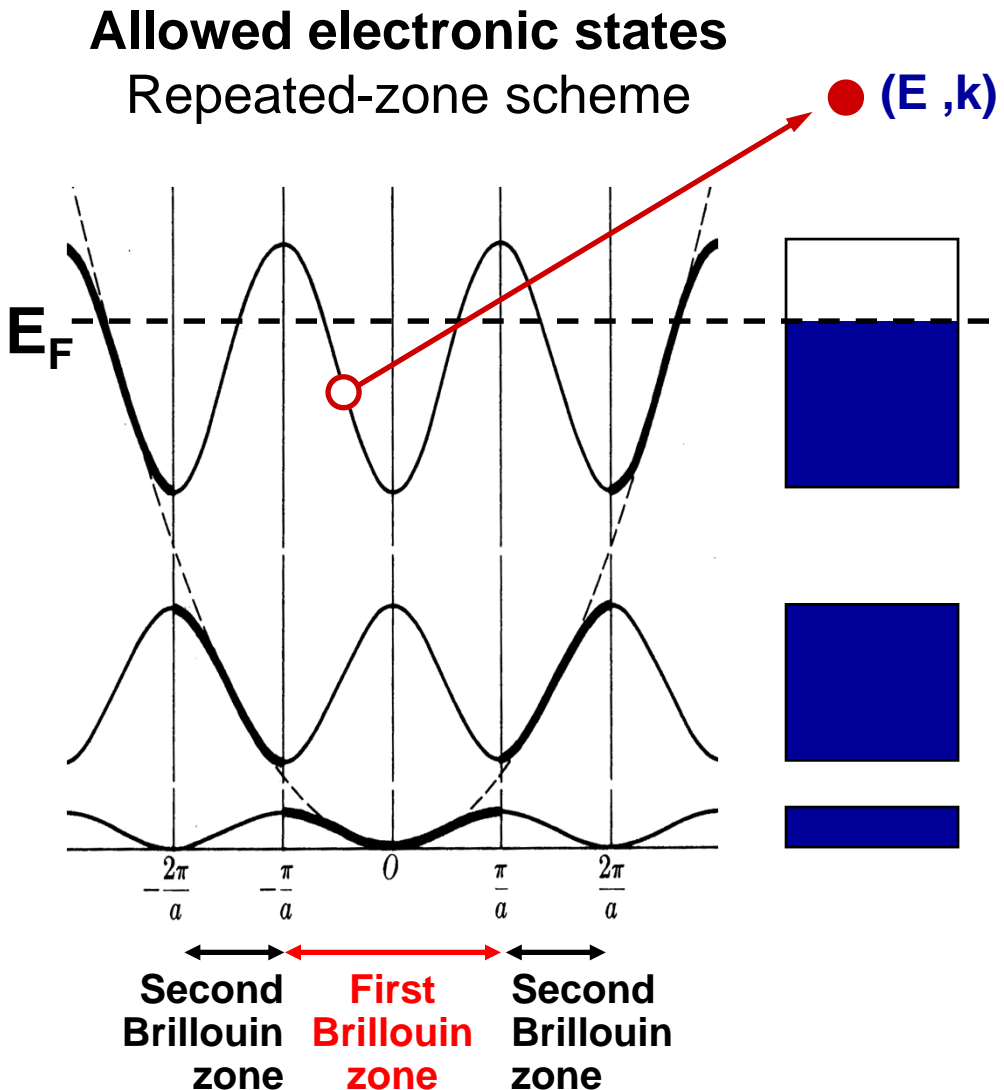
$$E_{kin} = h\nu - \phi - |E_B|$$

Solid State: Electrons in Reciprocal Space

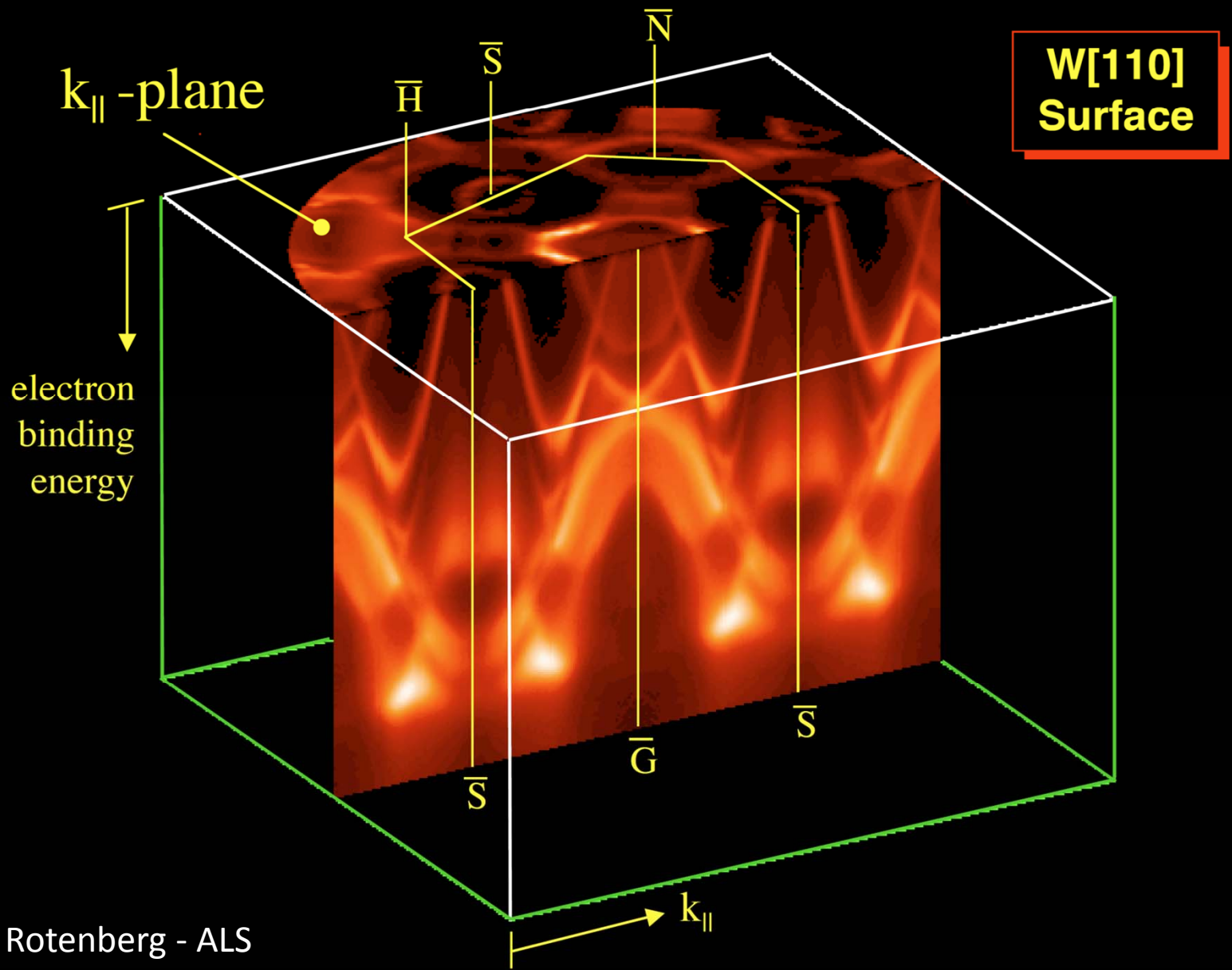
Many properties of a solids are determined by electrons near E_F (conductivity, magnetoresistance, superconductivity, magnetism)



Only a narrow energy slice around E_F is relevant for these properties ($kT=25$ meV at room temperature)

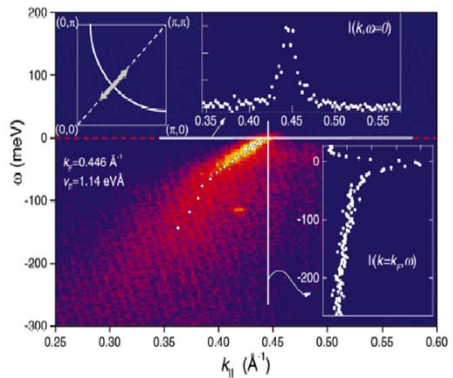


Band Mapping and Fermi Contours



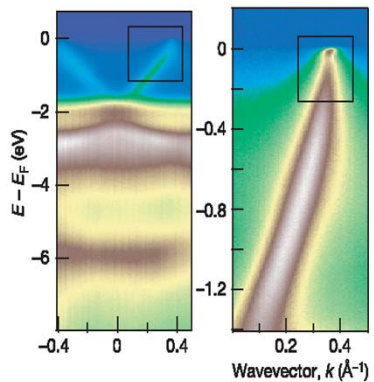
ARPES: Widespread Impact in Complex Materials

HTSC's



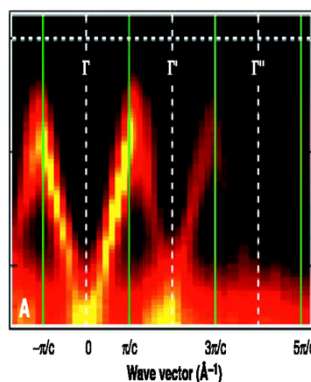
Science 1999

CMR's



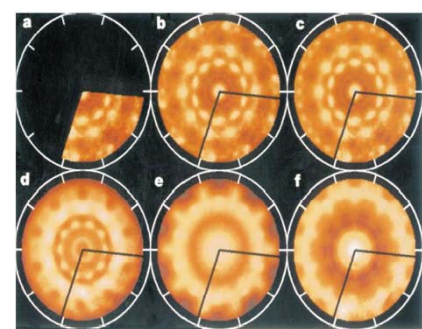
Nature 2005

CDW's



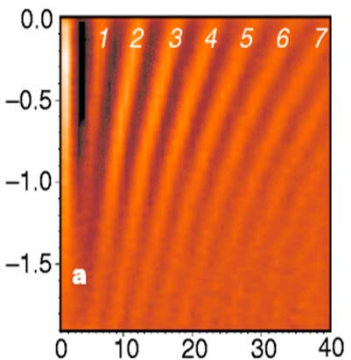
Science 2000

Quasicrystals



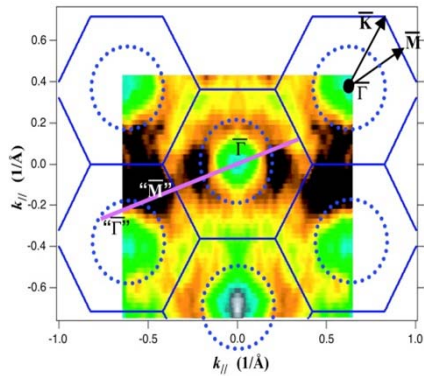
Nature 2000

Quantum Wells



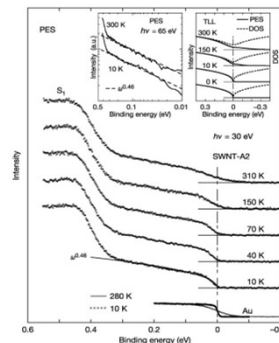
Nature 1999

C_{60}



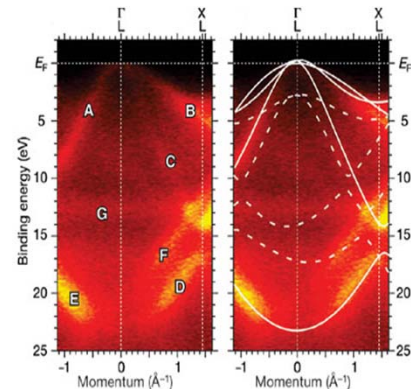
Science 2003

Nanotubes



Nature 2003

Diamond



Nature 2005

Band Velocity

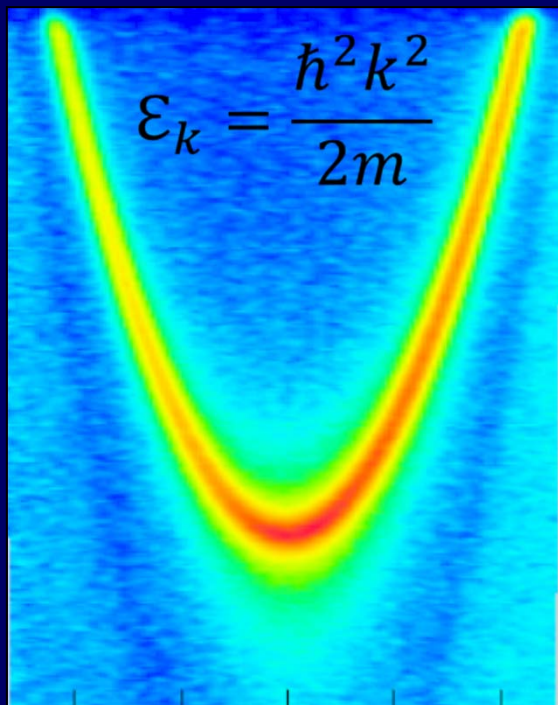
$$v_k = \frac{1}{\hbar} \frac{\partial \mathcal{E}_k}{\partial k}$$

Band Mass

$$\frac{1}{m_k} = \frac{1}{\hbar^2} \frac{\partial^2 \mathcal{E}_k}{\partial k^2}$$

Cu surface state

Energy

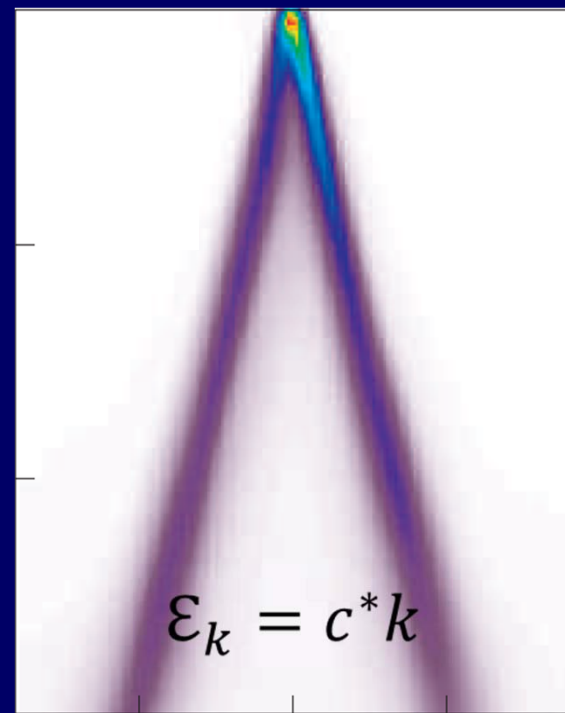


Momentum

Reinert & Hufner, NJP 2005

Graphene

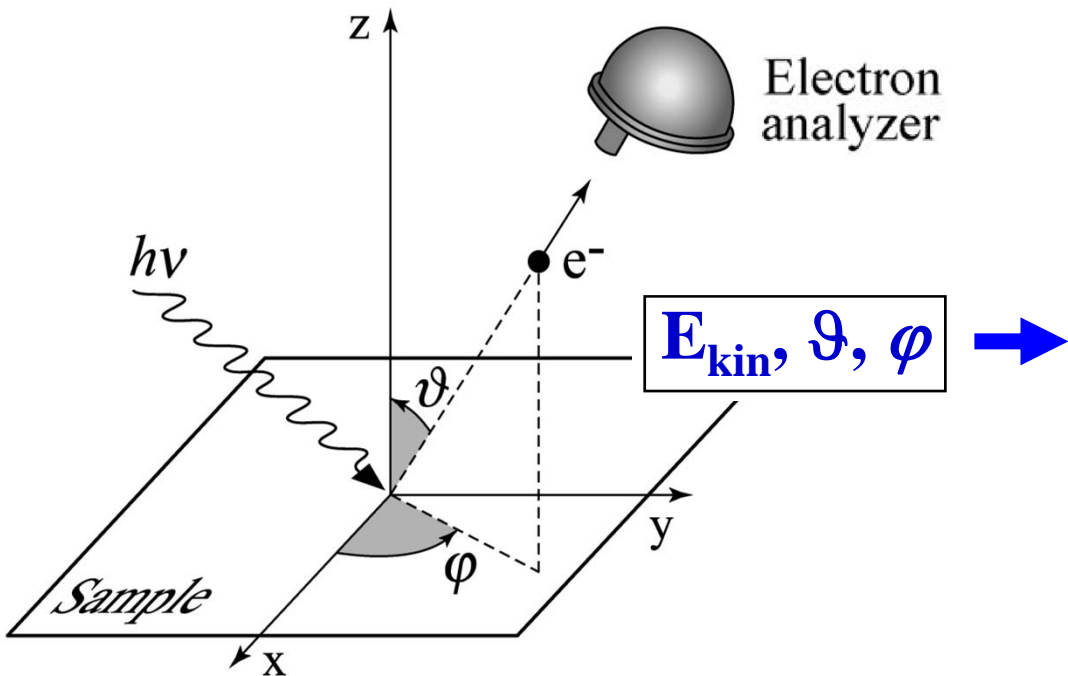
Energy



Momentum

Zhou et al., Nat. Phys. 2006

Angle-Resolved Photoemission Spectroscopy



$$\mathbf{K} = \mathbf{p}/\hbar = \sqrt{2mE_{kin}}/\hbar$$

$$K_x = \frac{1}{\hbar} \sqrt{2mE_{kin}} \sin \vartheta \cos \varphi$$

$$K_y = \frac{1}{\hbar} \sqrt{2mE_{kin}} \sin \vartheta \sin \varphi$$

$$K_z = \frac{1}{\hbar} \sqrt{2mE_{kin}} \cos \vartheta$$

Vacuum

$$E_{kin}$$

 \mathbf{K}

Conservation laws

$$E_f - E_i = h\nu$$
$$\mathbf{k}_f - \mathbf{k}_i = \cancel{\mathbf{k}_{\text{rel}}}$$

Solid

$$E_B$$

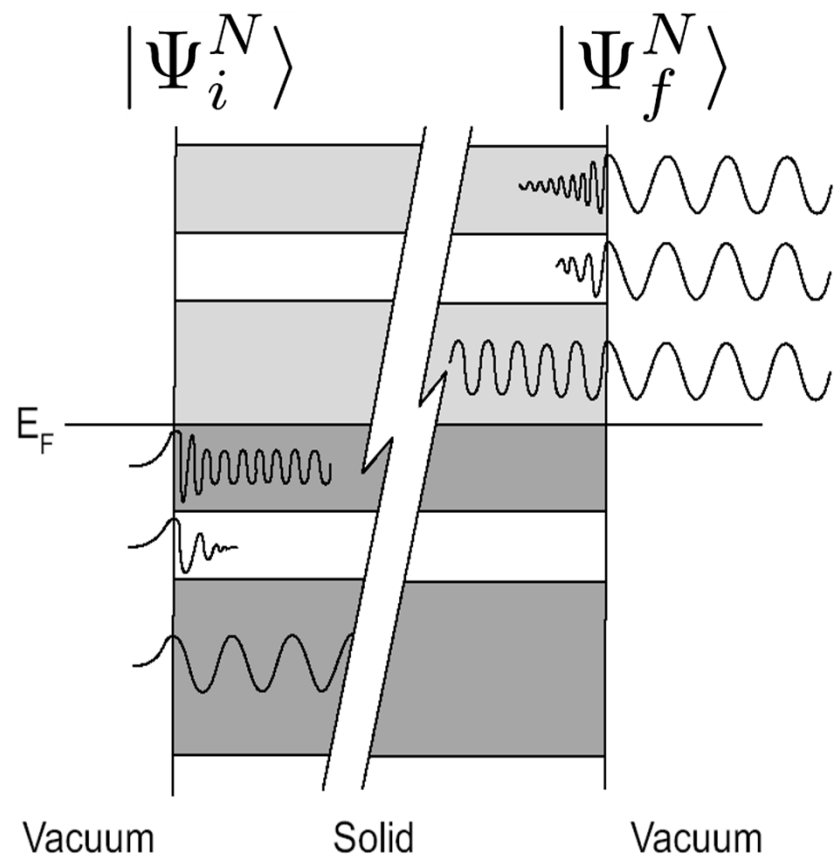
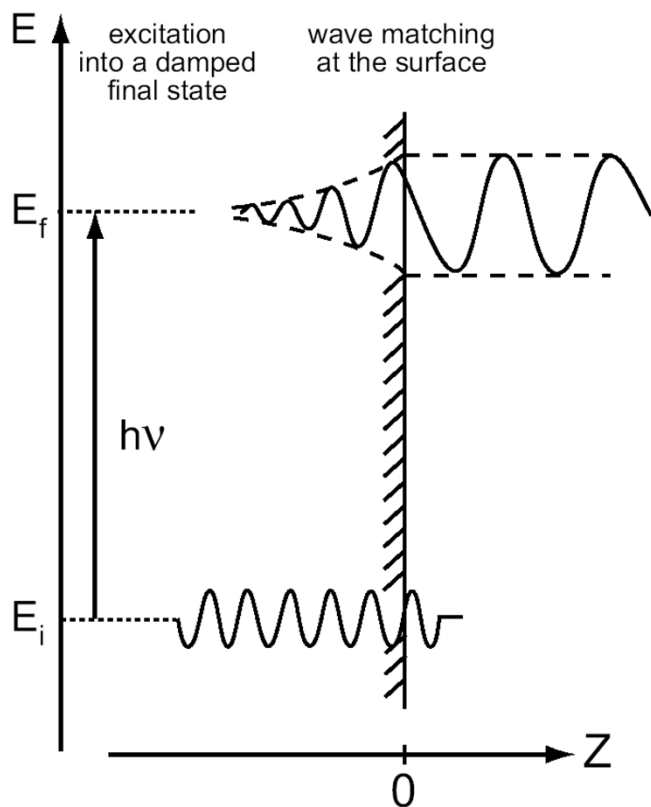
 \mathbf{k}

ARPES: One-Step vs Three-Step Model

Photoemission Intensity $I(k, \omega)$

$$w_{fi} \propto |\langle \Psi_f^N | \mathbf{A} \cdot \mathbf{p} | \Psi_i^N \rangle|^2 \delta(E_f^N - E_i^N - h\nu)$$

One-step model

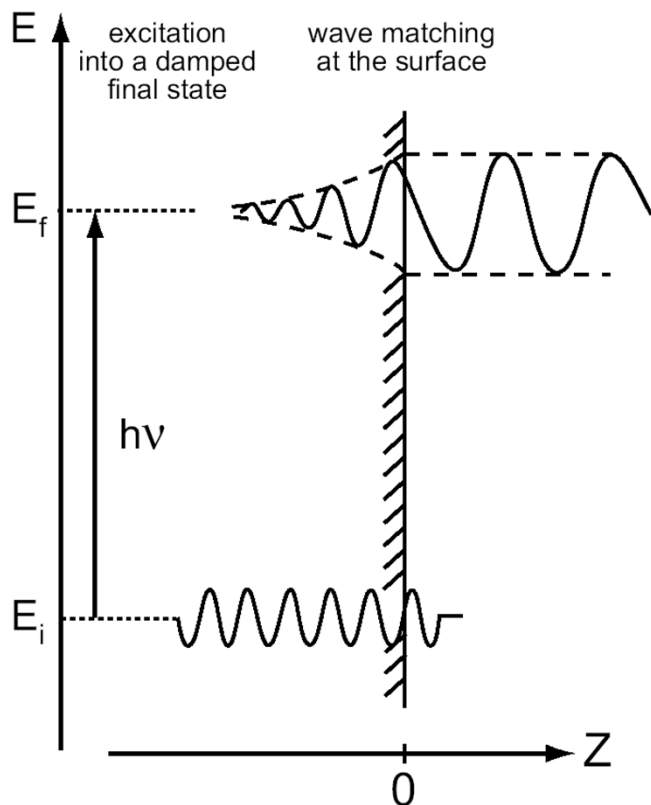


ARPES: One-Step vs Three-Step Model

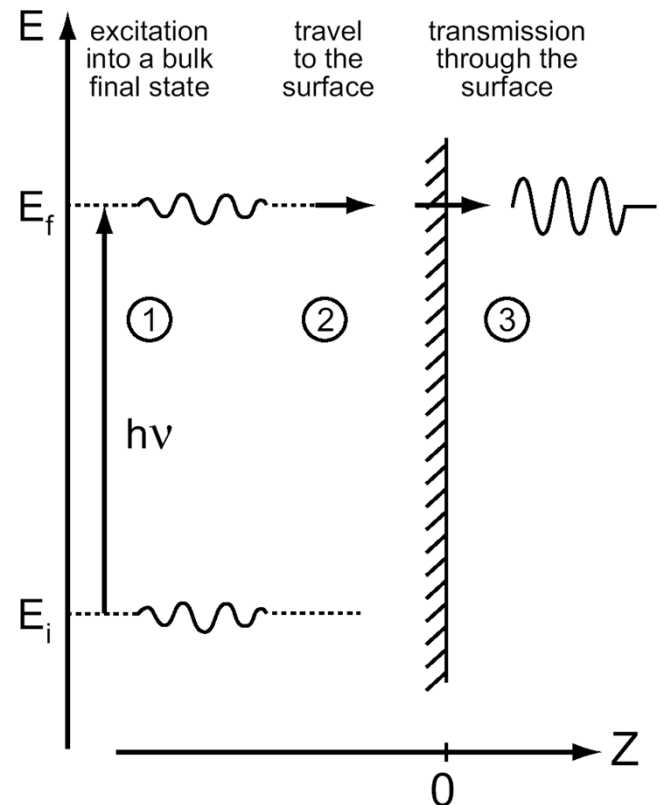
Photoemission Intensity $I(k, \omega)$

$$w_{fi} \propto |\langle \Psi_f^N | \mathbf{A} \cdot \mathbf{p} | \Psi_i^N \rangle|^2 \delta(E_f^N - E_i^N - h\nu)$$

One-step model



Three-step model



ARPES: The Sudden Approximation

Photoemission Intensity $I(k, \omega)$ } $w_{fi} \propto |\langle \Psi_f^N | \mathbf{A} \cdot \mathbf{p} | \Psi_i^N \rangle|^2 \delta(E_f^N - E_i^N - h\nu)$

Sudden approximation }
One Slater determinant }
 $\Psi_f^N = \mathcal{A} \phi_f^{\mathbf{k}} \Psi_f^{N-1}$
 $\Psi_i^N = \mathcal{A} \phi_i^{\mathbf{k}} \Psi_i^{N-1}$

ARPES: The Sudden Approximation

Photoemission Intensity $I(k, \omega)$ } $w_{fi} \propto |\langle \phi_f^k | \mathbf{A} \cdot \mathbf{p} | \phi_i^k \rangle \langle \Psi_m^{N-1} | \Psi_i^{N-1} \rangle|^2 \delta(\omega - h\nu)$

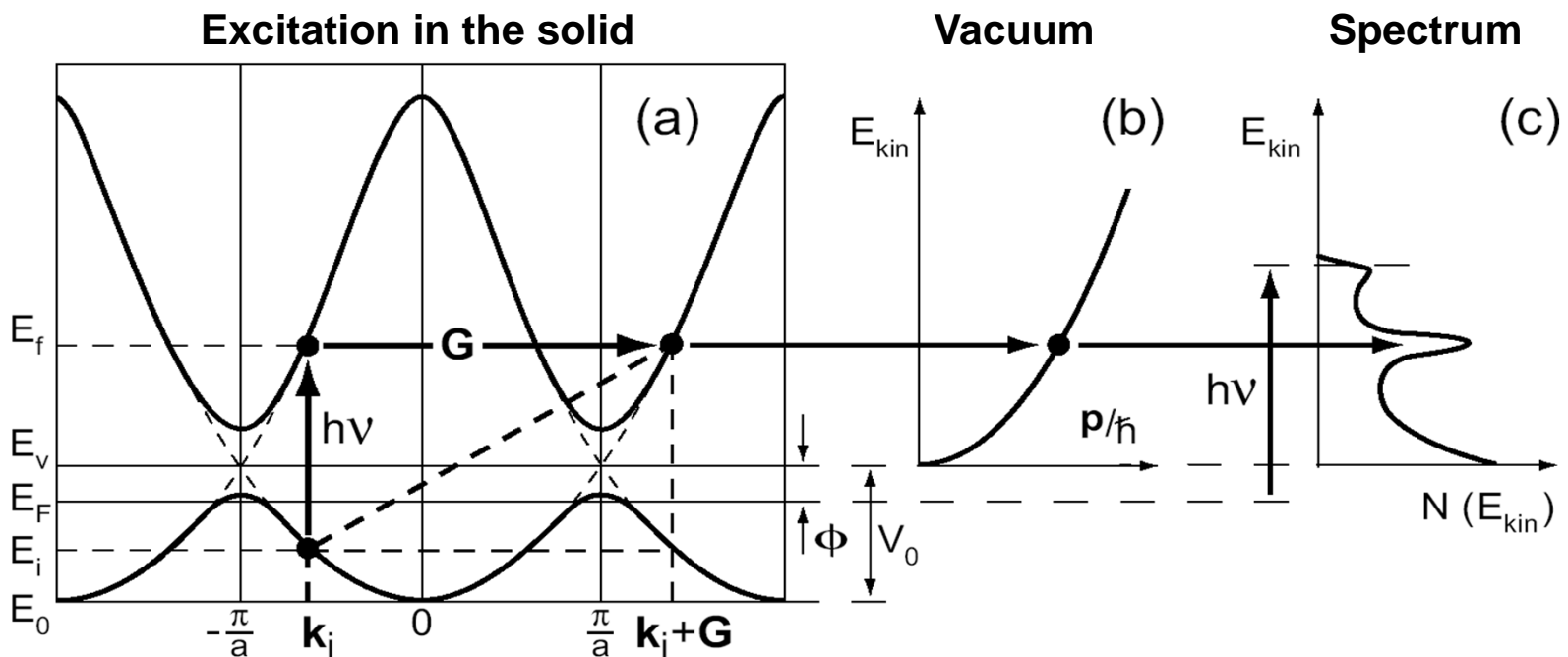
Sudden approximation }
One Slater determinant }

$$\begin{aligned}\Psi_f^N &= \mathcal{A} \phi_f^k \Psi_f^{N-1} \\ \Psi_i^N &= \mathcal{A} \phi_i^k \Psi_i^{N-1}\end{aligned}$$

ARPES: The Sudden Approximation

Photoemission Intensity $I(k, \omega)$ } $w_{fi} \propto |\langle \phi_f^k | \mathbf{A} \cdot \mathbf{p} | \phi_i^k \rangle \langle \Psi_m^{N-1} | \Psi_i^{N-1} \rangle|^2 \delta(\omega - h\nu)$

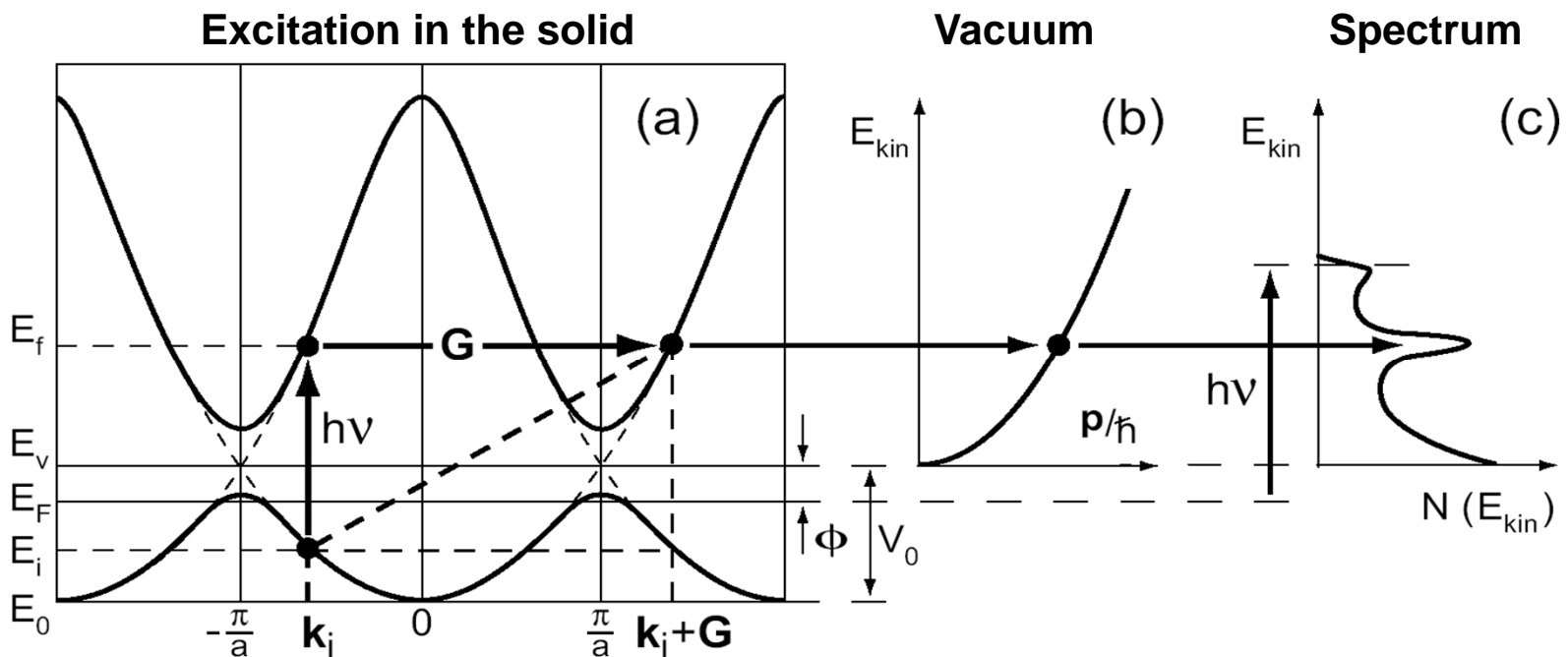
Sudden approximation }
One Slater determinant }

$$\Psi_f^N = \mathcal{A} \phi_f^k \Psi_f^{N-1}$$
$$\Psi_i^N = \mathcal{A} \phi_i^k \Psi_i^{N-1}$$


ARPES: Role of the Crystal Potential

Photoemission Intensity $I(k, \omega)$ } $w_{fi} \propto |\langle \phi_f^k | \underline{\mathbf{A} \cdot \nabla V} | \phi_i^k \rangle \langle \Psi_m^{N-1} | \Psi_i^{N-1} \rangle|^2 \delta(\omega - h\nu)$

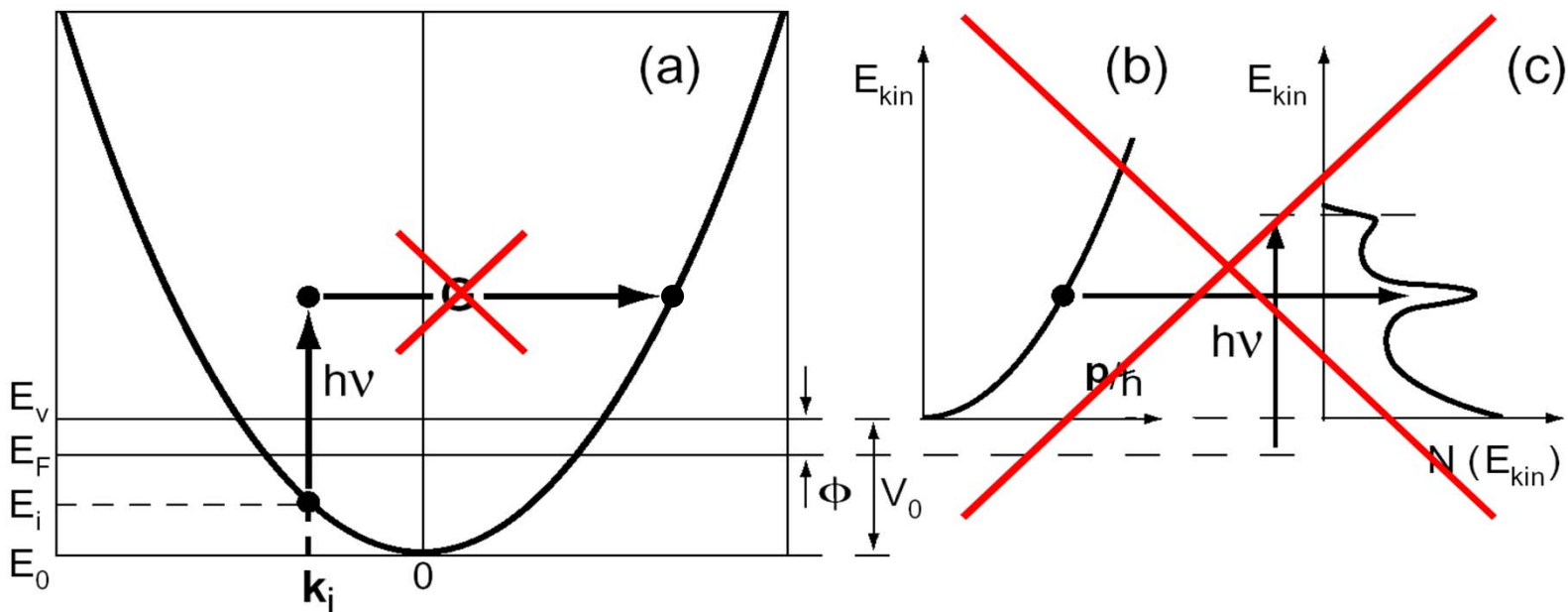
Sudden approximation } $\Psi_f^N = \mathcal{A} \phi_f^k \Psi_f^{N-1}$
One Slater determinant } $\Psi_i^N = \mathcal{A} \phi_i^k \Psi_i^{N-1}$



ARPES: Role of the Crystal Potential

Photoemission Intensity $I(k, \omega)$ } $w_{fi} \propto |\langle \phi_f^k | \underline{\mathbf{A} \cdot \nabla V} | \phi_i^k \rangle \langle \Psi_m^{N-1} | \Psi_i^{N-1} \rangle|^2 \delta(\omega - h\nu)$

Sudden approximation } $\Psi_f^N = \mathcal{A} \phi_f^k \Psi_f^{N-1}$
One Slater determinant } $\Psi_i^N = \mathcal{A} \phi_i^k \Psi_i^{N-1}$



ARPES: Role of the Crystal Potential

Photoemission Intensity $I(k, \omega)$ } $w_{fi} \propto |\langle \phi_f^k | \mathbf{A} \cdot \underline{\nabla V} | \phi_i^k \rangle \langle \Psi_m^{N-1} | \Psi_i^{N-1} \rangle|^2 \delta(\omega - h\nu)$

"In a nearly-free electron gas, optical absorption may be viewed as a two-step process. The absorption of the photon provides the electron with the additional energy it needs to get to the excited state. The crystal potential imparts to the electron the additional momentum it needs to reach the excited state. This momentum comes in multiples of the reciprocal-lattice vectors \mathbf{G} : So in a reduced zone picture, the transitions are vertical in wave-vector space. But in photoemission, it is more useful to think in an extended-zone scheme."

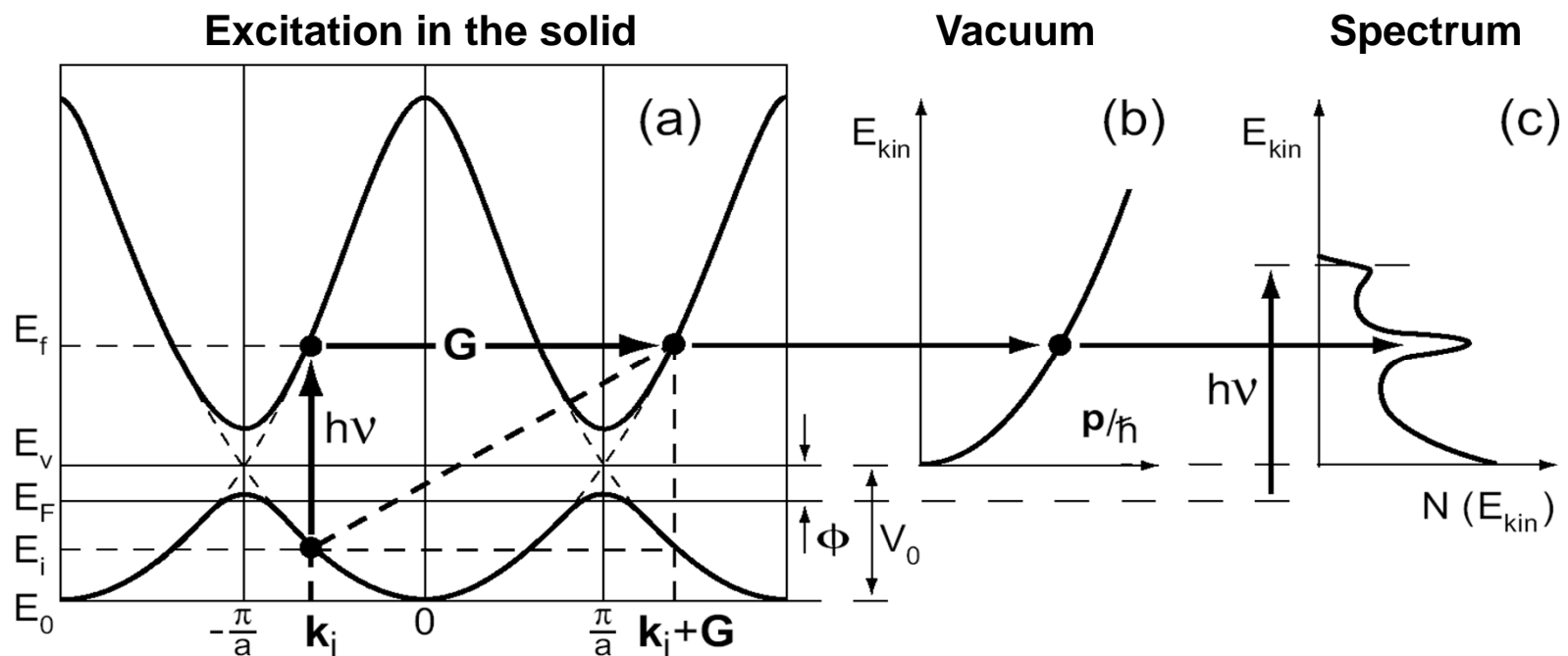
G.D. Mahan, Phys. Rev. B 2, 4334 (1970)

ARPES: Three-step Model & Sudden Approximation

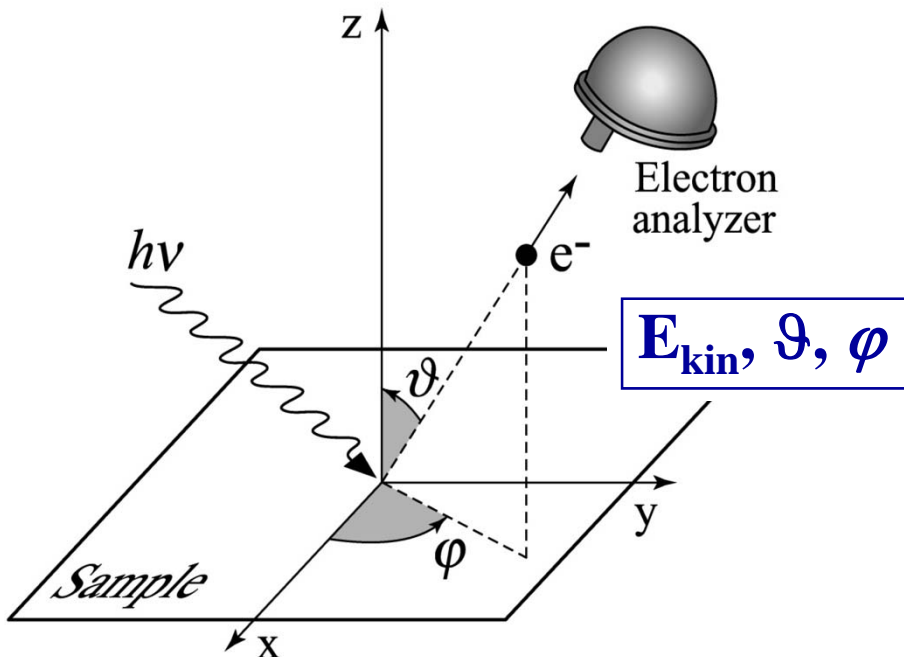
Photoemission Intensity $I(k, \omega)$

$$w_{fi} \propto |\langle \phi_f^k | \underline{\mathbf{A} \cdot \nabla V} | \phi_i^k \rangle \langle \Psi_m^{N-1} | \Psi_i^{N-1} \rangle|^2 \delta(\omega - h\nu)$$

The photoemission intensity for the SAME band is very DIFFERENT in various Brillouin zones



ARPES: Energetics and Kinematics

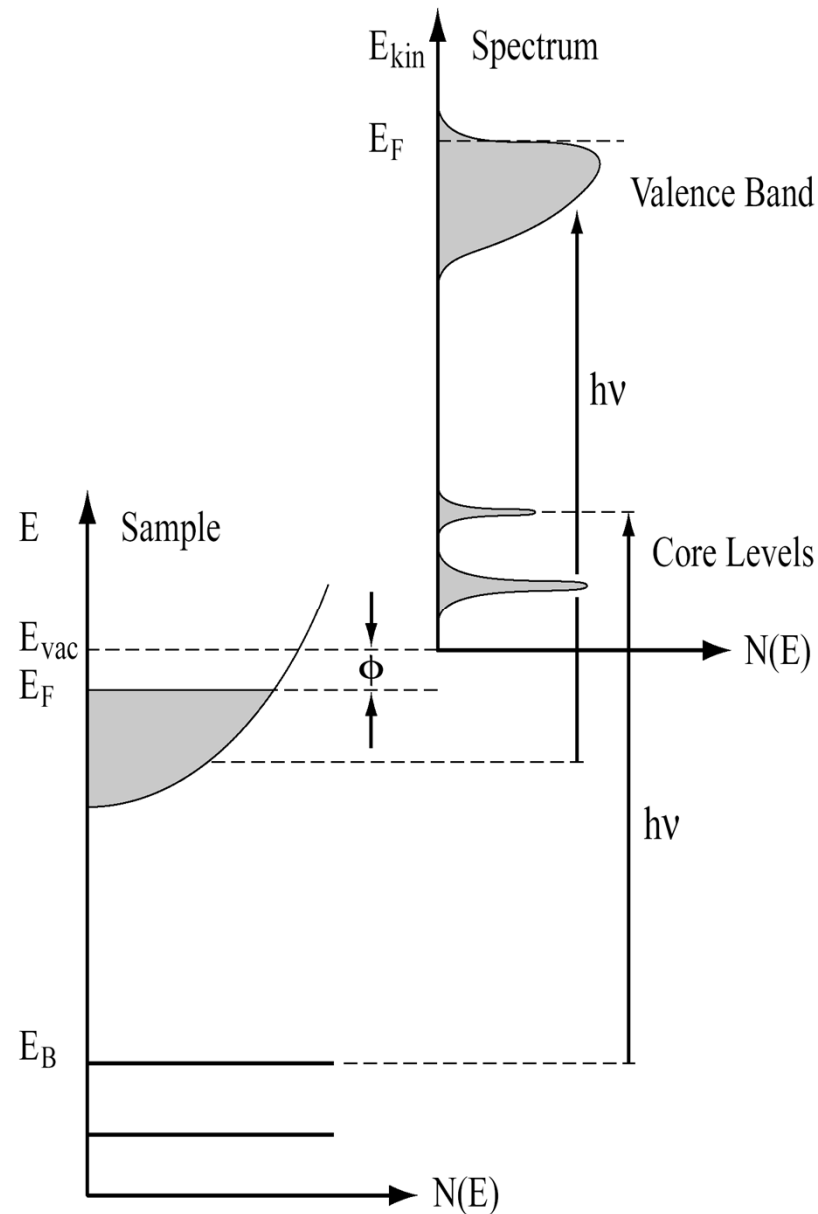


Energy Conservation

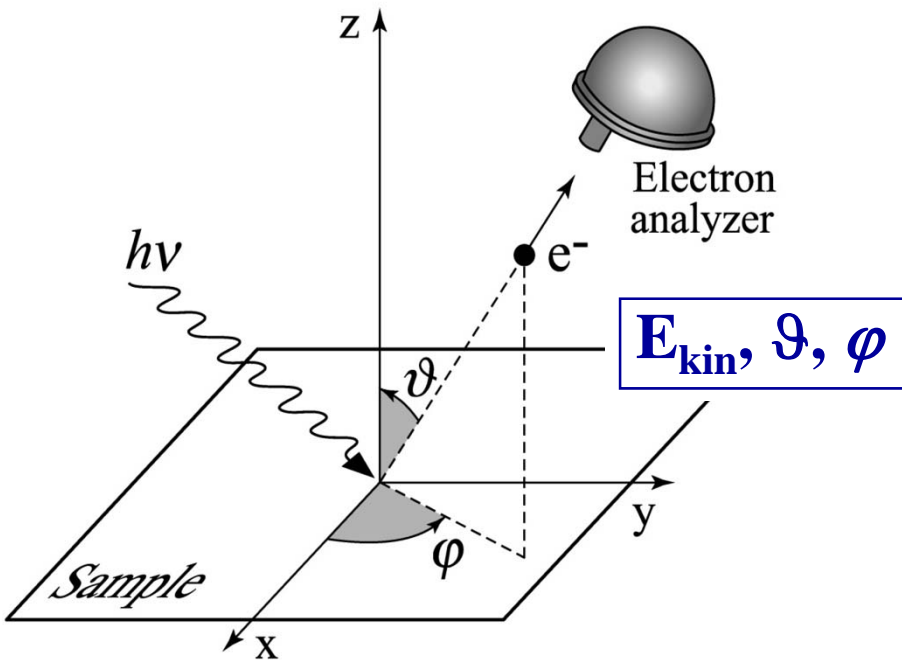
$$E_{kin} = h\nu - \phi - |\mathbf{E}_B|$$

Momentum Conservation

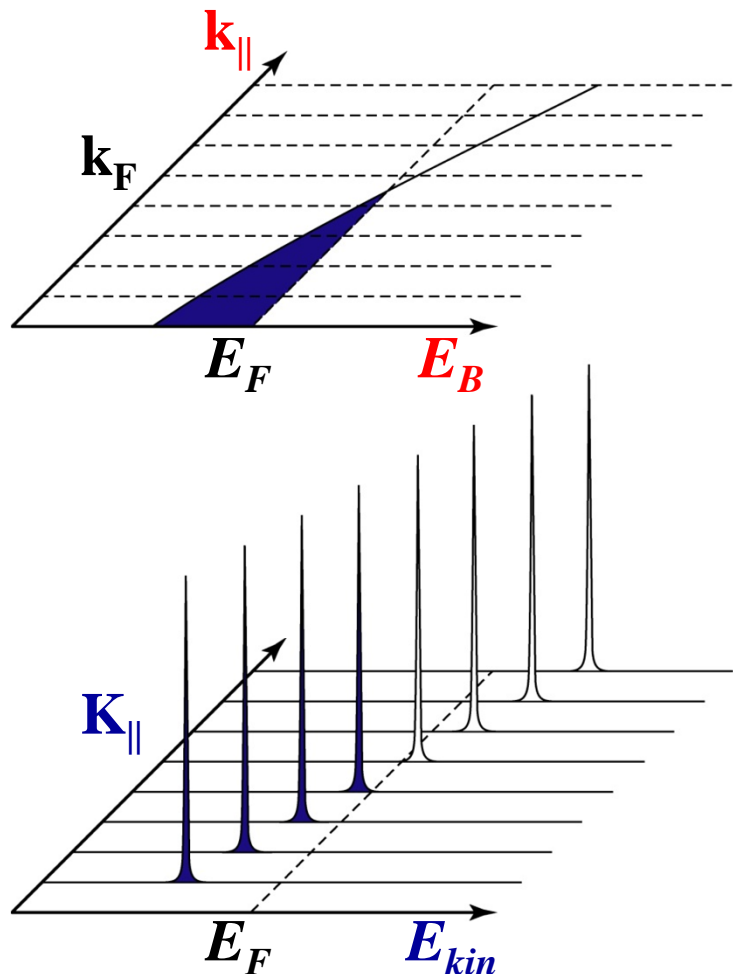
$$\hbar \mathbf{k}_{\parallel} = \hbar \mathbf{K}_{\parallel} = \sqrt{2m E_{kin}} \cdot \sin \vartheta$$



ARPES: Energetics and Kinematics



Electrons in Reciprocal Space



Energy Conservation

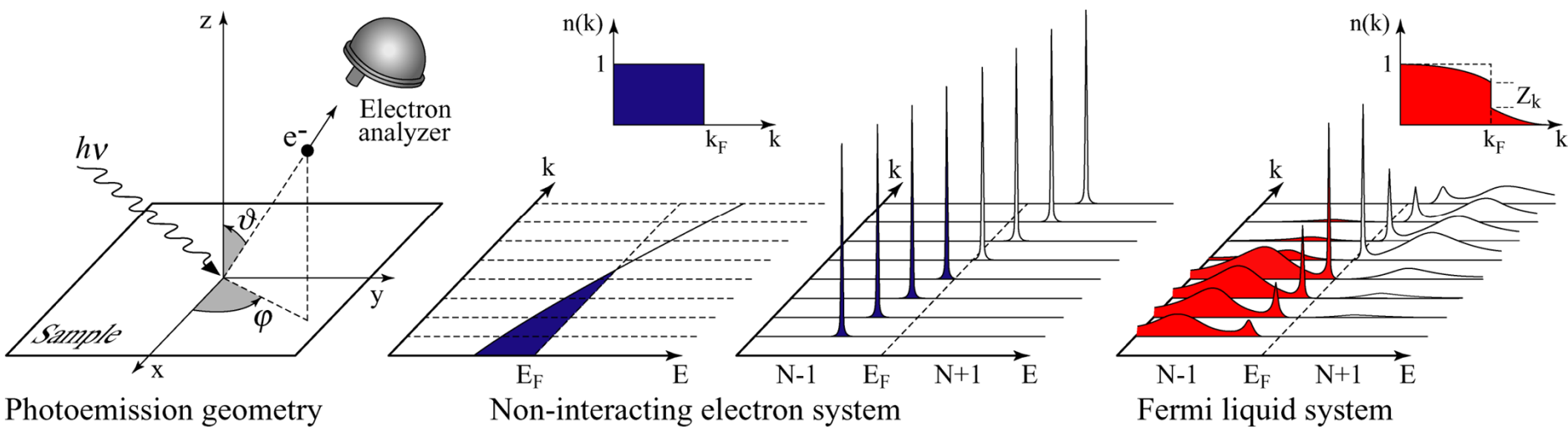
$$E_{kin} = h\nu - \phi - |\mathbf{E}_B|$$

Momentum Conservation

$$\hbar \mathbf{k}_{\parallel} = \hbar \mathbf{K}_{\parallel} = \sqrt{2m E_{kin}} \cdot \sin \vartheta$$

ARPES: Interacting Systems

A. Damascelli, Z. Hussain, Z.-X Shen, Rev. Mod. Phys. **75**, 473 (2003)



Photoemission intensity: $I(\mathbf{k}, E_{kin}) = \sum_{f,i} w_{f,i}$

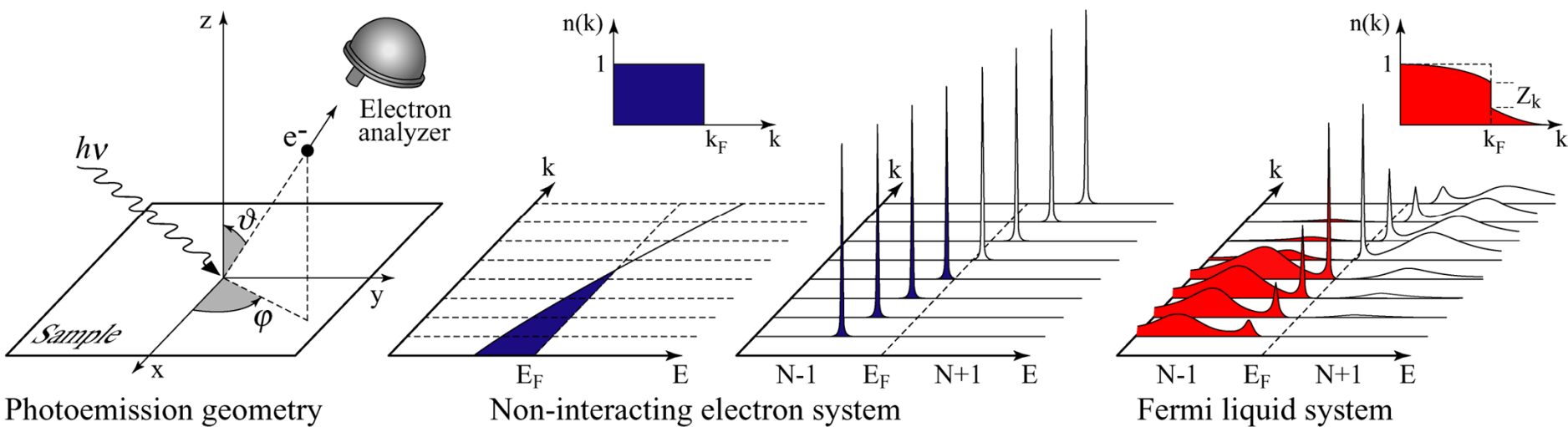
$$I(\mathbf{k}, E_{kin}) \propto \sum_{f,i} |M_{f,i}^{\mathbf{k}}|^2 \sum_m |c_{m,i}|^2 \delta(E_{kin} + E_m^{N-1} - E_i^N - h\nu)$$

$$|M_{f,i}^{\mathbf{k}}|^2 \equiv |\langle \phi_f^{\mathbf{k}} | \mathbf{A} \cdot \mathbf{p} | \phi_i^{\mathbf{k}} \rangle|^2 \quad |c_{m,i}|^2 = |\langle \Psi_m^{N-1} | \Psi_i^{N-1} \rangle|^2$$

In general $\Psi_i^{N-1} = c_{\mathbf{k}} \Psi_i^N$ **NOT orthogonal** Ψ_m^{N-1}

ARPES: Interacting Systems

A. Damascelli, Z. Hussain, Z.-X Shen, Rev. Mod. Phys. **75**, 473 (2003)



Photoemission intensity: $I(\mathbf{k}, E_{kin}) = \sum_{f,i} w_{f,i}$

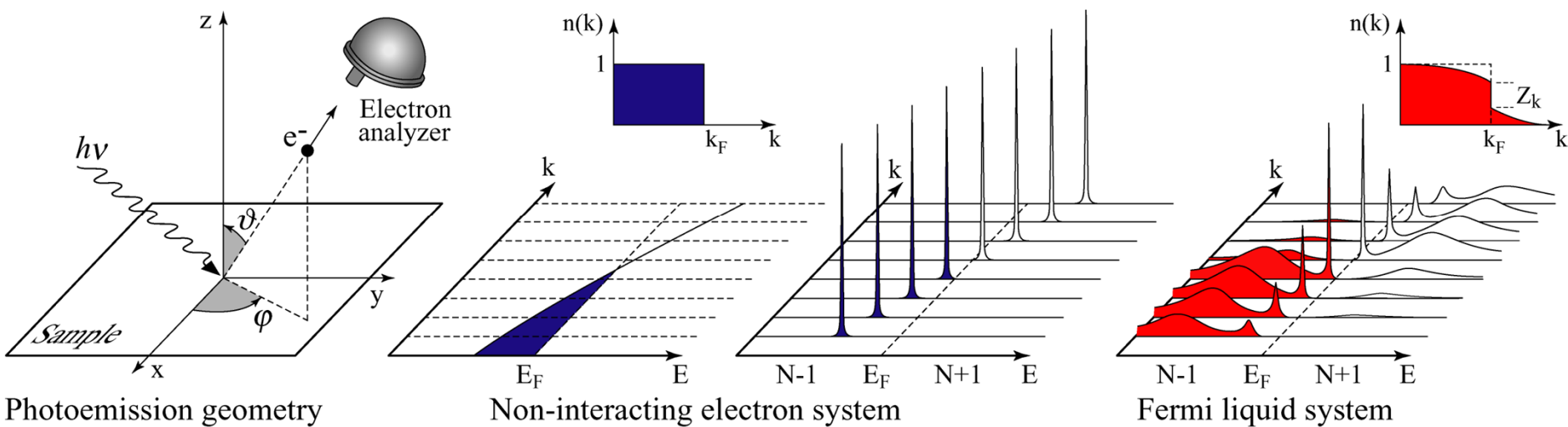
$$I(\mathbf{k}, E_{kin}) \propto \sum_{f,i} |M_{f,i}^{\mathbf{k}}|^2 \sum_m |c_{m,i}|^2 \delta(E_{kin} + E_m^{N-1} - E_i^N - h\nu)$$

$$|M_{f,i}^{\mathbf{k}}|^2 \equiv |\langle \phi_f^{\mathbf{k}} | \mathbf{A} \cdot \mathbf{p} | \phi_i^{\mathbf{k}} \rangle|^2 \quad |c_{m,i}|^2 = |\langle \Psi_m^{N-1} | \Psi_i^{N-1} \rangle|^2$$

“Like removing a stone from a water bucket”

ARPES: Fermi Liquid Description

A. Damascelli, Z. Hussain, Z.-X Shen, Rev. Mod. Phys. **75**, 473 (2003)



$$\text{Photoemission intensity: } I(k, \omega) = I_0 / M(k, \omega)^2 f(\omega) A(k, \omega)$$

Non-interacting

$$A(\mathbf{k}, \omega) = \delta(\omega - \epsilon_{\mathbf{k}})$$

No Renormalization
Infinite lifetime

Fermi Liquid

$$A(\mathbf{k}, \omega) = Z_{\mathbf{k}} \frac{\Gamma_{\mathbf{k}}/\pi}{(\omega - \varepsilon_{\mathbf{k}})^2 + \Gamma_{\mathbf{k}}^2} + A_{inc}$$

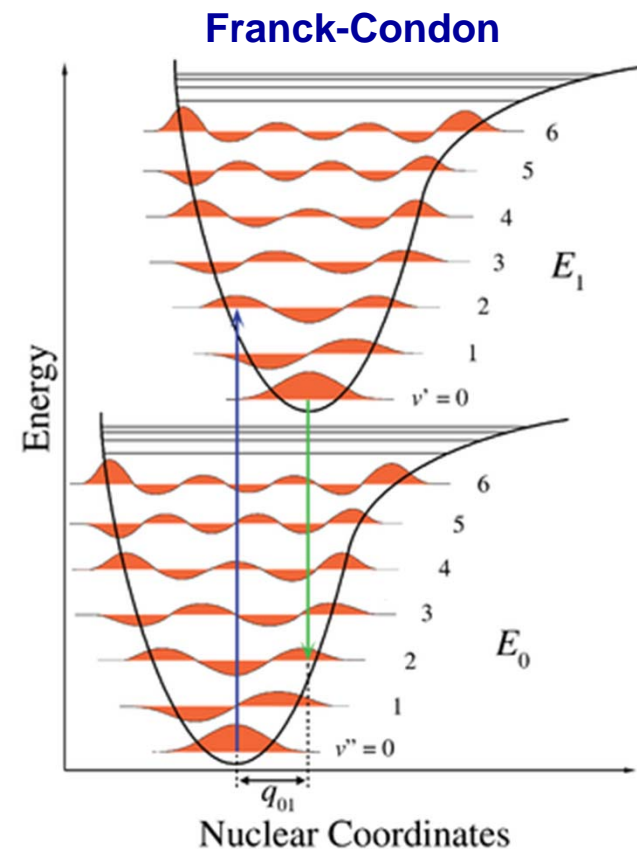
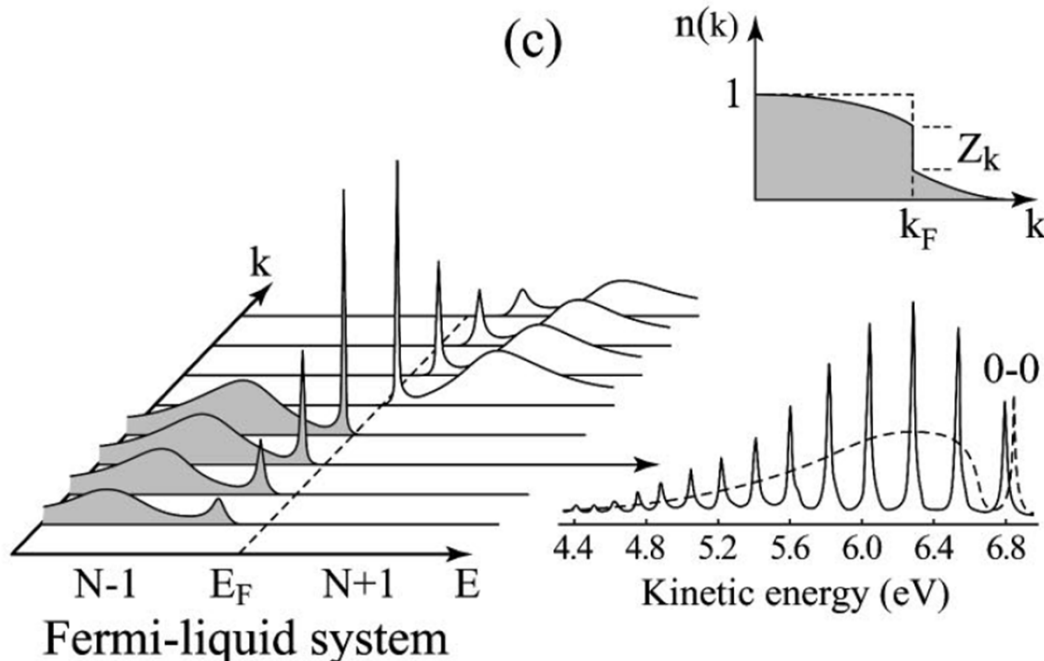
$$m^* > m \quad |\varepsilon_{\mathbf{k}}| < |\epsilon_{\mathbf{k}}|$$

$$\tau_{\mathbf{k}} = 1/\Gamma_{\mathbf{k}}$$

$\Sigma(\mathbf{k}, \omega)$: the “self-energy” captures the effects of interactions

Testing Fermi-liquid models

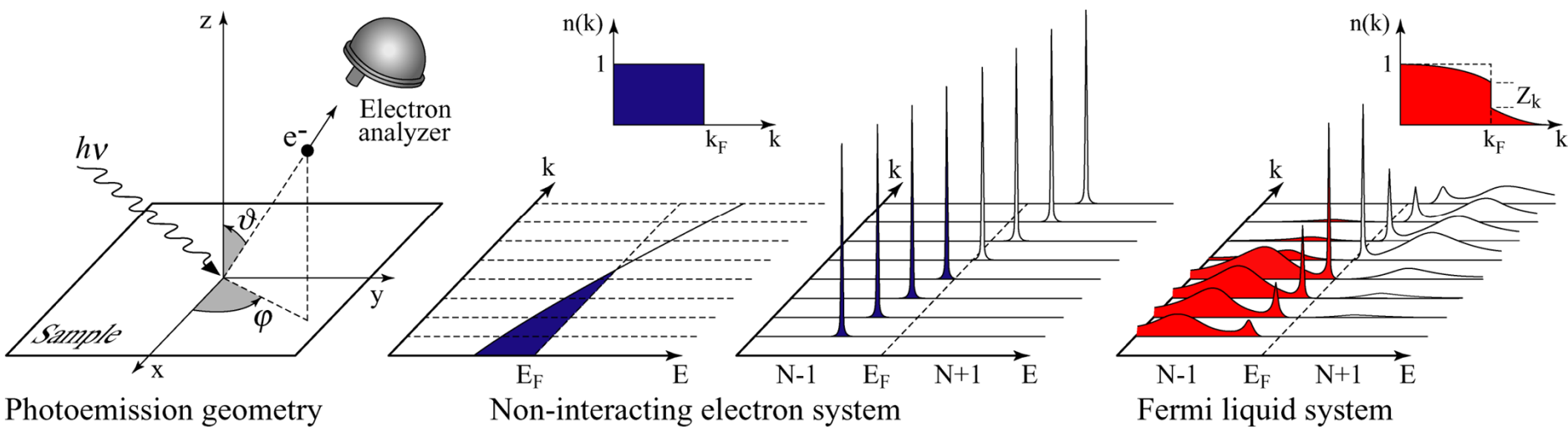
G.A. Sawatzky



"In gaseous hydrogen, the equilibrium bond length is dependent on the degree of occupation of that level. The electrons are dressed by interatomic displacements. The intensities are given by the Franck-Condon factors, the molecular equivalent of the sudden approximation. The ARPES spectrum of solid hydrogen, developed from the molecular spectrum, will be angle dependent but for some angle will resemble the broken line. The fundamental transition (0-0) becomes the solid state quasiparticle peak. The phonon excitations develop into a broad, incoherent quasicontinuum."

ARPES: The One-Particle Spectral Function

A. Damascelli, Z. Hussain, Z.-X Shen, Rev. Mod. Phys. **75**, 473 (2003)



Photoemission intensity: $I(k, \omega) = I_0 / M(k, \omega)^2 f(\omega) A(k, \omega)$

Single-particle spectral function

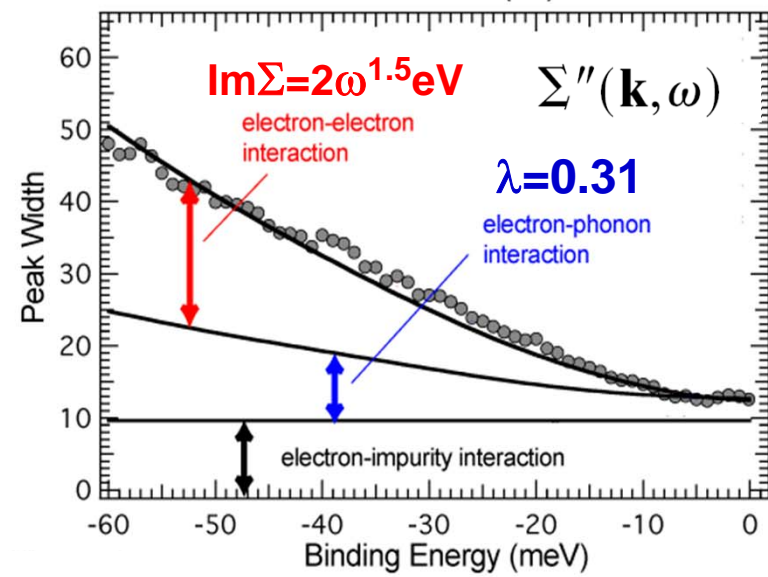
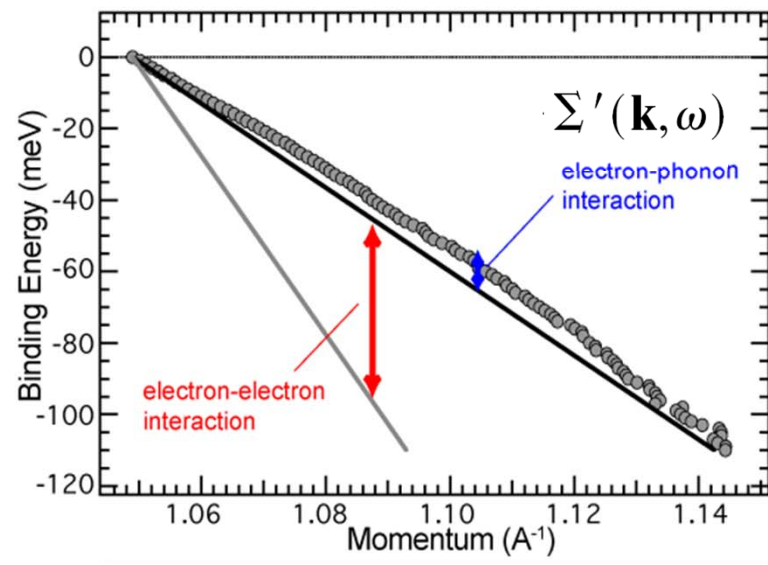
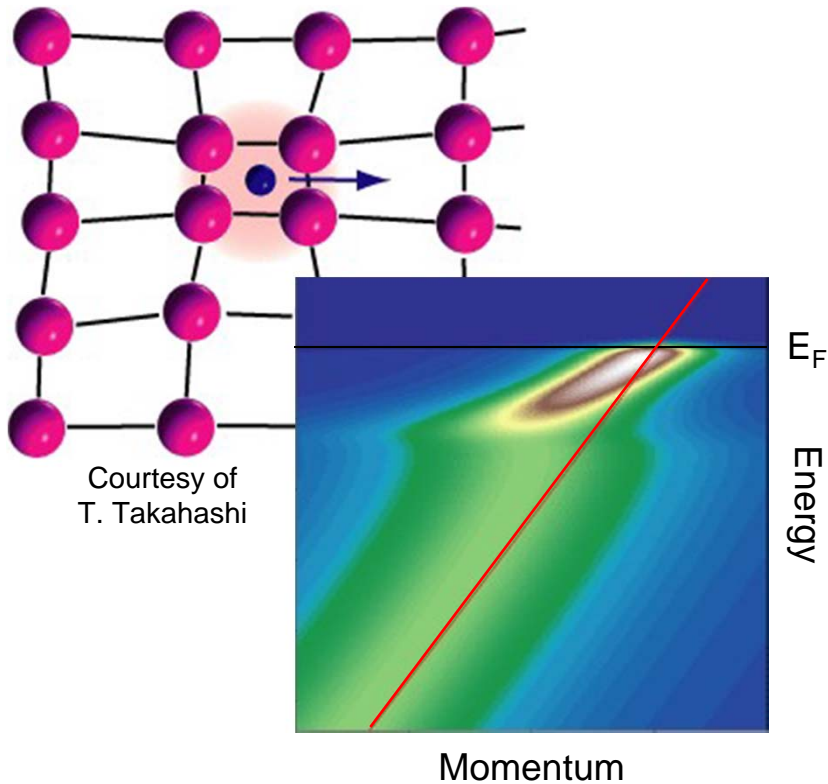
$$A(\mathbf{k}, \omega) = -\frac{1}{\pi} \frac{\Sigma''(\mathbf{k}, \omega)}{[\omega - \epsilon_{\mathbf{k}} - \Sigma'(\mathbf{k}, \omega)]^2 + [\Sigma''(\mathbf{k}, \omega)]^2}$$

$\Sigma(\mathbf{k}, \omega)$: the “self-energy” captures the effects of interactions

Many-Body Correlation Effects in Sr_2RuO_4

Single-particle spectral function

$$A(\mathbf{k}, \omega) = -\frac{1}{\pi} \frac{\Sigma''(\mathbf{k}, \omega)}{[\omega - \epsilon_{\mathbf{k}} - \Sigma'(\mathbf{k}, \omega)]^2 + [\Sigma''(\mathbf{k}, \omega)]^2}$$





UNIVERSITY OF BRITISH COLUMBIA

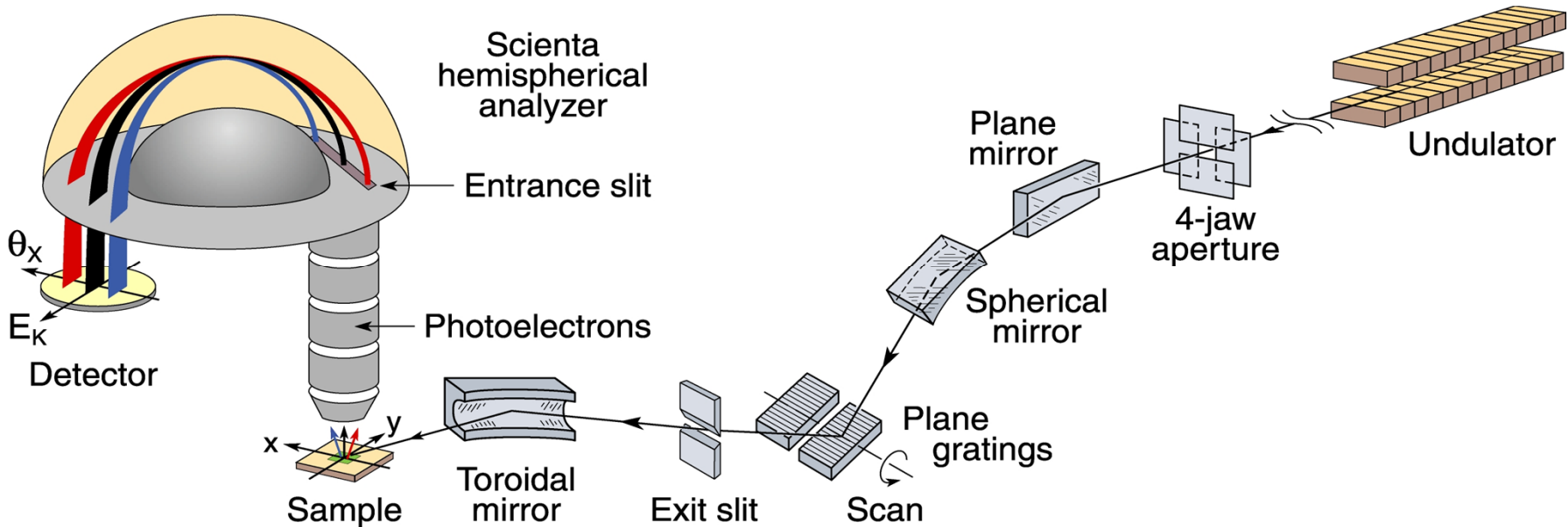


Outline Part I

ARPES: Technique and developments

CUSO Lecture – Lausanne 02/2011

Angle-Resolved Photoemission Spectroscopy



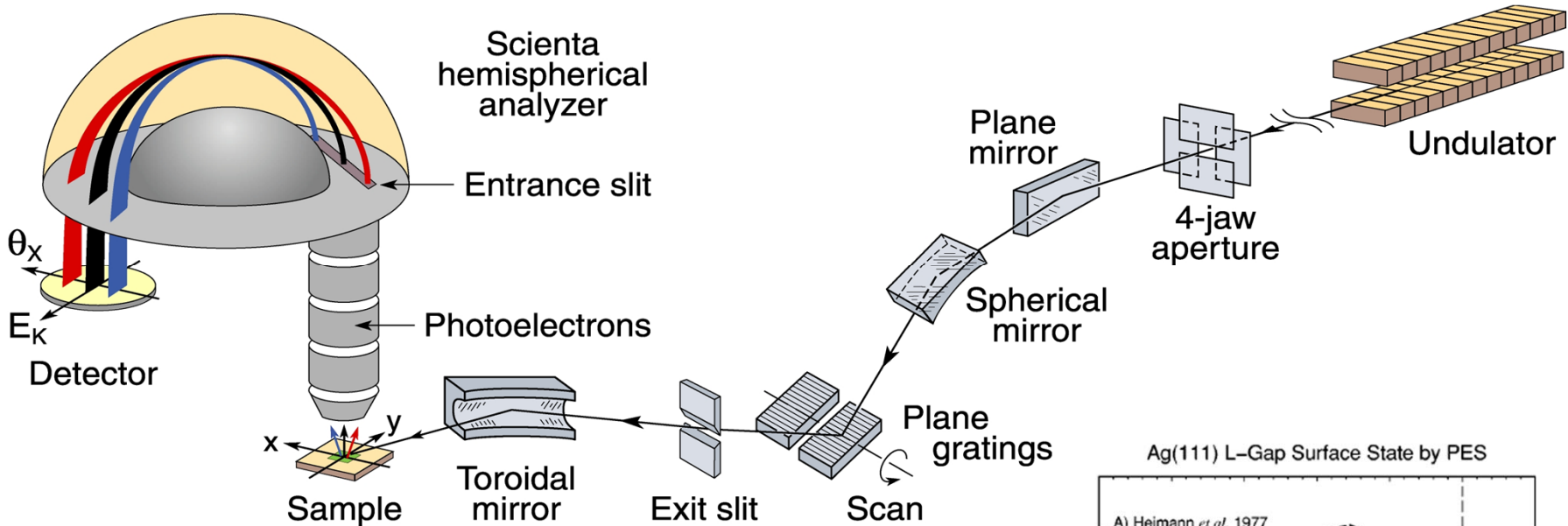
Parallel multi-angle recording

- Improved energy resolution
- Improved momentum resolution
- Improved data-acquisition efficiency

	ΔE (meV)	$\Delta\theta$
past	20-40	2°
now	1-10	0.2°



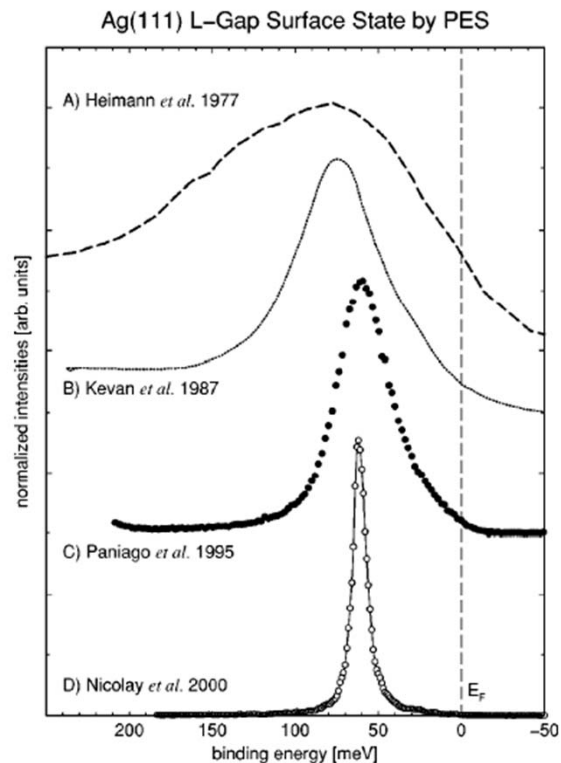
Angle-Resolved Photoemission Spectroscopy



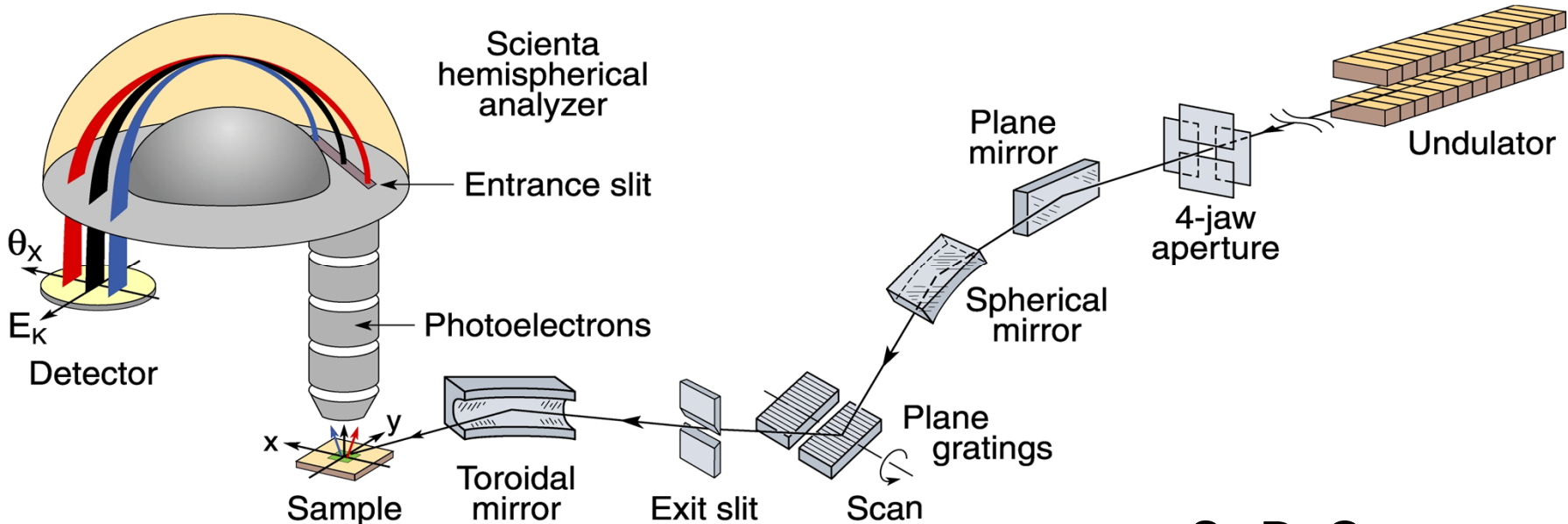
Parallel multi-angle recording

- Improved energy resolution
- Improved momentum resolution
- Improved data-acquisition efficiency

	ΔE (meV)	$\Delta \theta$
past	20-40	2°
now	1-10	0.2°



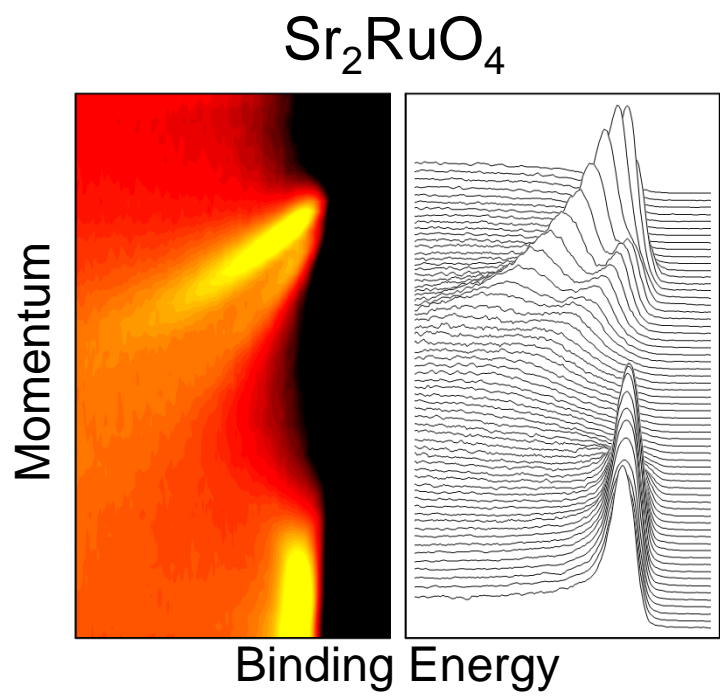
Angle-Resolved Photoemission Spectroscopy



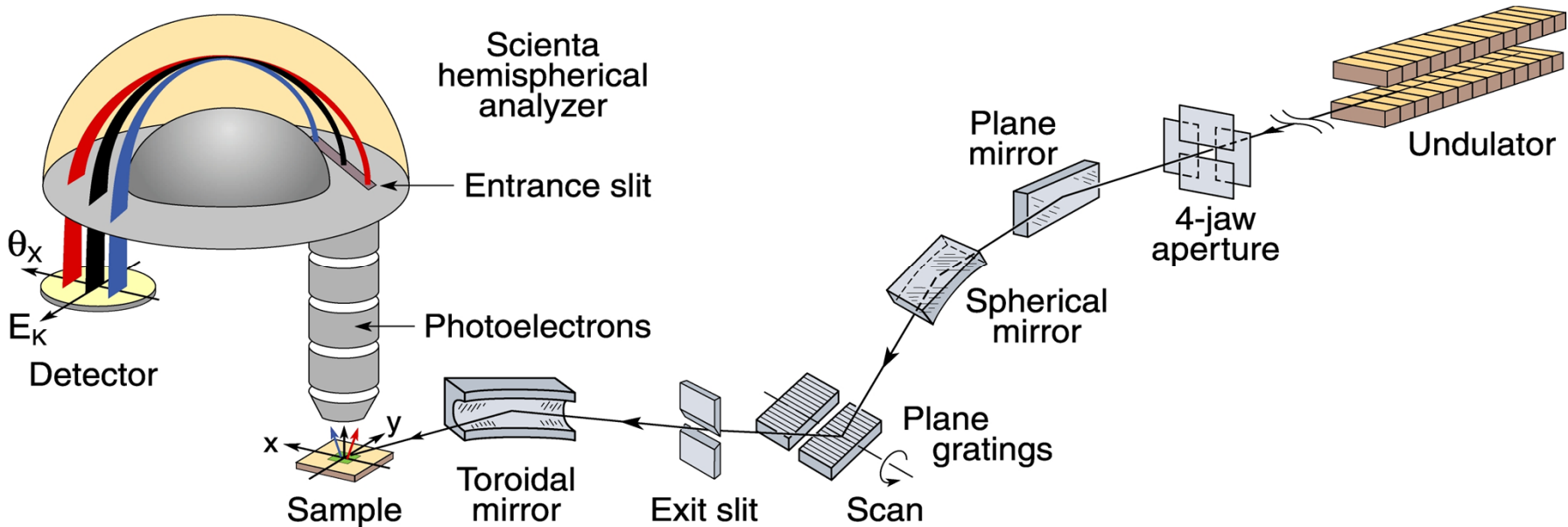
Parallel multi-angle recording

- Improved energy resolution
- Improved momentum resolution
- Improved data-acquisition efficiency

	ΔE (meV)	$\Delta \theta$
past	20-40	2°
now	1-10	0.2°



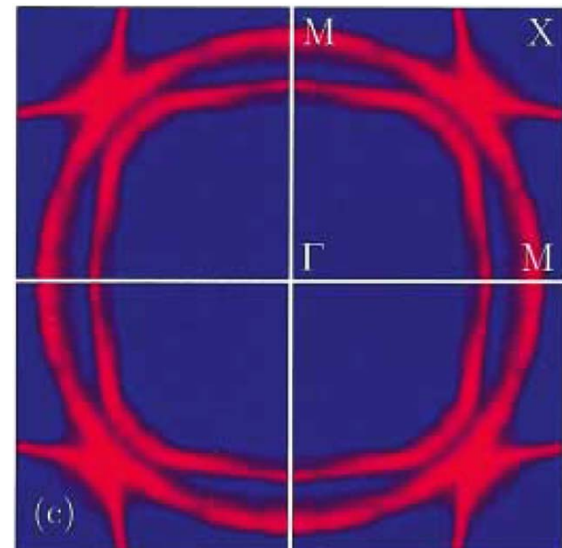
Angle-Resolved Photoemission Spectroscopy



Parallel multi-angle recording

- Improved energy resolution
- Improved momentum resolution
- Improved data-acquisition efficiency

	ΔE (meV)	$\Delta \theta$
past	20-40	2°
now	1-10	0.2°

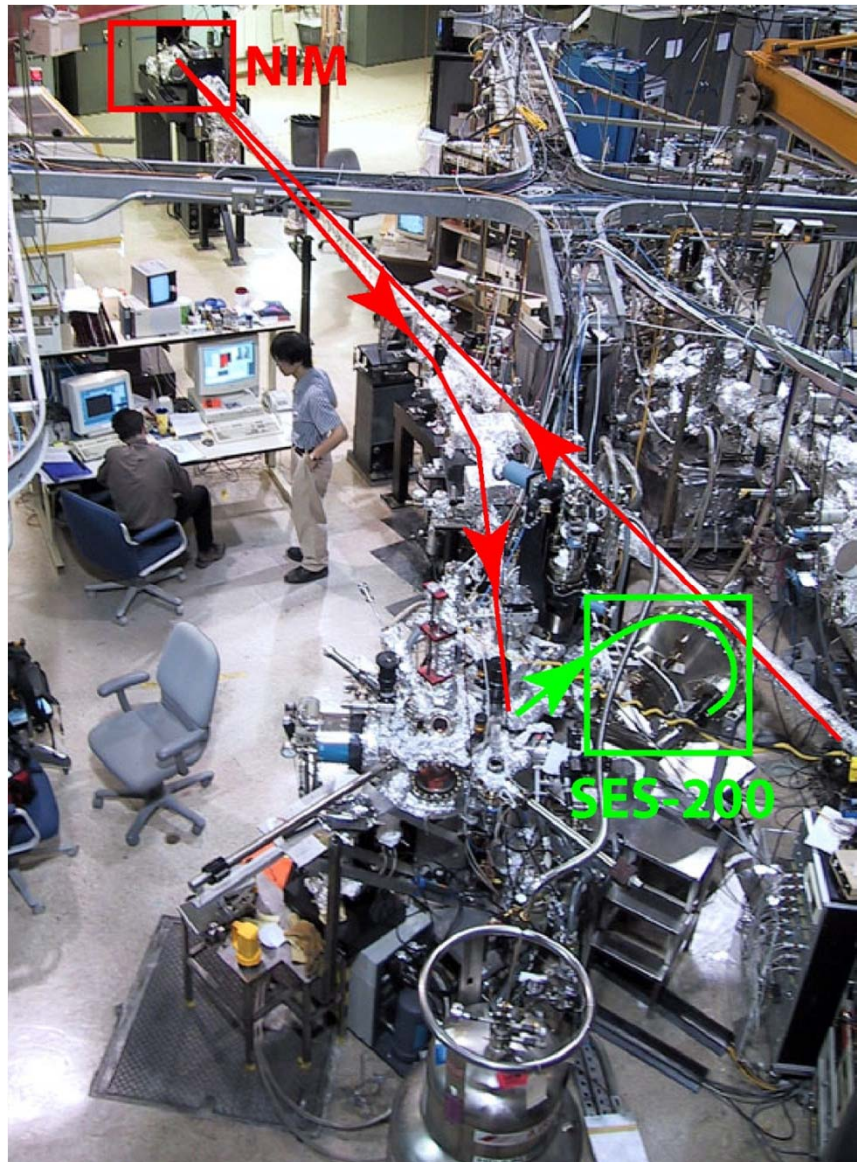
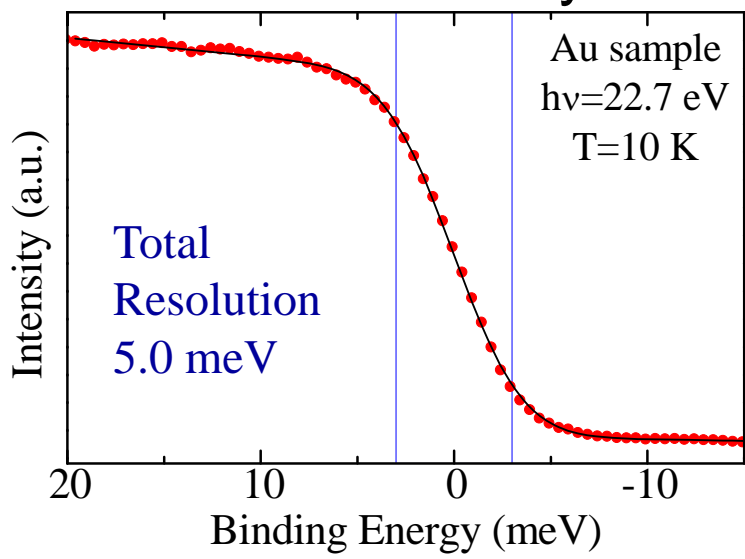


Angle-Resolved Photoemission Spectroscopy



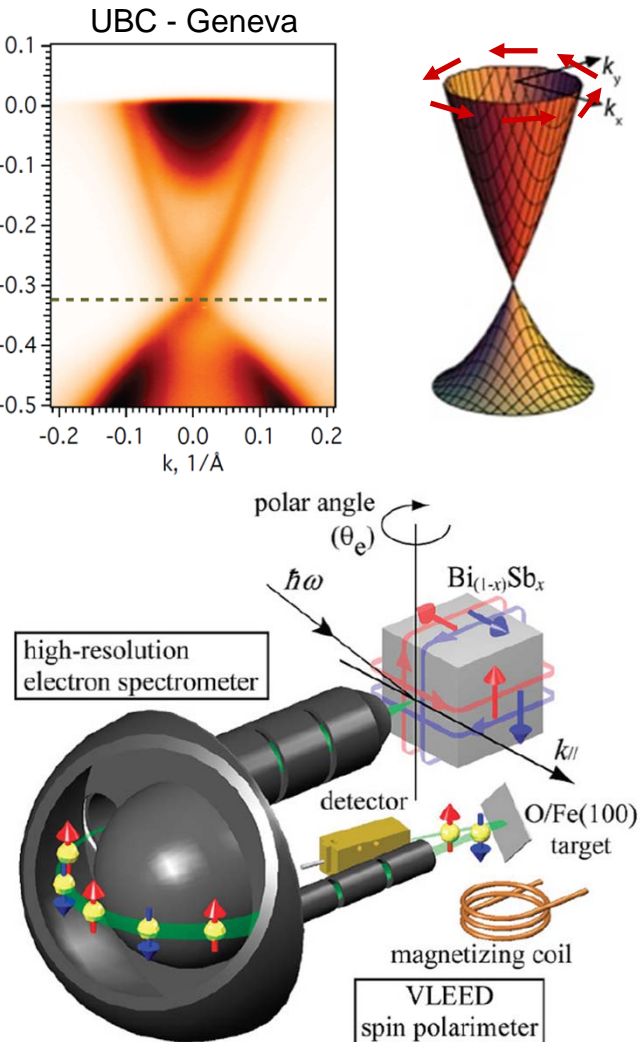
ΔE (meV)	$\Delta\theta$
1-10	0.2°

NIM/SCIENTA System



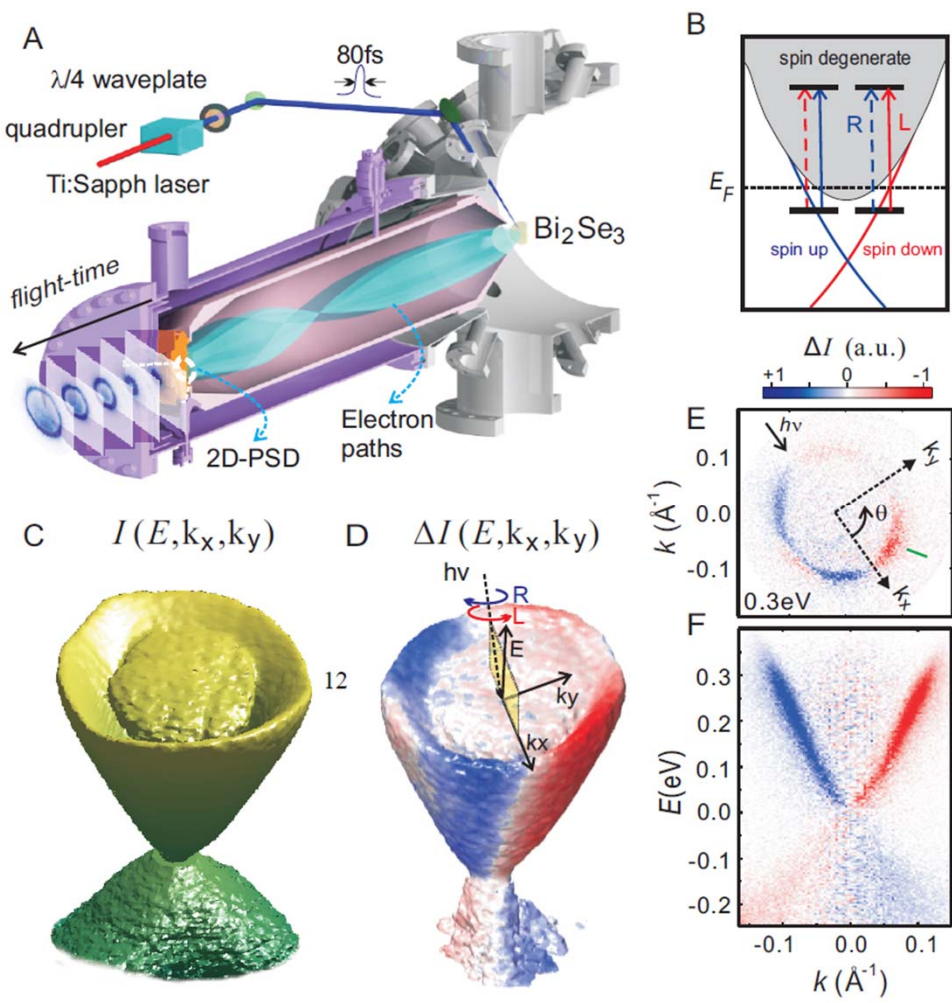
New Developments: ARPES + Spin + Time

ARPES+Spin polarimeter



Nishide et al., New J. Phys. 12, 065011 (2010)

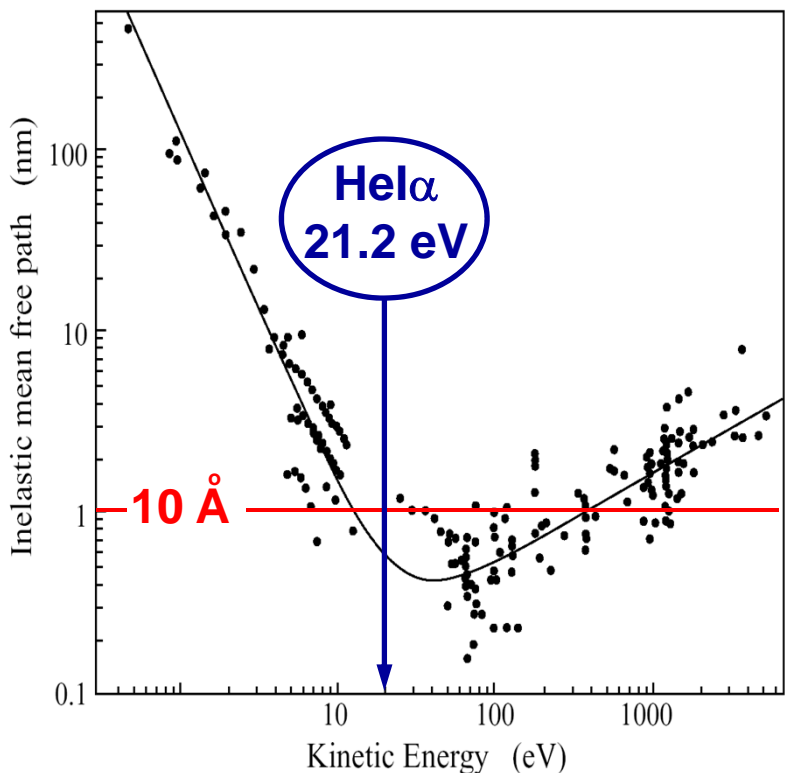
ARPES+Time of Flight



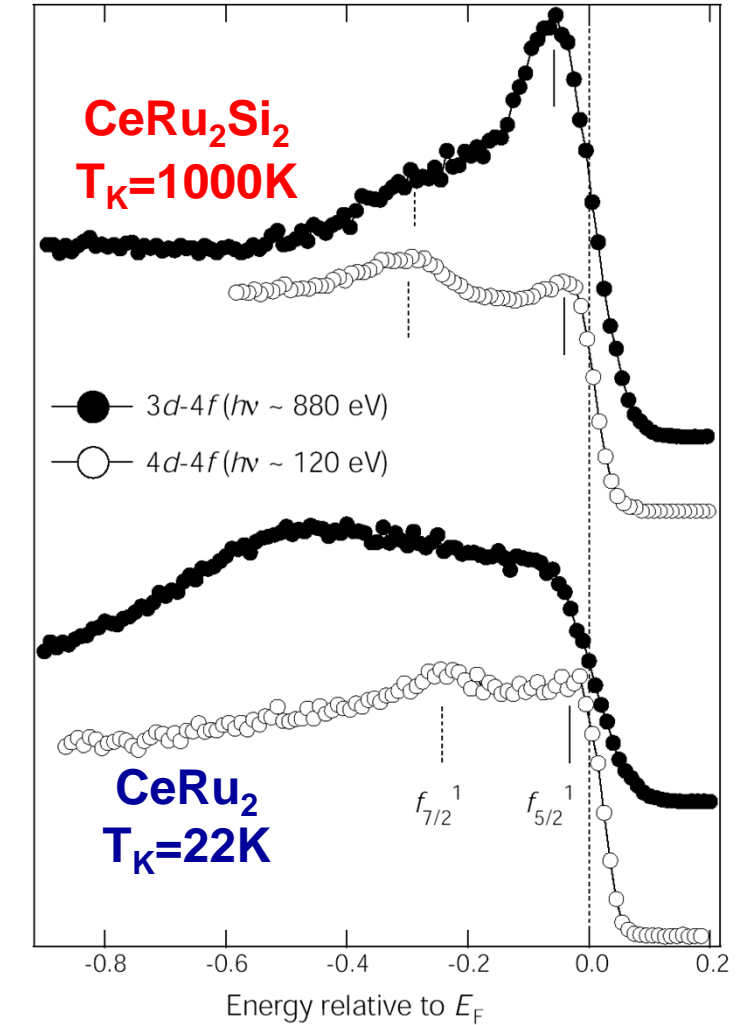
Wang et al., arXiv:1101.5636 (2011)

ARPES: Surface vs Bulk Sensitivity

Mean-free path for excited electrons



Seah, Dench *et al.*, SIA 1, 2 (1979)



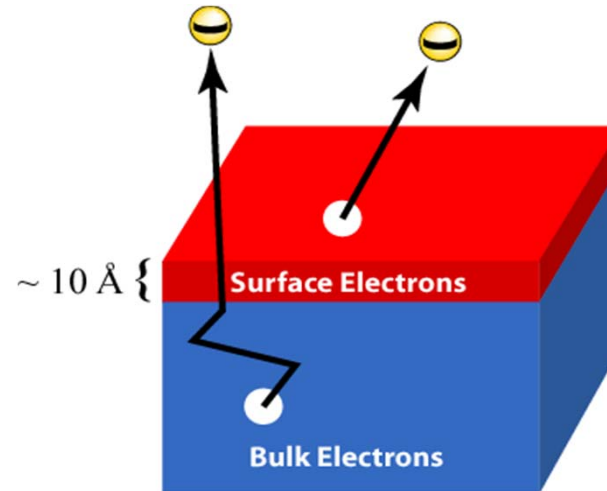
Sekiyama *et al.*, Nature 403, 396 (2000)

ARPES: Advantages and Limitations

Advantages

- Direct information about the electronic states!
- Straightforward comparison with theory - little or no modeling.
- High-resolution information about **BOTH energy and momentum**
- **Surface-sensitive probe**
- Sensitive to “**many-body**” effects
- Can be applied to small samples (100 μm x 100 μm x 10 nm)

Limitations



- Not bulk sensitive
- Requires clean, atomically flat surfaces in **ultra-high vacuum**
- Cannot be studied as a function of pressure or magnetic field



UNIVERSITY OF BRITISH COLUMBIA



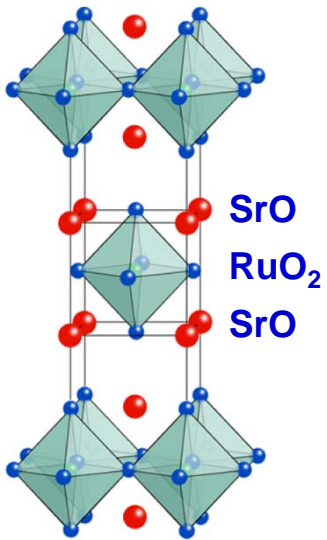
Outline Part II

Sr_2RuO_4 : A Fermi liquid with spin-orbit coupling

CUSO Lecture – Lausanne 02/2011

Sr_2RuO_4 : p-wave Superconductivity

2D perovskite

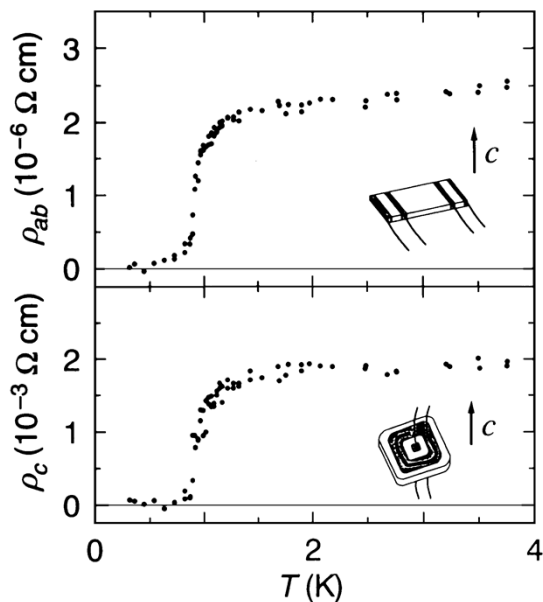


Unconventional superconductivity

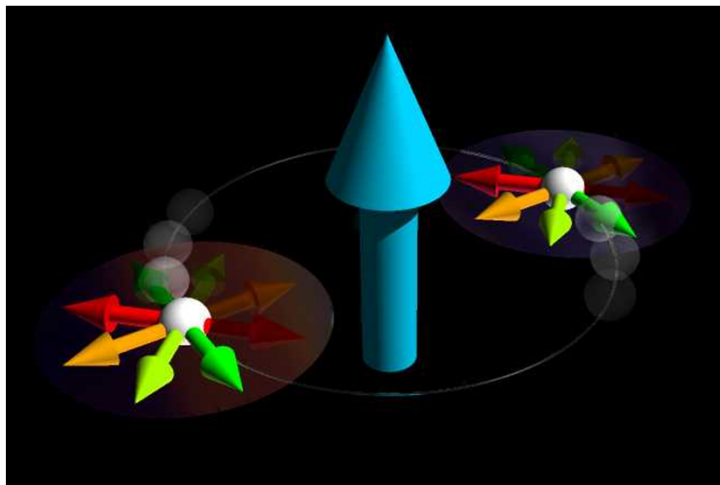
- Pairing mechanism ?
- Order parameter ?
- FM-AF fluctuations ?

Rice & Sigrist, JPCM 7, L643 (1995)

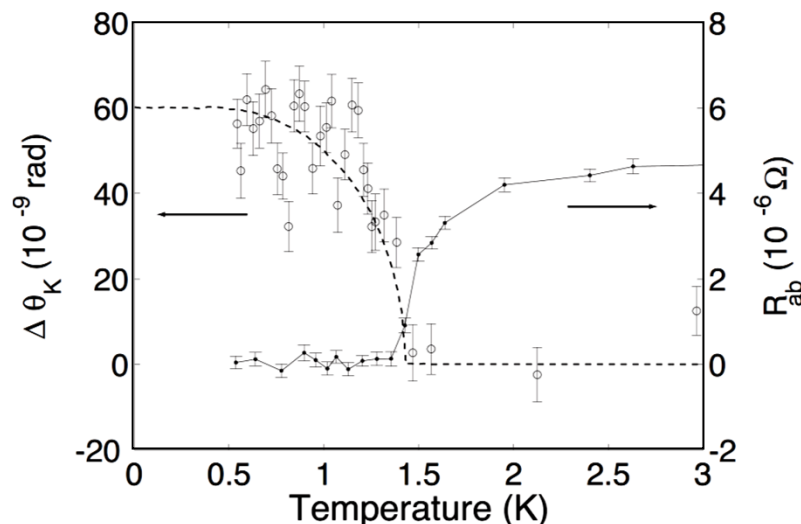
Maeno *et al.*, Nature 372, 532 (1994)



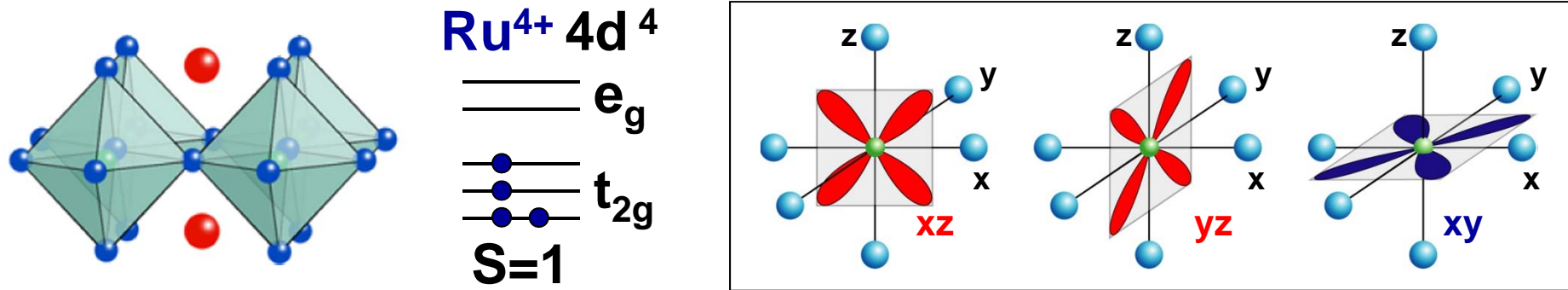
Mackenzie & Maeno, RMP 75, 657 (2003)



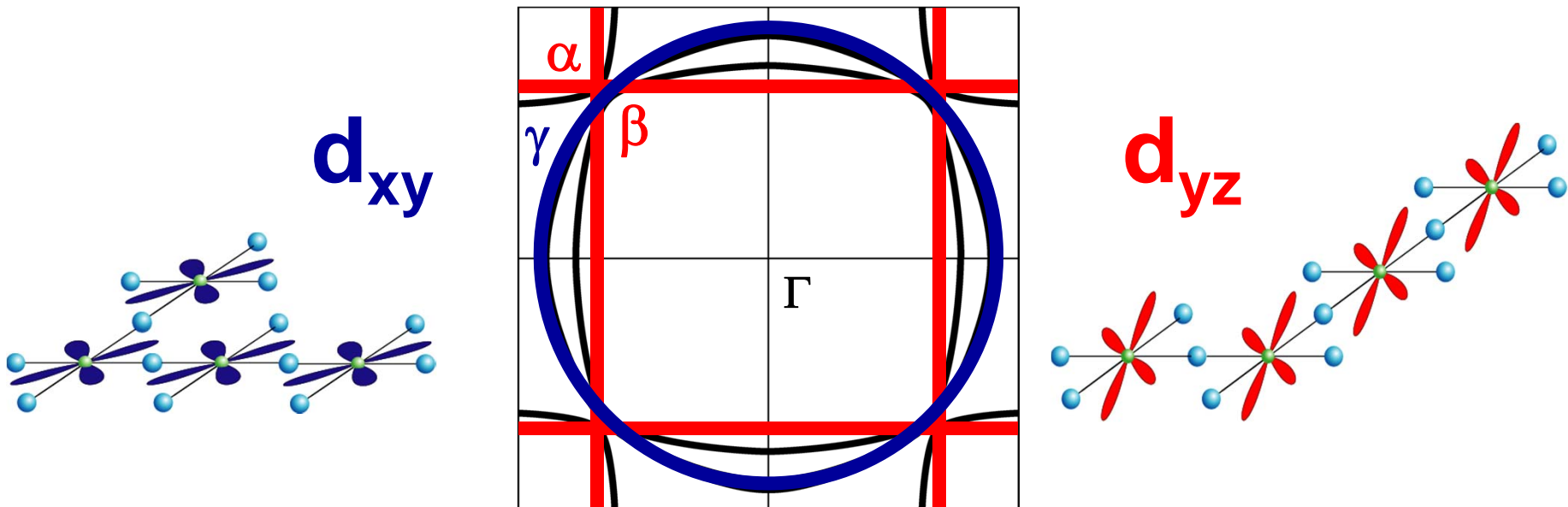
Xia *et al.*, PRL 97, 167002 (2006)



1D ($d_{xz,yz}$) versus 2D (d_{xy}) Superconductivity ?

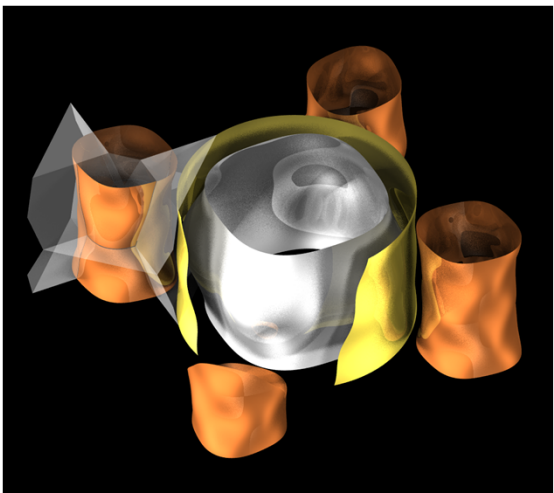


► Band structure calculation: 3 t_{2g} bands crossing E_F



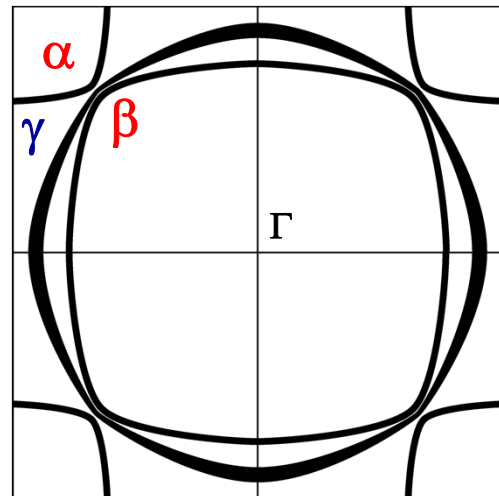
The Fermi Surface of Sr_2RuO_4

de Haas-van Alphen



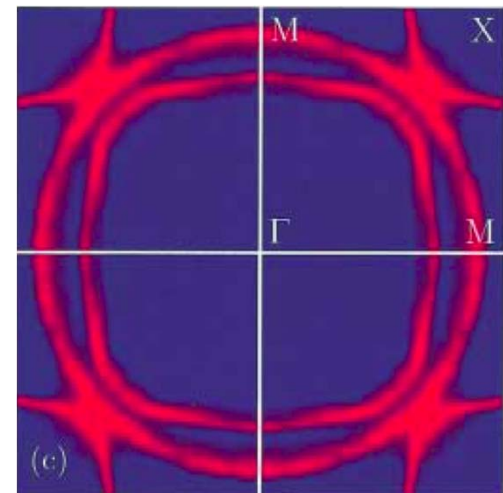
Bergemann *et al.*, PRL **84**, 2662 (2000)

LDA



Mazin *et al.*, PRL **79**, 733 (1997)

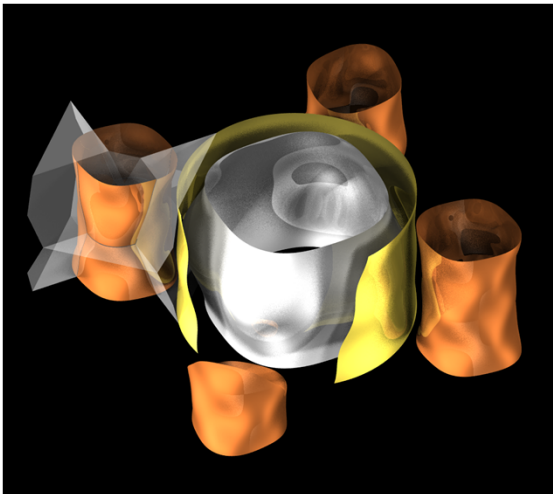
ARPES



Damascelli *et al.*, PRL **85**, 5194 (2000)

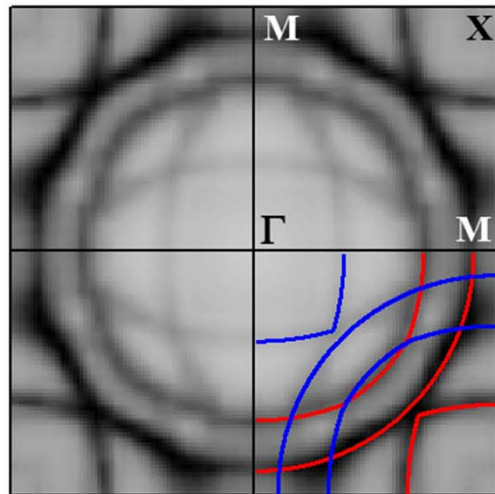
The Fermi Surface of Sr_2RuO_4

de Haas-van Alphen



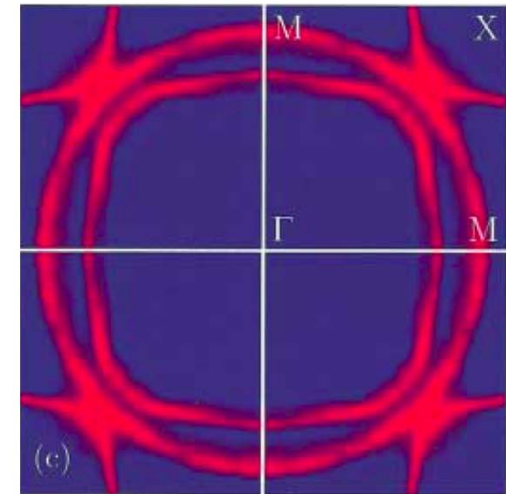
Bergemann *et al.*, PRL **84**, 2662 (2000)

Surface



Damascelli *et al.*, PRL **85**, 5194 (2000)

Bulk



Damascelli *et al.*, PRL **85**, 5194 (2000)

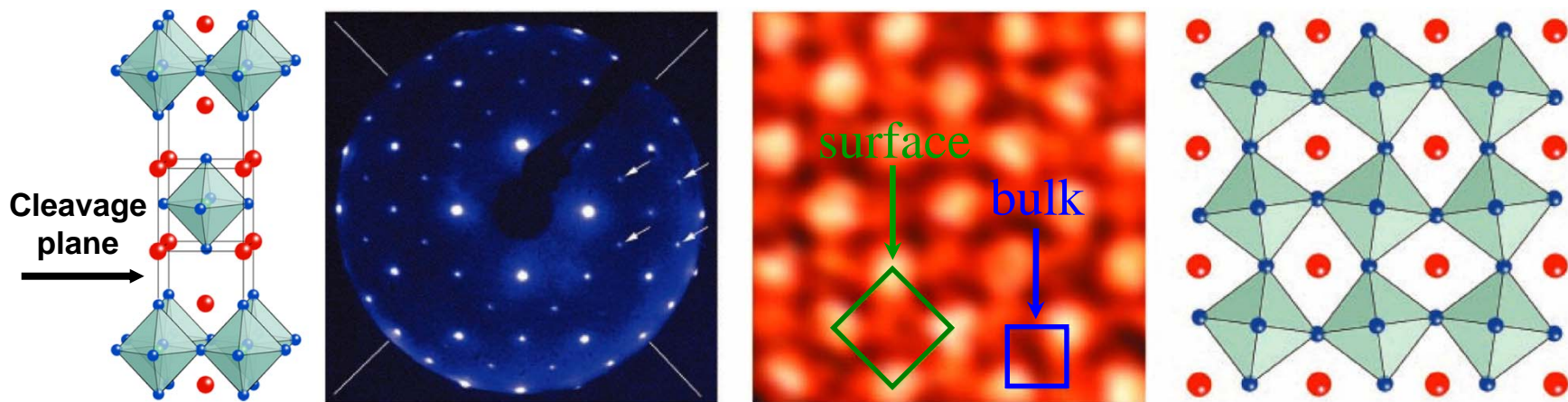
Cleaved at 10K

Cleaved at 200K

Structural surface reconstruction: rotation of RuO_6 octahedra

R. Matzdorf *et al.*, Science **289**, 746 (2000)

Surface reconstruction of cleaved Sr_2RuO_4



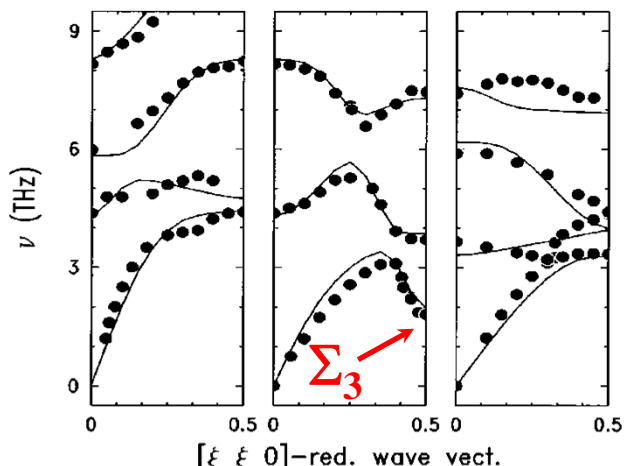
R. Matzdorf *et al.*, Science **289**, 746 (2000)

Rotation of the RuO_6 octahedra around the c axis

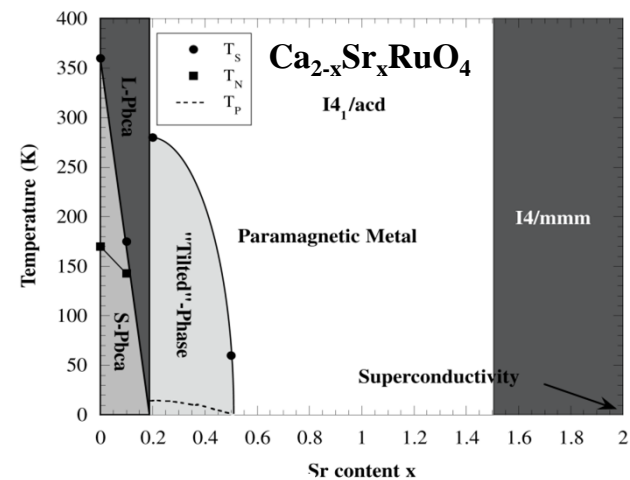
Soft S_3 phonon branch



Rotation instability of $\text{Ca}_{2-x}\text{Sr}_x\text{RuO}_4$



M. Braden *et al.*, PRB **57**, 1236 (1998)

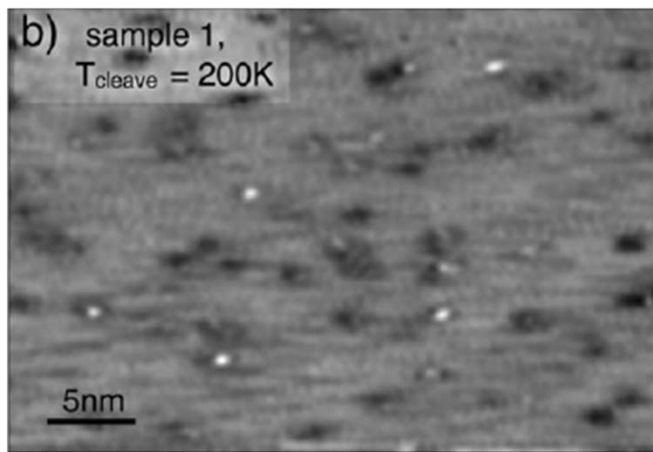
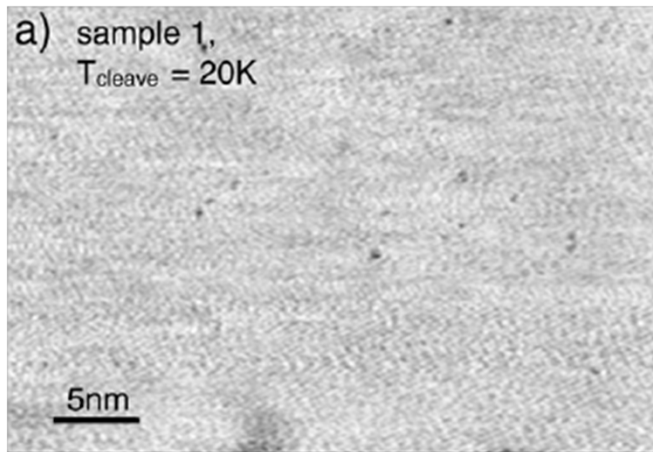


O. Friedt *et al.*, PRB **63**, 174432 (2001)

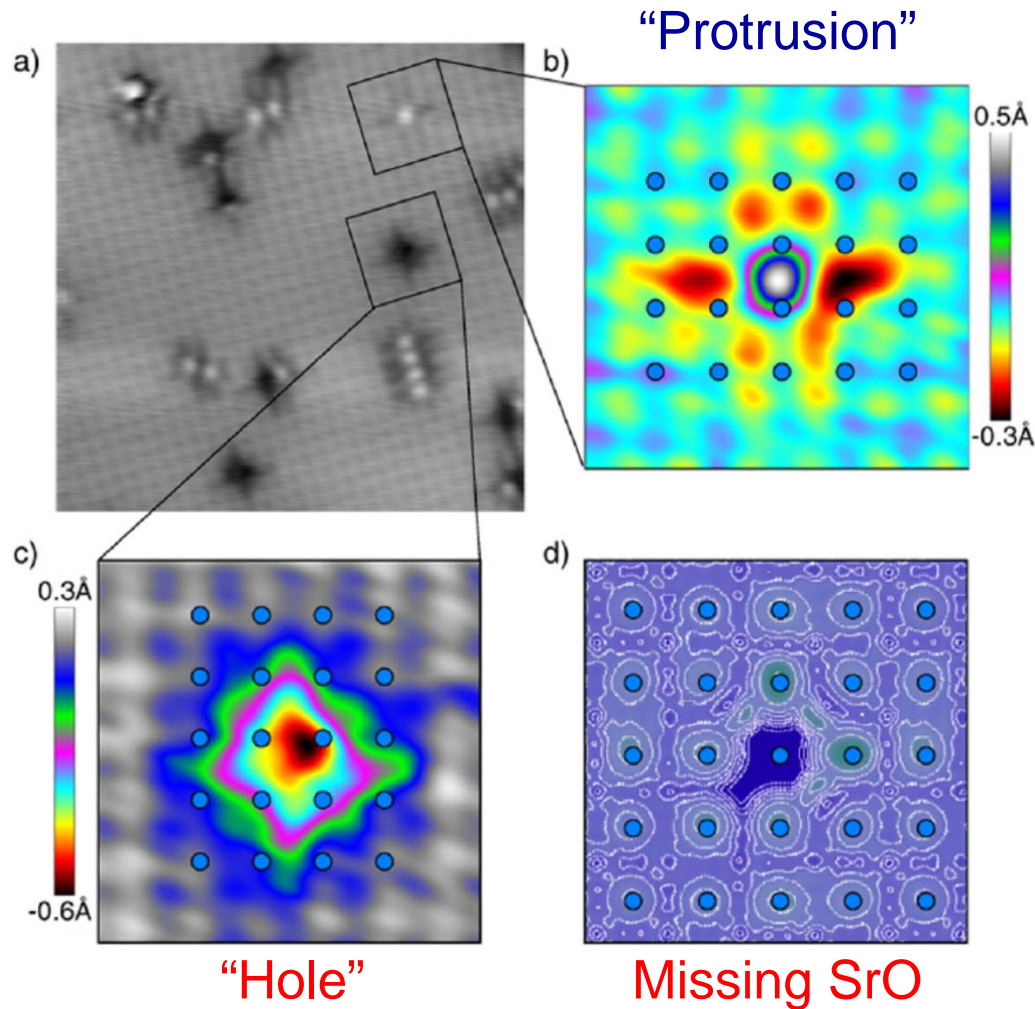
Cleaving-Temperature Dependence of Sr_2RuO_4 Surfaces

Temperature dependent STM

~ 0.002 defects/nm²

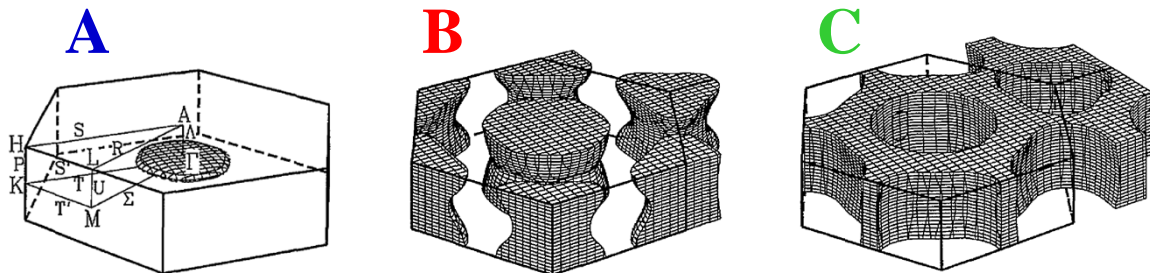
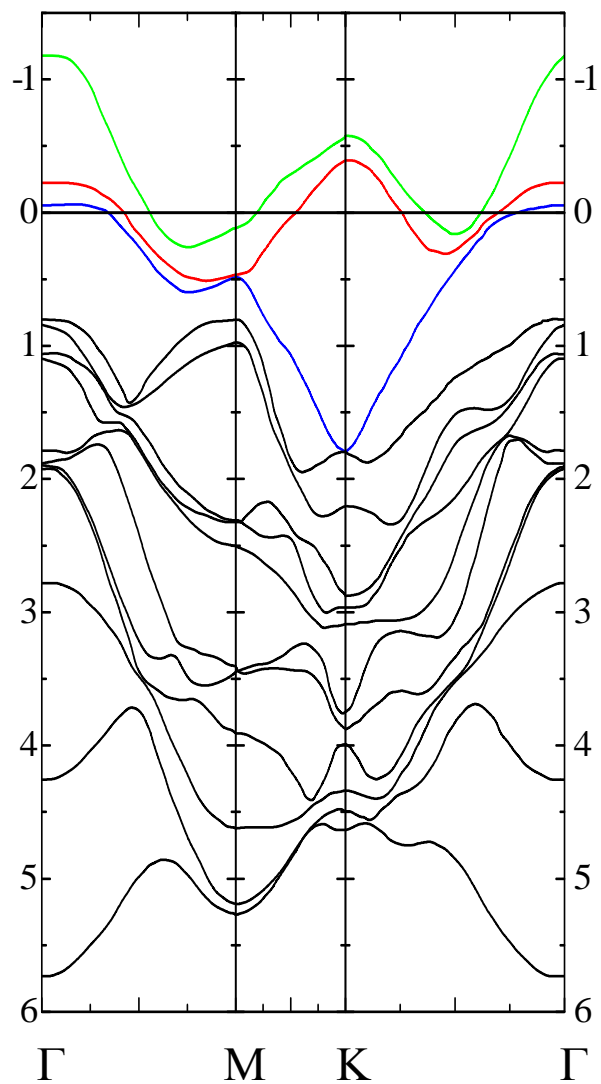


0.056 ± 0.01 defects/nm²

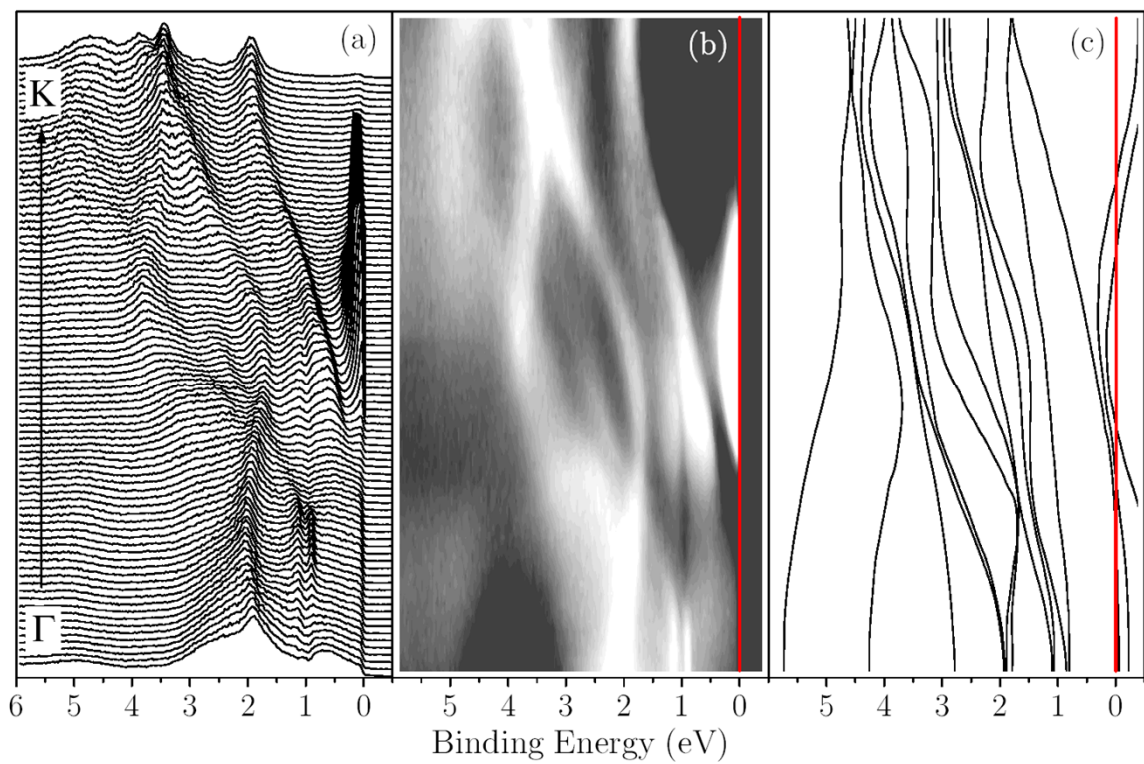


2H-NbSe₂: Normal State Electronic Structure

Corcoran *et al.*, JPCM **6**, 4479 (1994)

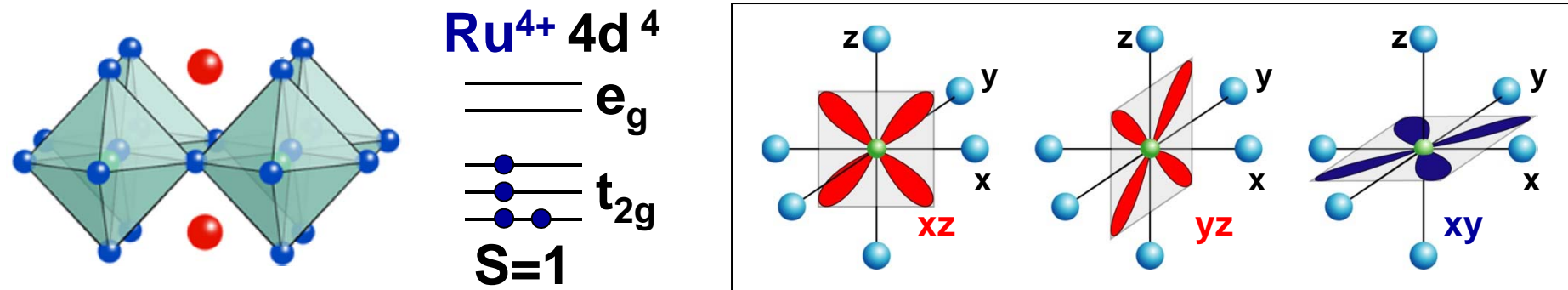


Damascelli *et al.* (2000)

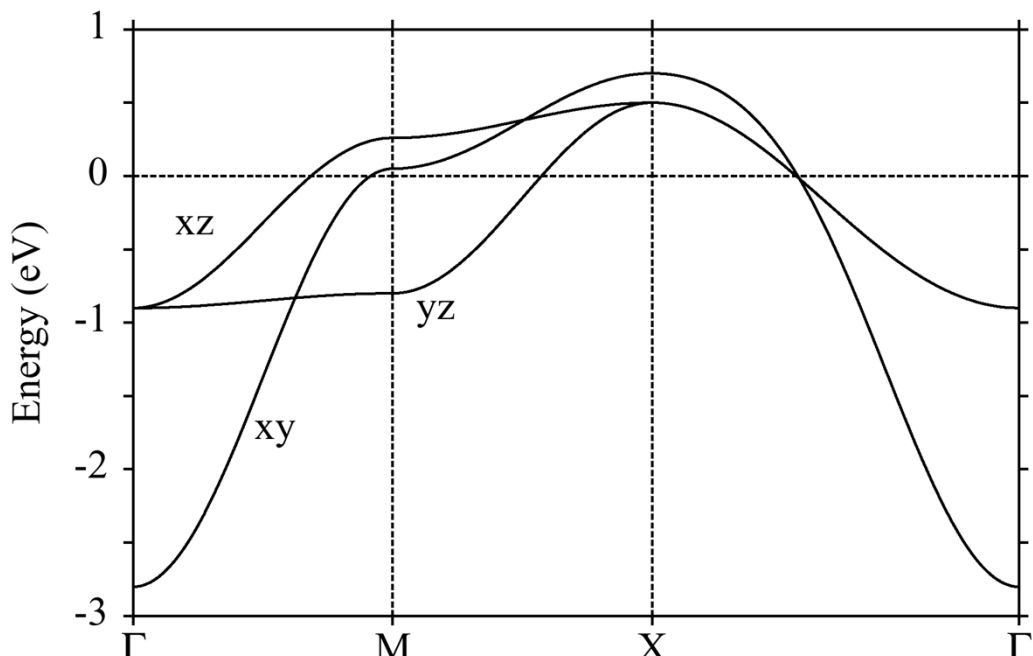


Here electronic correlations are weak: 1 to 1 matching with DFT

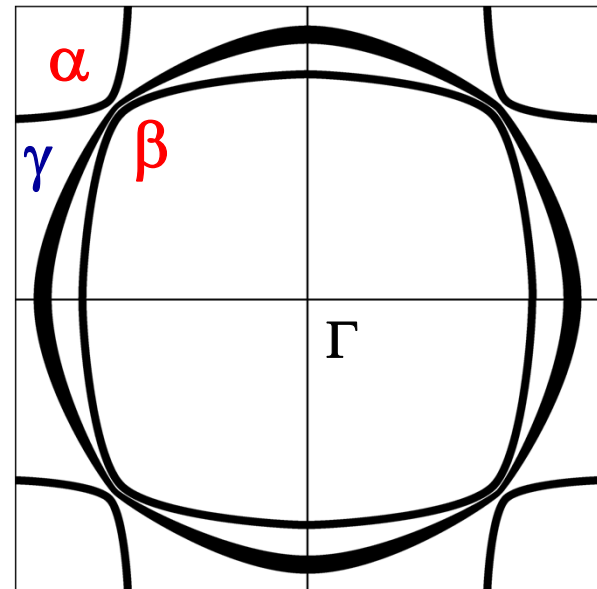
Band Renormalization by Electronic Correlations



► Band structure calculation: 3 t_{2g} bands crossing E_F

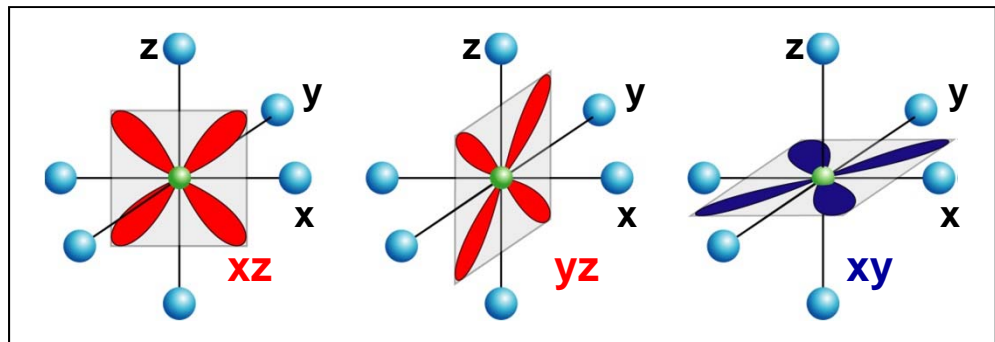
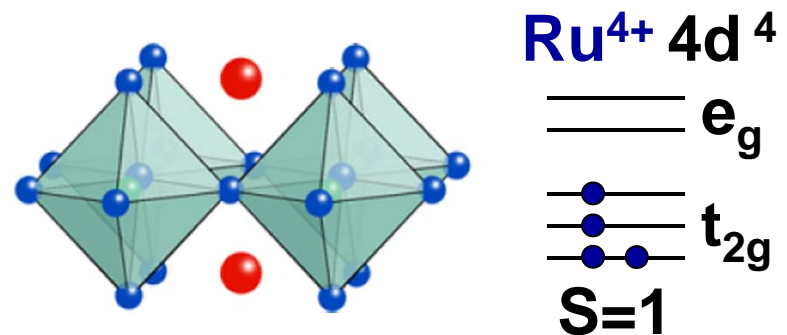


A. Liebsch et al., PRL 84, 1591 (2000)

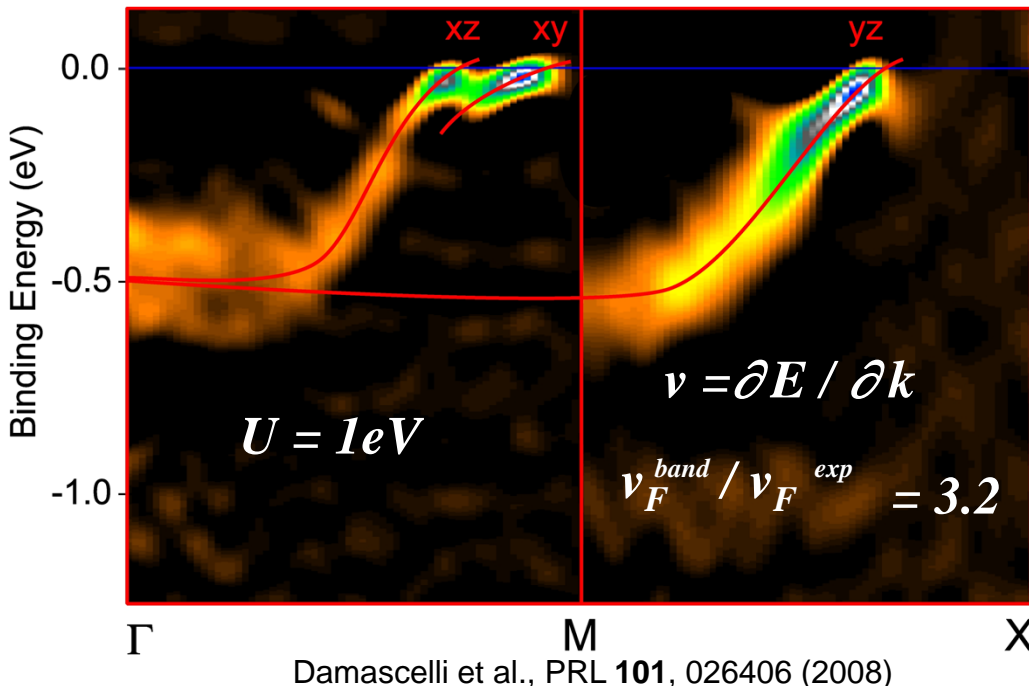
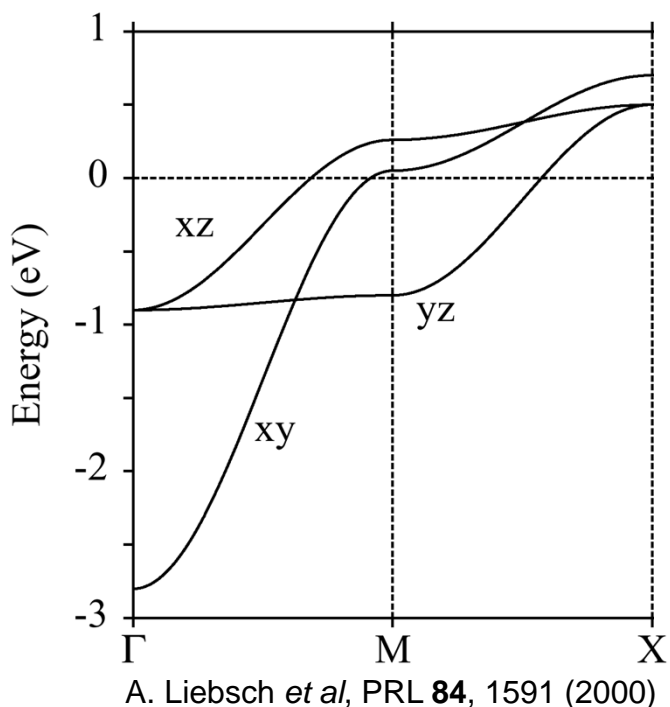


Mazin et al., PRL 79, 733 (1997)

Band Renormalization by Electronic Correlations



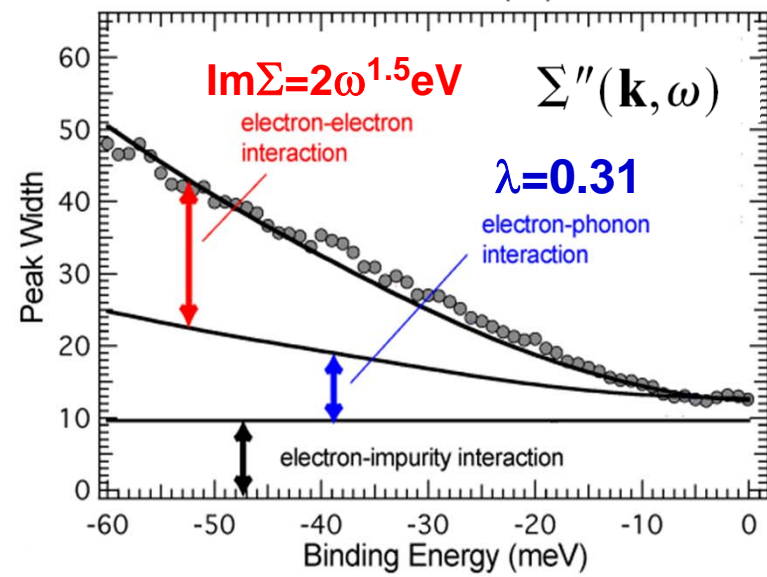
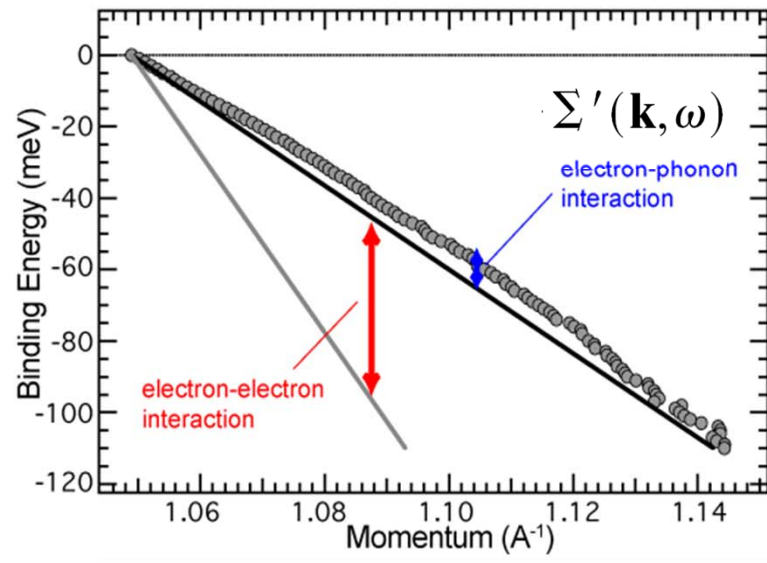
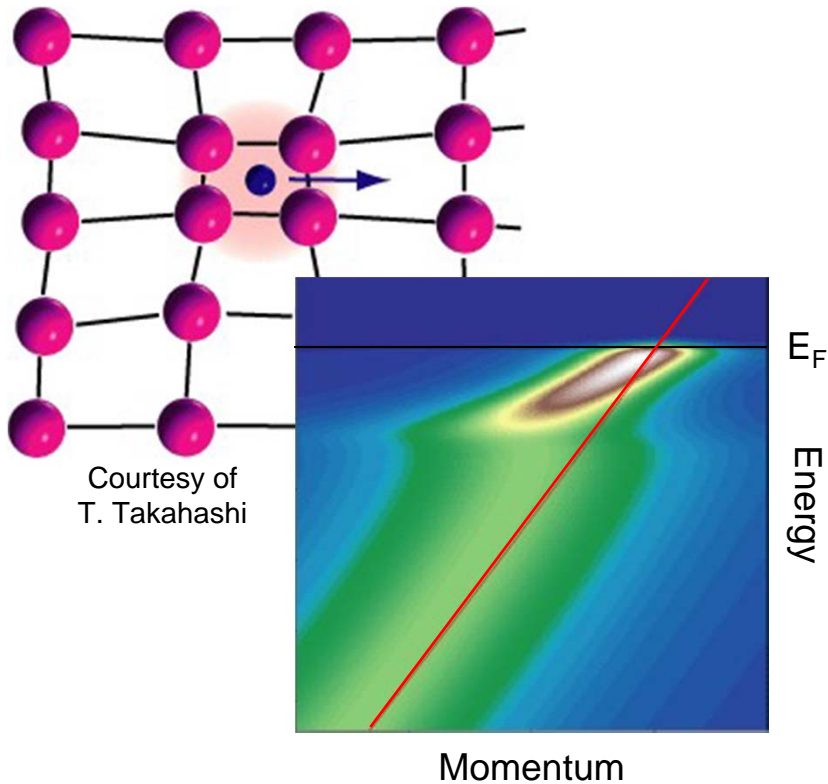
► The first indication of correlations is band narrowing



Many-Body Correlation Effects in Sr_2RuO_4

Single-particle spectral function

$$A(\mathbf{k}, \omega) = -\frac{1}{\pi} \frac{\Sigma''(\mathbf{k}, \omega)}{[\omega - \epsilon_{\mathbf{k}} - \Sigma'(\mathbf{k}, \omega)]^2 + [\Sigma''(\mathbf{k}, \omega)]^2}$$



What is the role of spin-orbit coupling in Ru-oxides?

In Sr_2RuO_4 it has been effectively mostly ignored!

PRL 101, 026406 (2008)

PHYSICAL REVIEW LETTERS

week ending
11 JULY 2008

Strong Spin-Orbit Coupling Effects on the Fermi Surface of Sr_2RuO_4 and Sr_2RhO_4

M. W. Haverkort,¹ I. S. Elfimov,² L. H. Tjeng,¹ G. A. Sawatzky,² and A. Damascelli²

¹*II. Physikalisches Institut, Universität zu Köln, Zülpicher Straße 77, 50937 Köln, Germany*

²*Department of Physics and Astronomy, University of British Columbia, Vancouver, British Columbia, Canada V6T 1Z1*

(Received 29 February 2008; published 11 July 2008)

PRL 101, 026408 (2008)

PHYSICAL REVIEW LETTERS

week ending
11 JULY 2008

Coulomb-Enhanced Spin-Orbit Splitting: The Missing Piece in the Sr_2RhO_4 Puzzle

Guo-Qiang Liu, V. N. Antonov, O. Jepsen, and O. K. Andersen.

Max-Planck Institut für Festkörperforschung, D-70569 Stuttgart, Germany

(Received 2 April 2008; published 11 July 2008)

Eigenstates with Spin-Orbit Coupling

Starting from degenerate t_{2g} orbitals

$$\sqrt{1/2} (-d_{xz} - i d_{yz}) = d_I$$

$$\sqrt{1/2} (d_{xz} - i d_{yz}) = d_{-I}$$

$$d_{xy}$$

3-orbitals with orbital momentum 0, +/- 1
like p -orbitals

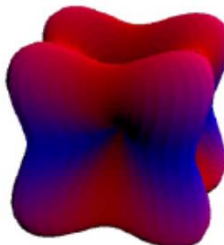
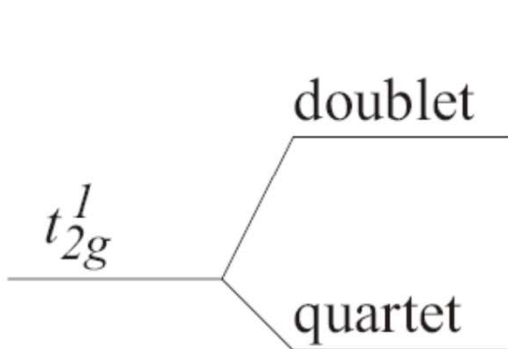
$$H = \zeta \sum_i \mathbf{l}_i \cdot \mathbf{s}_i$$

Atomic relativistic SOC

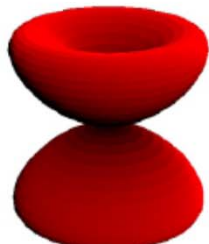
$$\text{Ru}^{4+} \quad \zeta = 161 \text{ meV}$$

$$\text{Rh}^{4+} \quad \zeta = 191 \text{ meV}$$

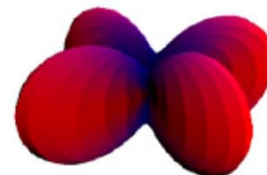
Earnshaw, JCS **601**, 3132 (1961)



$$L_z = +\frac{2}{3}, -\frac{2}{3}$$
$$S_z = +\frac{1}{6}, -\frac{1}{6}$$

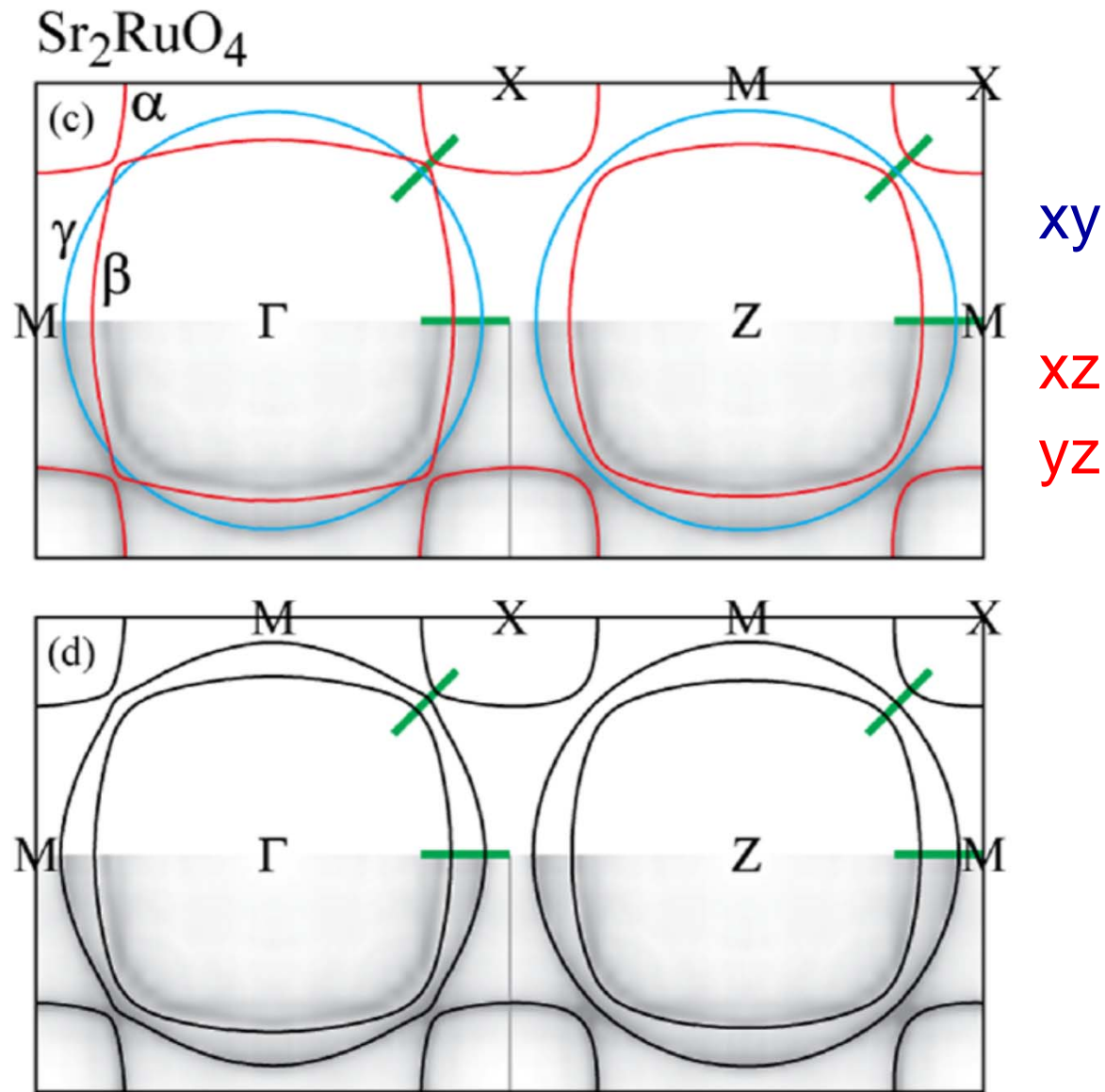
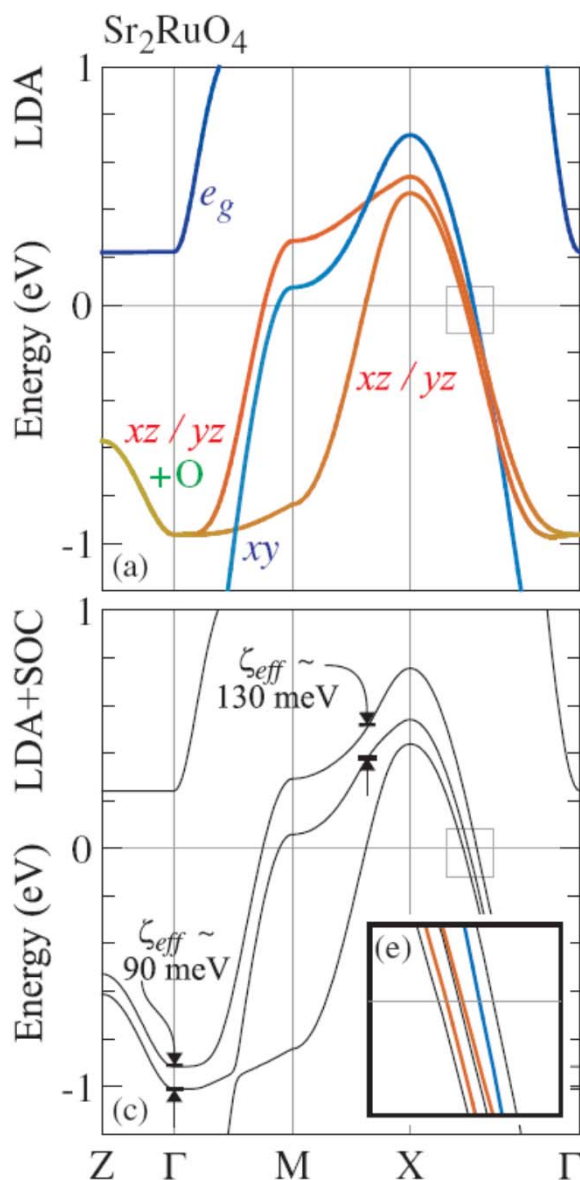


$$L_z = +\frac{1}{2}, -\frac{1}{2}$$
$$S_z = +1, -1$$



$$L_z = +\frac{1}{3}, -\frac{1}{3}$$
$$S_z = +\frac{1}{6}, -\frac{1}{6}$$

Importance of Spin-Orbit Coupling in 4d Oxides





UNIVERSITY OF BRITISH COLUMBIA



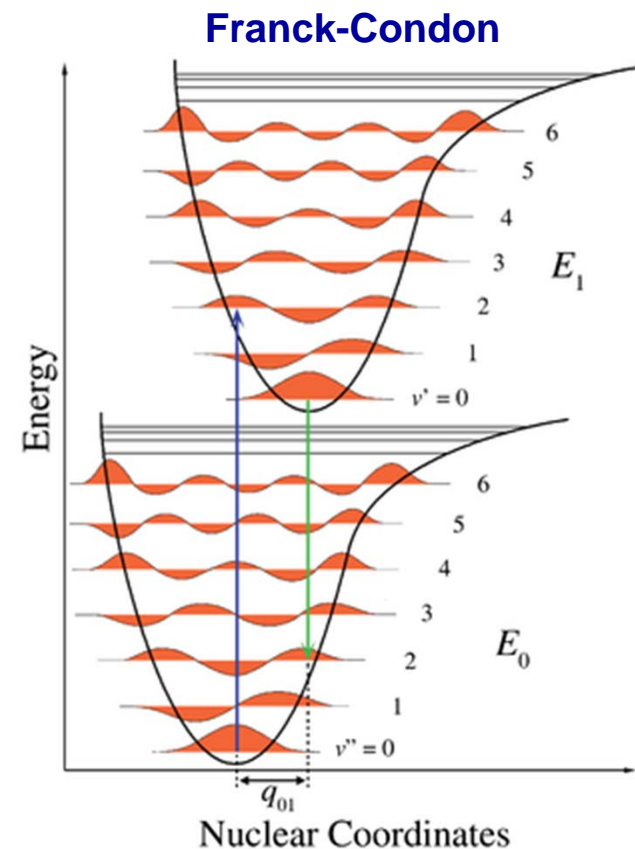
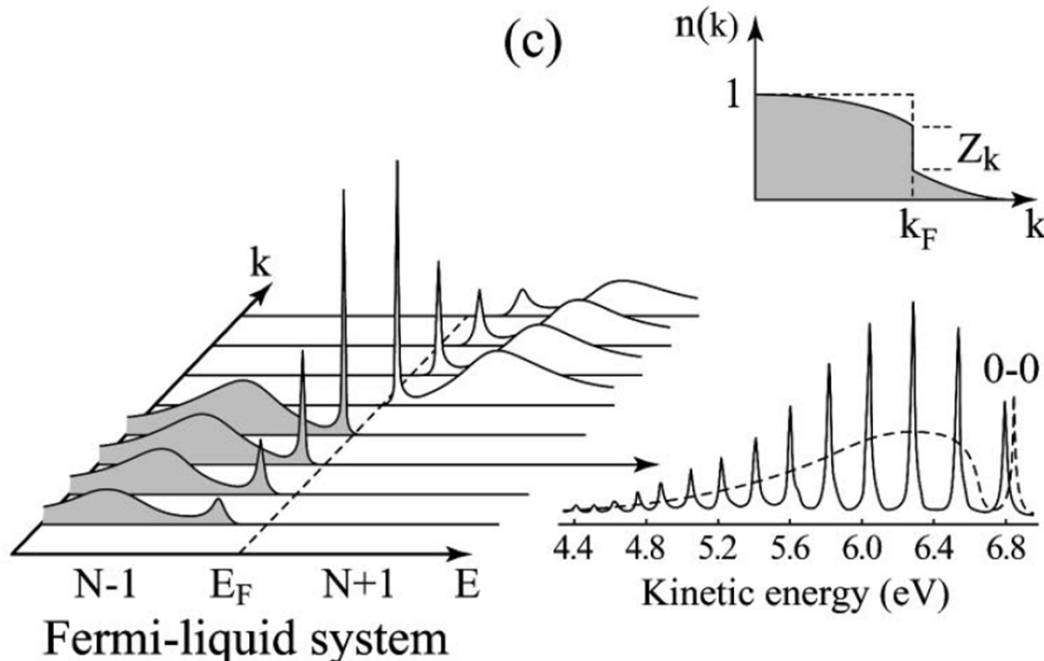
Outline Part II

Polarons and sudden approximation

CUSO Lecture – Lausanne 02/2011

Testing Fermi-liquid models

G.A. Sawatzky



"In gaseous hydrogen, the equilibrium bond length is dependent on the degree of occupation of that level. The electrons are dressed by interatomic displacements. The intensities are given by the Franck-Condon factors, the molecular equivalent of the sudden approximation. The ARPES spectrum of solid hydrogen, developed from the molecular spectrum, will be angle dependent but for some angle will resemble the broken line. The fundamental transition (0-0) becomes the solid state quasiparticle peak. The phonon excitations develop into a broad, incoherent quasicontinuum."

Development of Low-Energy LASER-ARPES

PRL 94, 057001 (2005)

PHYSICAL REVIEW LETTERS

week ending
11 FEBRUARY 2005

Photoemission Spectroscopic Evidence of Gap Anisotropy in an *f*-Electron Superconductor

T. Kiss,^{1,*} F. Kanetaka,¹ T. Yokoya,^{1,†} T. Shimojima,¹ K. Kanai,¹ S. Shin,^{1,2} Y. Onuki,^{3,4} T. Togashi,² C. Zhang,⁵ C. T. Chen,⁵ and S. Watanabe¹

¹Institute for Solid State Physics (ISSP), University of Tokyo, Kashiwa, Chiba 277-8581, Japan

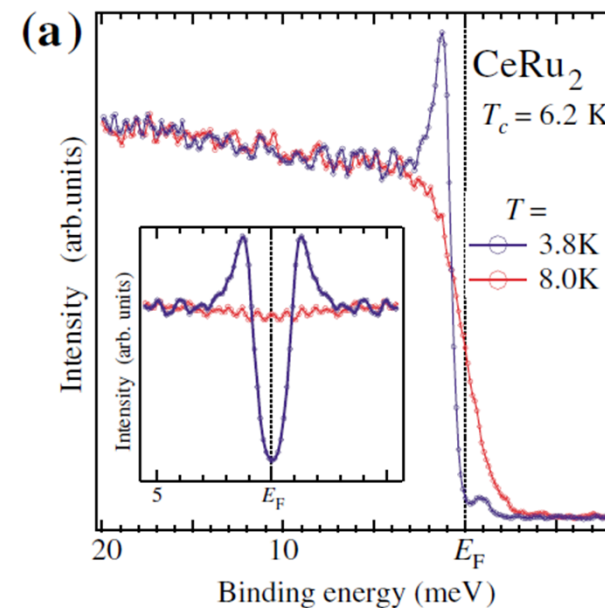
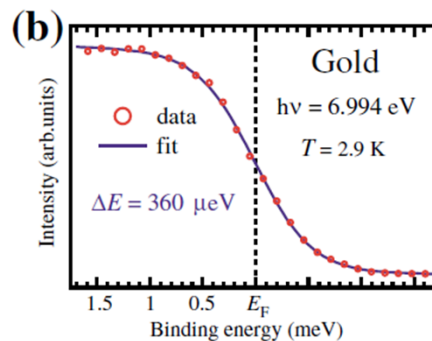
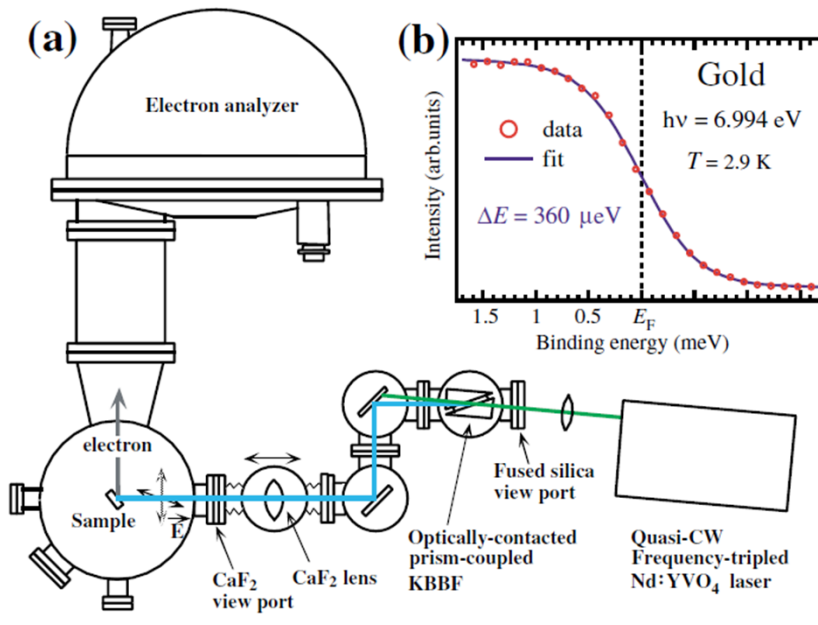
²The Institute of Physical and Chemical Research (RIKEN), Sayo-gun, Hyogo 679-5143, Japan

³Graduate School of Science, Osaka University, Toyonaka, Osaka 560-0043, Japan

⁴Advanced Science Research Center, JAERI, Tokai Ibaraki 319-1195, Japan

⁵Beijing Center for Crystal R&D, Chinese Academy of Science, Zhongguancun, Beijing 100080, China

(Received 5 June 2004; published 7 February 2005)



Development of Low-Energy LASER-ARPES

PRL 94, 057001 (2005)

PHYSICAL REVIEW LETTERS

week ending
11 FEBRUARY 2005

Photoemission Spectroscopic Evidence of Gap Anisotropy in an *f*-Electron Superconductor

T. Kiss,^{1,*} F. Kanetaka,¹ T. Yokoya,^{1,†} T. Shimojima,¹ K. Kanai,¹ S. Shin,^{1,2} Y. Onuki,^{3,4} T. Togashi,² C. Zhang,⁵ C. T. Chen,⁵ and S. Watanabe¹

¹*Institute for Solid State Physics (ISSP), University of Tokyo, Kashiwa, Chiba 277-8581, Japan*

²*The Institute of Physical and Chemical Research (RIKEN), Sayo-gun, Hyogo 679-5143, Japan*

³*Graduate School of Science, Osaka University, Toyonaka, Osaka 560-0043, Japan*

⁴*Advanced Science Research Center, JAERI, Tokai Ibaraki 319-1195, Japan*

⁵*Beijing Center for Crystal R&D, Chinese Academy of Science, Zhongguancun, Beijing 100080, China*

(Received 5 June 2004; published 7 February 2005)

Low energy ARPES is now becoming popular as a new tool for spectroscopy

- Advantages:
- Higher bulk sensitivity: material specific, depending on relaxations
 - Narrow excitation linewidth: higher energy resolution
 - Smaller light spot: higher angular resolution

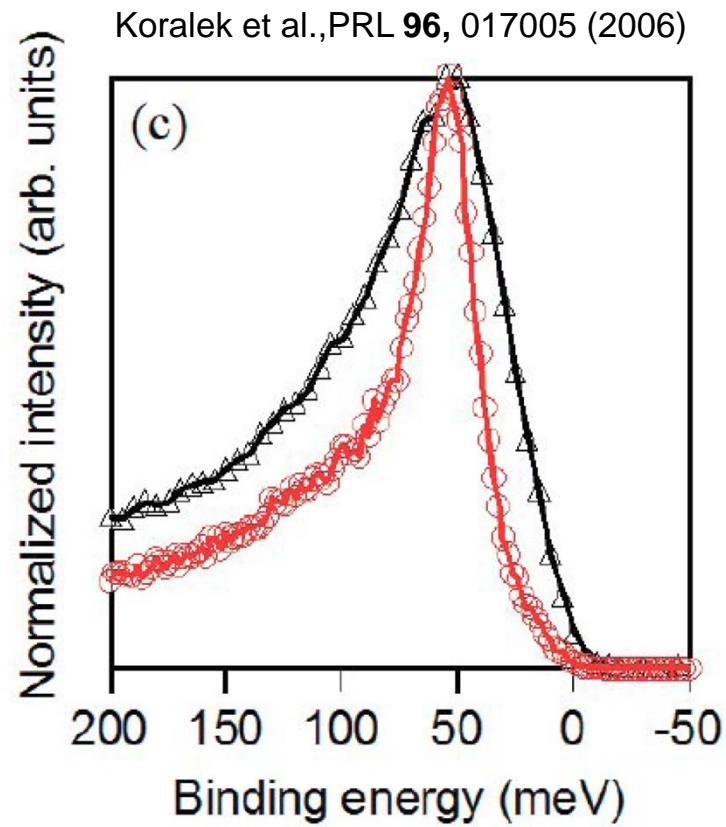
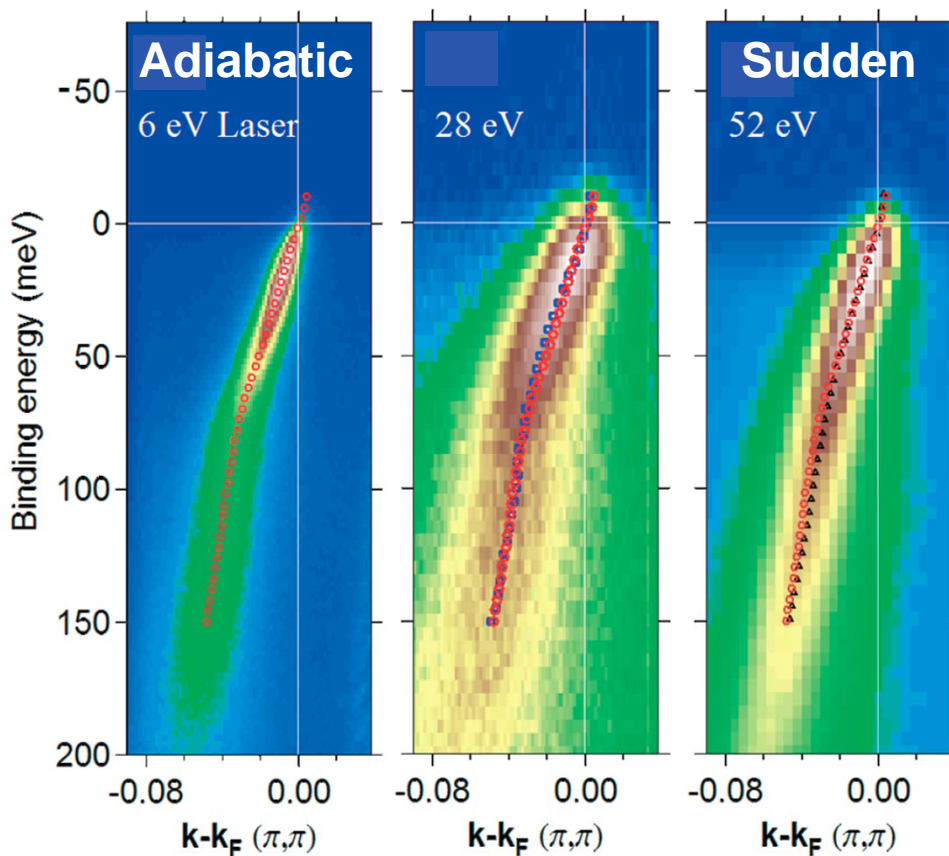
- Drawbacks:
- Breakdown of sudden approximation?
 - Higher sensitivity to final state effects
 - Smaller amount of k-space accessible

Sudden approximation

$$w_{fi} \propto |\langle \phi_f^k | \mathbf{A} \cdot \mathbf{p} | \phi_i^k \rangle \langle \Psi_m^{N-1} | \Psi_i^{N-1} \rangle|^2 \delta(\omega - h\nu)|$$

The N-1 system eigenstates don't change

But the projection of final on initial states does!



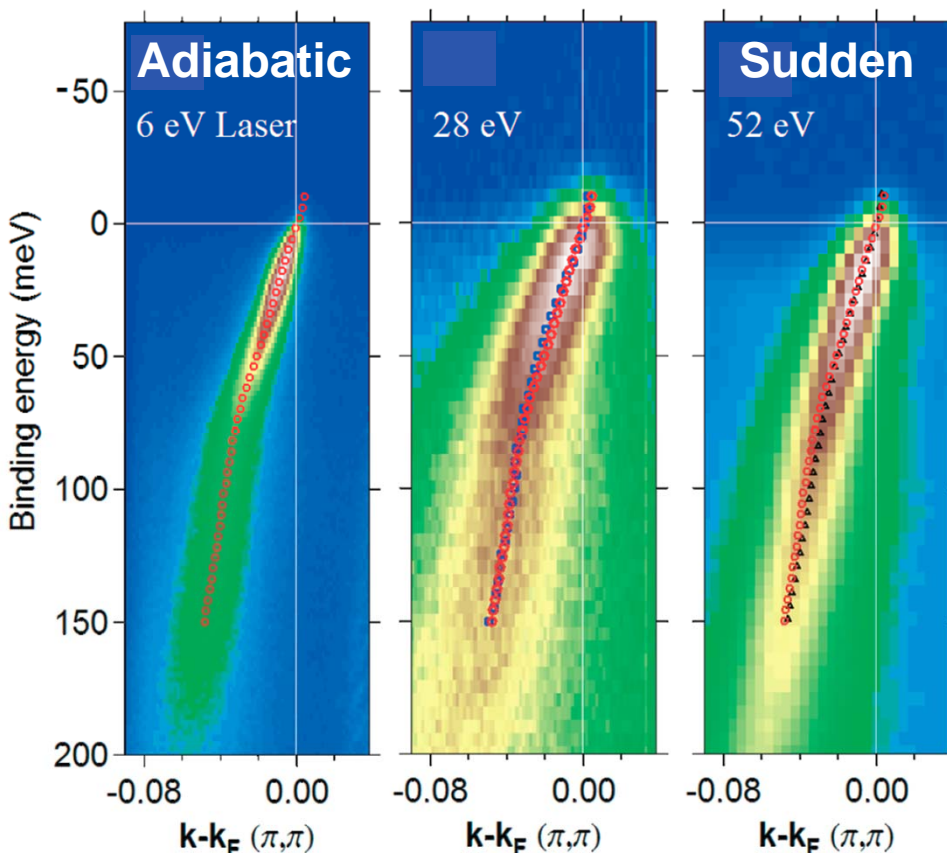
The intensity changes but not the dispersion!

Sudden approximation

$$w_{fi} \propto |\langle \phi_f^k | \mathbf{A} \cdot \mathbf{p} | \phi_i^k \rangle \langle \Psi_m^{N-1} | \Psi_i^{N-1} \rangle|^2 \delta(\omega - h\nu)|$$

The N-1 system eigenstates don't change

But the projection of final on initial states does!



If the sudden approximation breaks down, the electron will be emitted with the highest possible kinetic energy and most of its spectral weight will be in a sharp line since the incoherent continuum is suppressed).

This does NOT prevent detecting features in the experiments due to correlation effects, because the (many-body) eigenstates of the N-1 particle system remain the same.

However, the ratio of intensity between coherent and incoherent parts of the spectral function will change, which WILL prevent a determination of Z from the evolution of the spectral weight detected by ARPES.

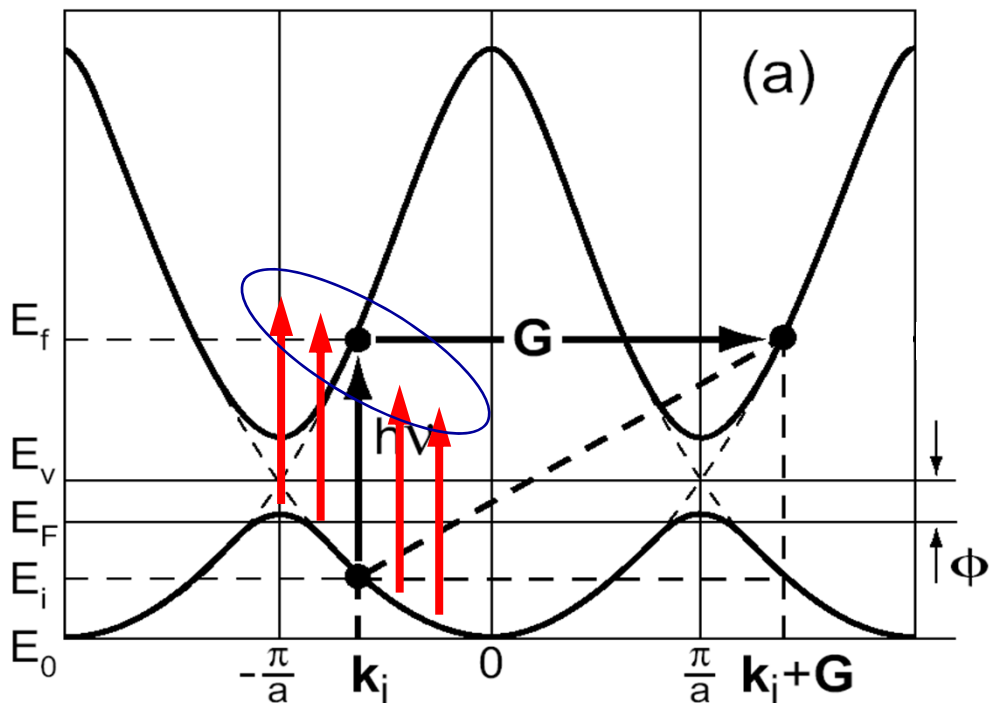
The intensity changes but not the dispersion!

Low-Energy ARPES and Final State Effects

Photoemission Intensity $I(k, \omega)$

$$w_{fi} \propto |\langle \phi_f^k | \mathbf{A} \cdot \mathbf{p} | \phi_i^k \rangle \langle \Psi_m^{N-1} | \Psi_i^{N-1} \rangle|^2 \delta(\omega - h\nu)$$

Excitation in the solid



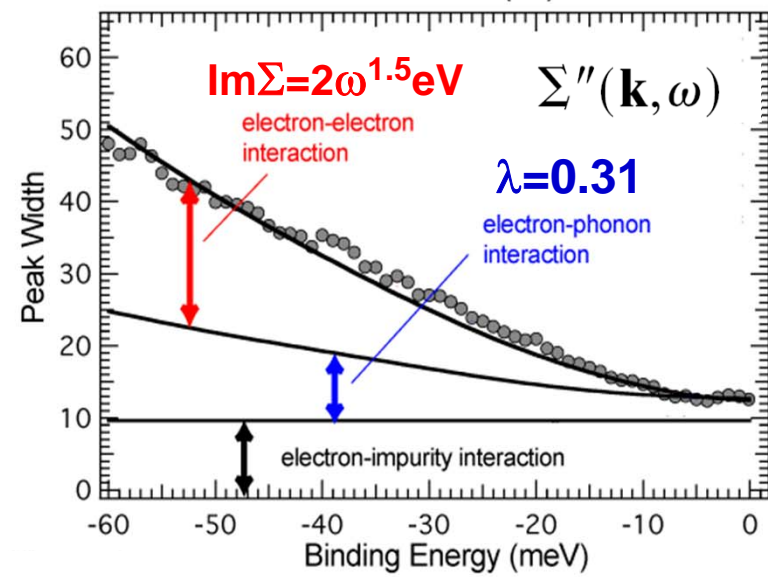
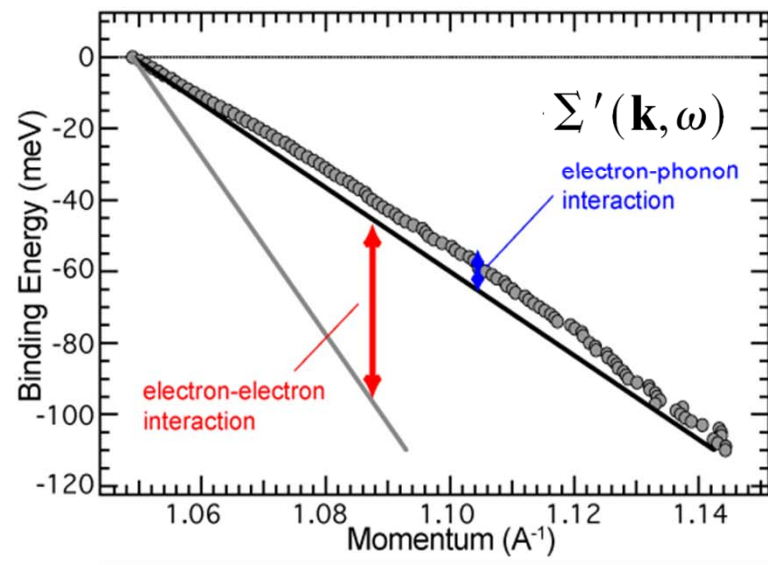
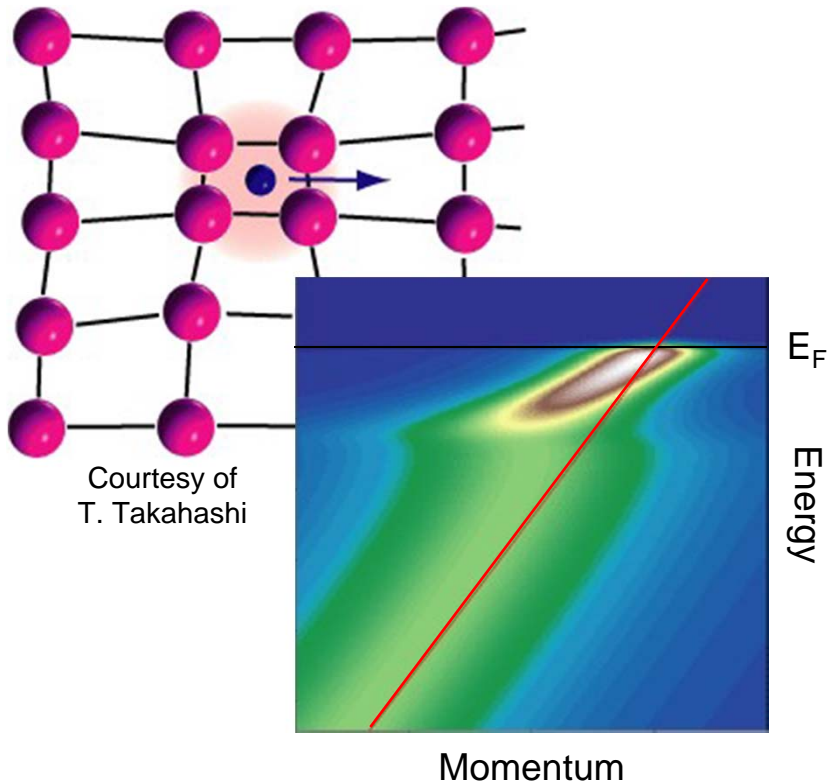
Working at high photon energies the electron is excited in a continuum of high-energy states; a final state is always available and the photoemission process can take place (with intensity still dependent on matrix elements).

At low photon energy photoemission is affected by the kinematic constrain deriving from energy and momentum conservation, and the k -dependent structure of the final states. For some initial state there is no final state that can be reached at a given photon energy and the intensity vanishes.

Many-Body Correlation Effects in Sr_2RuO_4

Single-particle spectral function

$$A(\mathbf{k}, \omega) = -\frac{1}{\pi} \frac{\Sigma''(\mathbf{k}, \omega)}{[\omega - \epsilon_{\mathbf{k}} - \Sigma'(\mathbf{k}, \omega)]^2 + [\Sigma''(\mathbf{k}, \omega)]^2}$$



Many-Body effects in the High- T_c Cuprates

Devereaux et al., Phys. Rev. Lett. **93**, 117004 (2004)

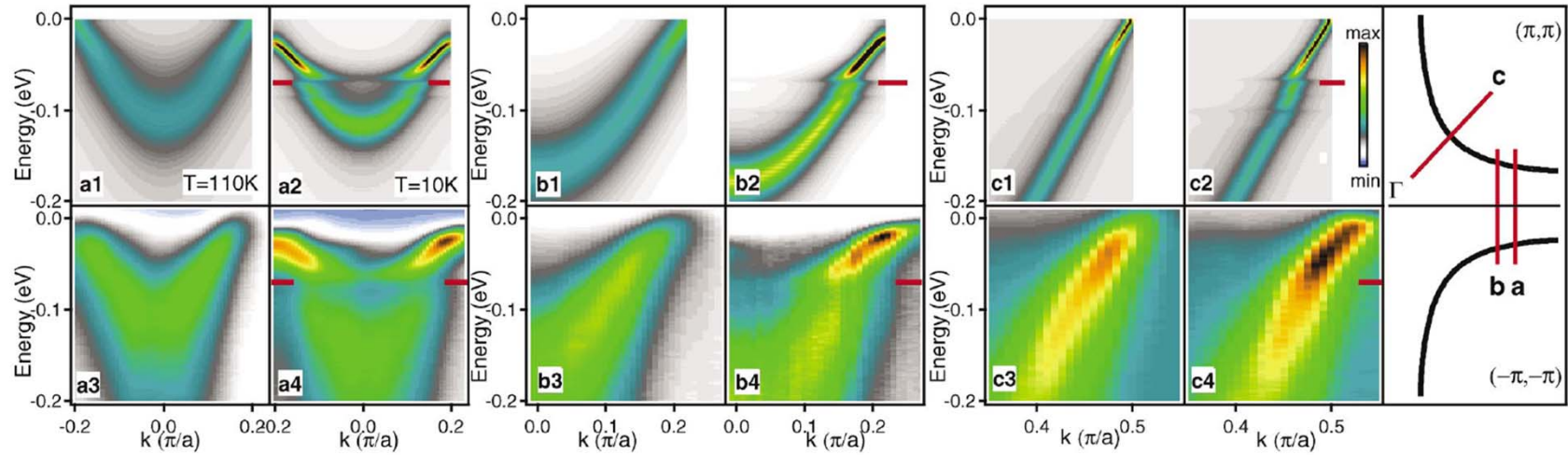
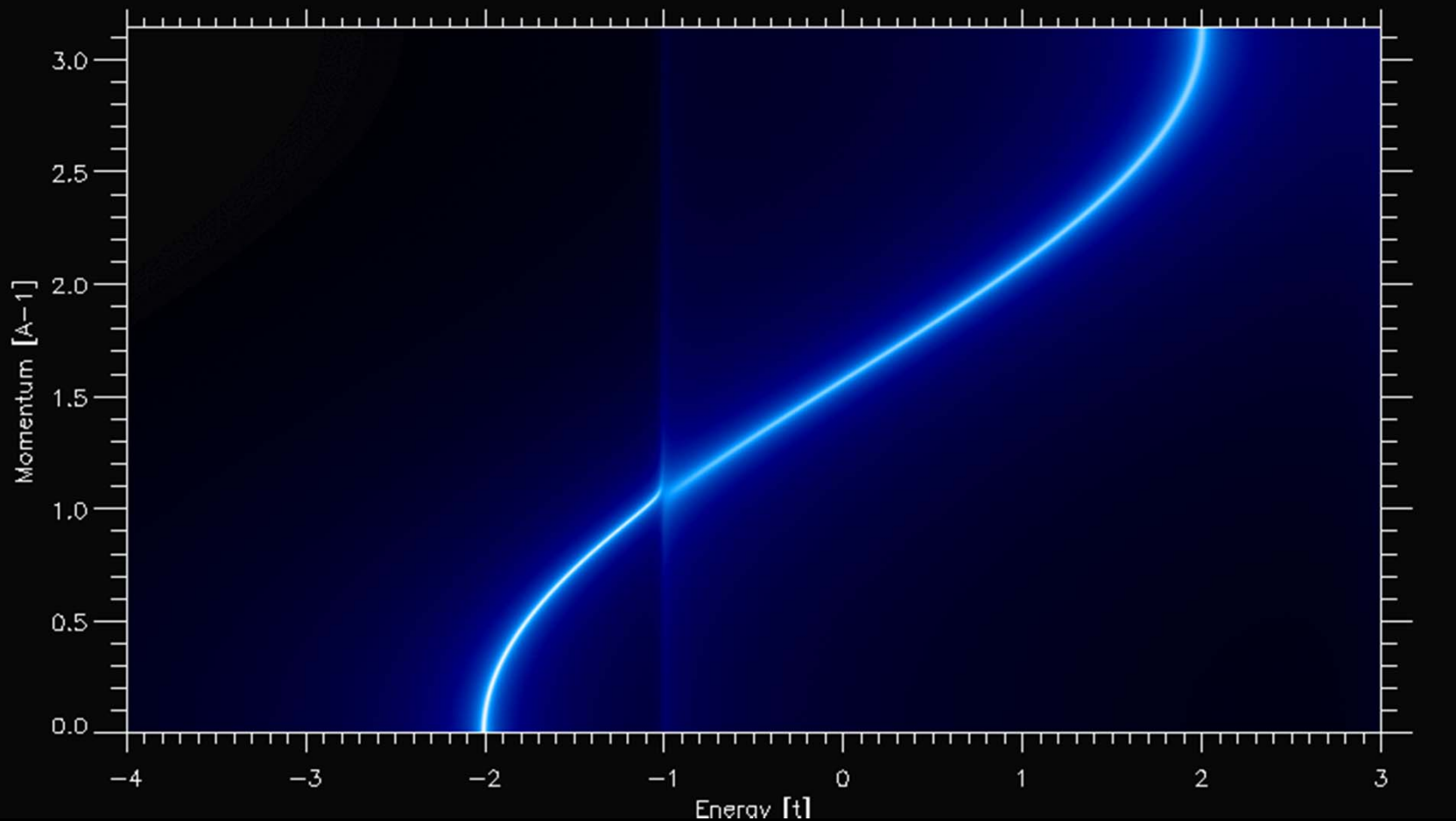


FIG. 3 (color). Image plots of the calculated spectral functions in the normal (a1,b1,c1) and superconducting (a2,b2,c2) states compared to the spectral functions in the normal (a3,b3,c3) and superconducting (a4,b4,c4) states measured in $\text{Bi}_2\text{Sr}_2\text{Ca}_{0.92}\text{Y}_{0.08}\text{Cu}_2\text{O}_{8+\delta}$ (Bi-2212) [6] for momentum cuts a, b, c shown in the rightmost panel and in Fig. 2. The same color scale is used for the normal or superconducting pairs within each cut, but the scaling for the data and the calculation are separate. The red markers indicate 70 meV in the superconducting state.

Mechanism for High- T_c { Magnetic fluctuations ?
Electron-phonon coupling ?

$$\mathcal{H} = \sum_k \varepsilon_k^b c_k^\dagger c_k + \Omega \sum_Q b_Q^\dagger b_Q + \frac{g}{\sqrt{N}} \sum_{k,Q} c_{k-Q}^\dagger c_k (b_Q^\dagger + b_{-Q})$$



Veenstra, Goodvin, Berciu, Damascelli, PRB **82**, 012504 (2010)

Renormalization of Polaronic Quasiparticles

$$\mathcal{H} = \sum_k \varepsilon_k^b c_k^\dagger c_k + \Omega \sum_Q b_Q^\dagger b_Q + \frac{g}{\sqrt{N}} \sum_{k,Q} c_{k-Q}^\dagger c_k (b_Q^\dagger + b_{-Q})$$

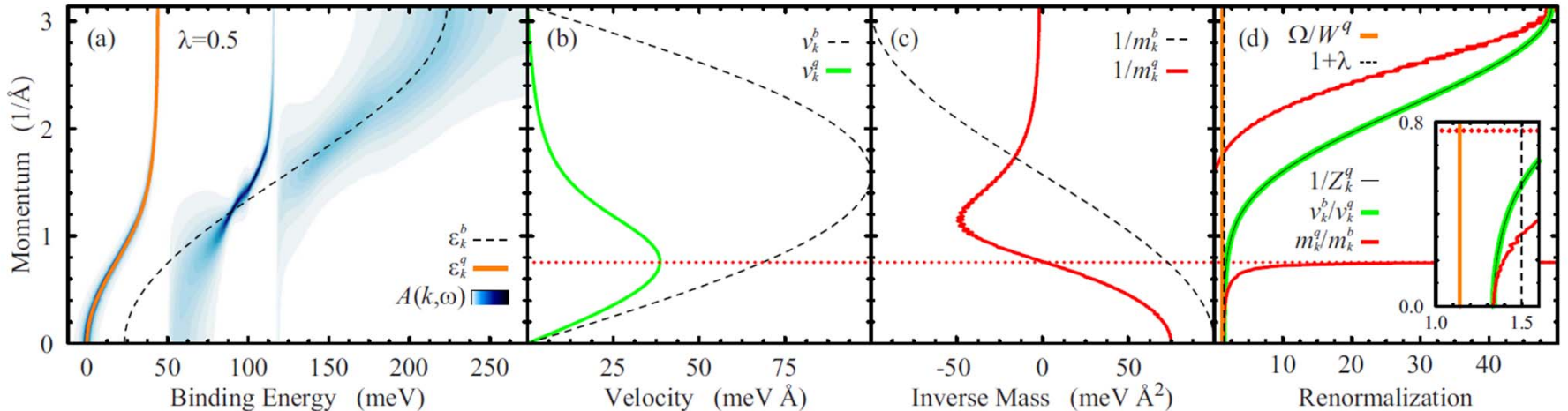
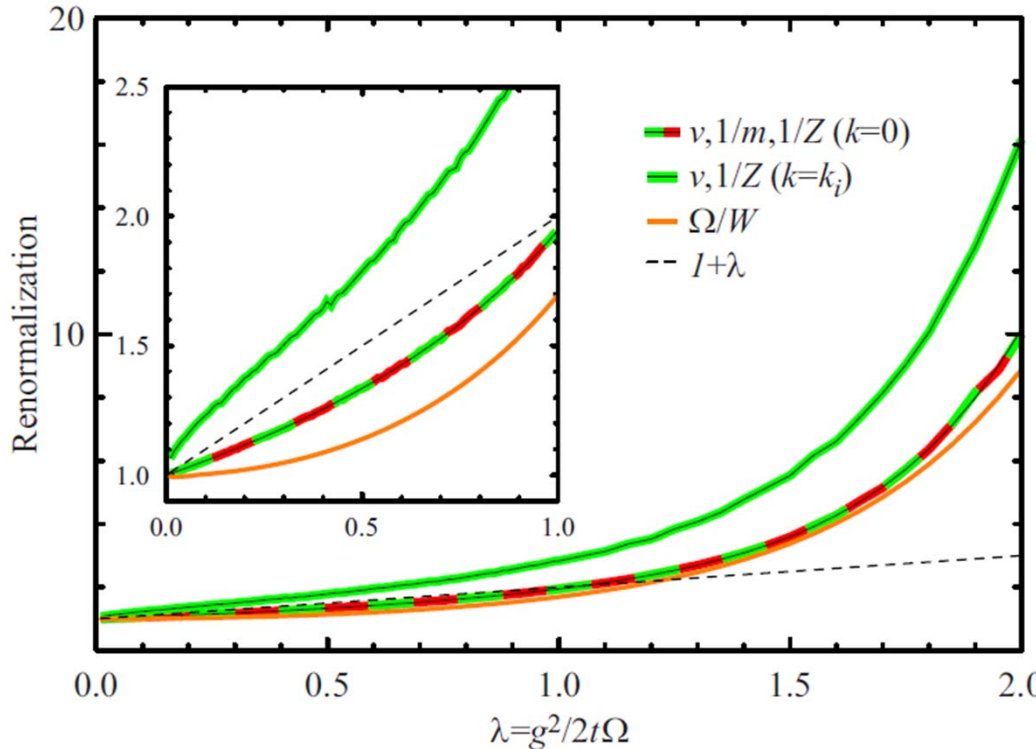


FIG. 1. (Color online) (a) $A(k, \omega)$ calculated within MA⁽¹⁾ for $\Omega=50$ meV and $\lambda=0.5$; the quasiparticle dispersion ε_k^q and the bare band ε_k^b are also shown. (b) Quasiparticle and bare-band velocities, v_k^q and v_k^b , and (c) corresponding inverse masses, $1/m_k^q$ and $1/m_k^b$, according to the definitions $v_k = \partial \varepsilon_k / \partial k$ and $1/m_k = \partial^2 \varepsilon_k / \partial k^2$. (d) Momentum-dependent quasiparticle renormalization as obtained from v_k^b/v_k^q , m_k^q/m_k^b , and the inverse quasiparticle coherence $1/Z_k^q$, where $Z_k^q = \int q A(k, \omega) d\omega$ is the quasiparticle-only integrated spectral weight; in the inset, these quantities are compared near $k=0$ to the renormalization factors Ω/W^q and $(1+\lambda)$, obtained from quasiparticle bandwidth W^q and dimensionless coupling $\lambda=g^2/2t\Omega$ in our model.

Far from the Migdal limit ($\Omega \ll E_F$ for a parabolic band), the effective coupling parameters deduced from the renormalization of quasiparticle mass, velocity, and spectral weight are momentum dependent and, in general, distinct from the true microscopic coupling; the latter is thus not readily accessible in the quasiparticle dispersion revealed by ARPES through the mass enhancement factor $1/(1+\lambda)$.

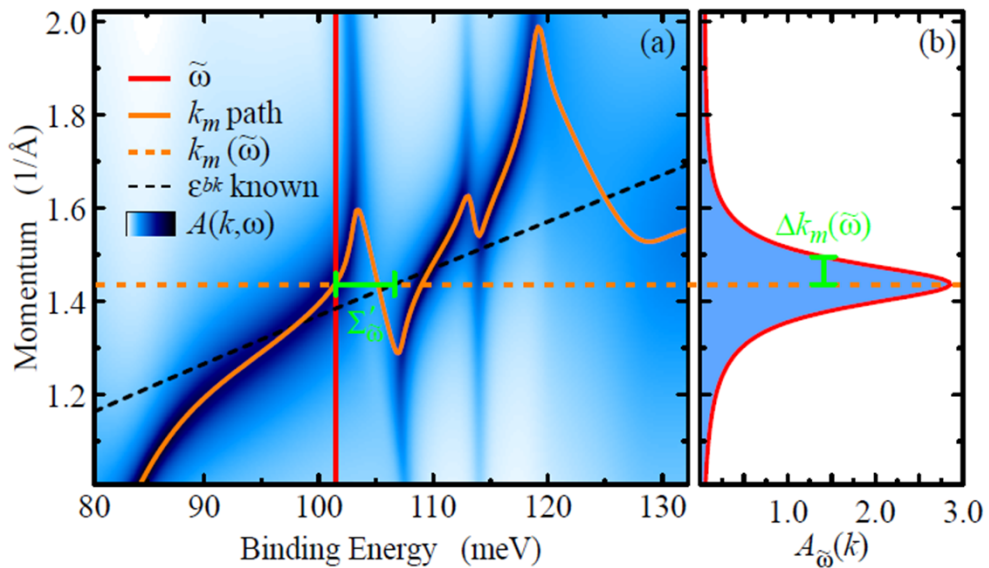
Renormalization of Polaronic Quasiparticles

$$\mathcal{H} = \sum_k \varepsilon_k^b c_k^\dagger c_k + \Omega \sum_Q b_Q^\dagger b_Q + \frac{g}{\sqrt{N}} \sum_{k,Q} c_{k-Q}^\dagger c_k (b_Q^\dagger + b_{-Q})$$

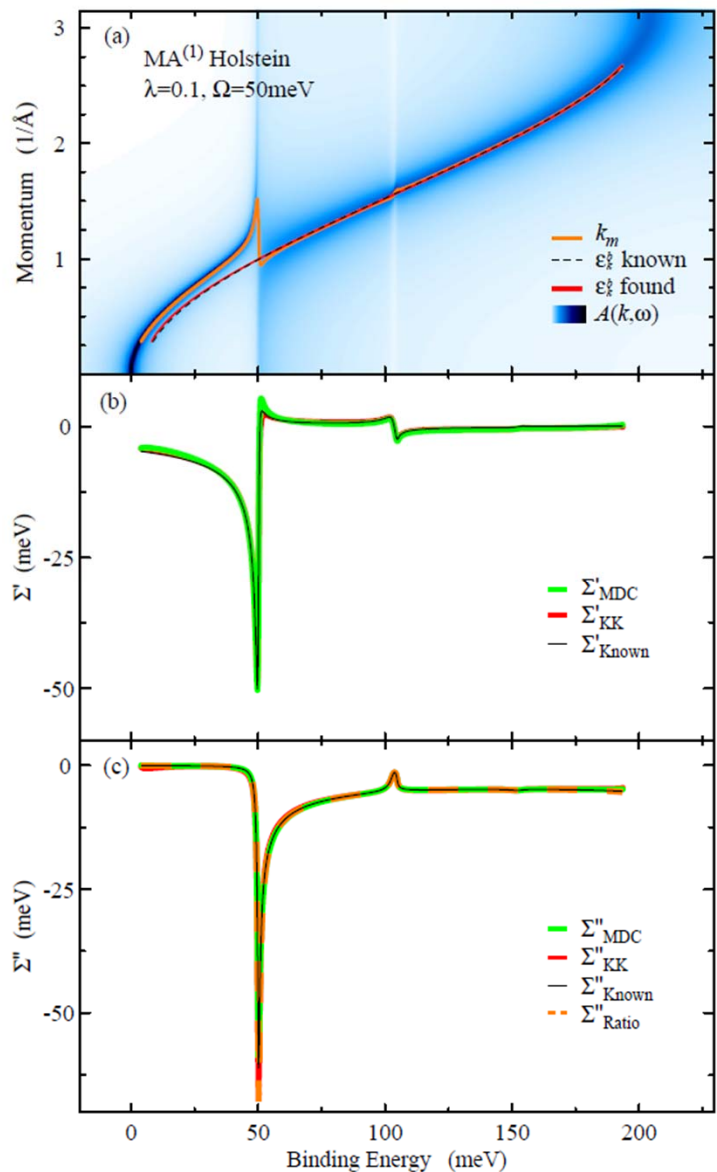


Based on the renormalization parameters and the mass enhancement factor $1/(1+\lambda)$, one can overestimate the true electron phonon microscopic coupling even by a factor of 10.

Renormalization of Polaronic Quasiparticles



Instead of extracting directly λ , one can estimate real and imaginary part of the self energy through bare -band fitting and Kramers-Kronig analysis.





UNIVERSITY OF BRITISH COLUMBIA

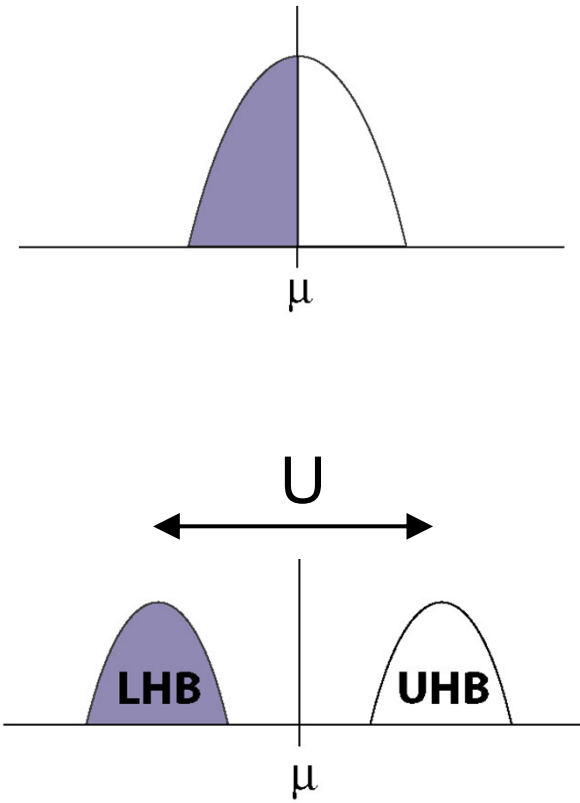


Outline Part II

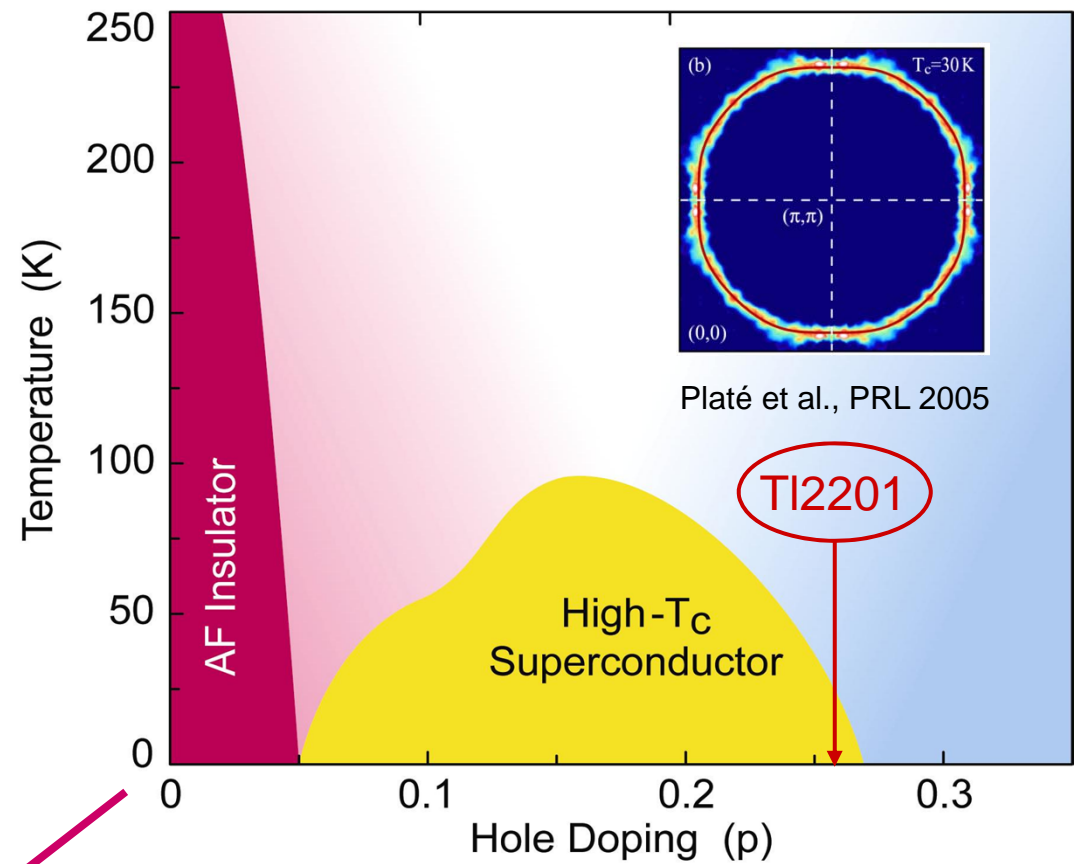
HTSC: The fate of quasiparticle strength

CUSO Lecture – Lausanne 02/2011

From Fermi Liquid to Mott Insulator



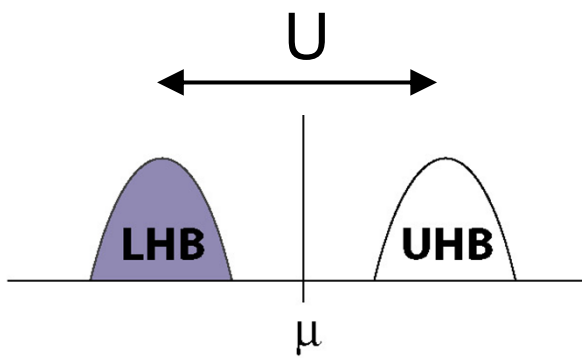
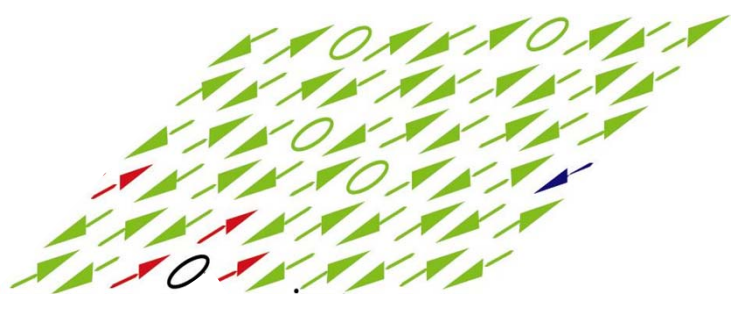
Mott insulator



Normal state properties

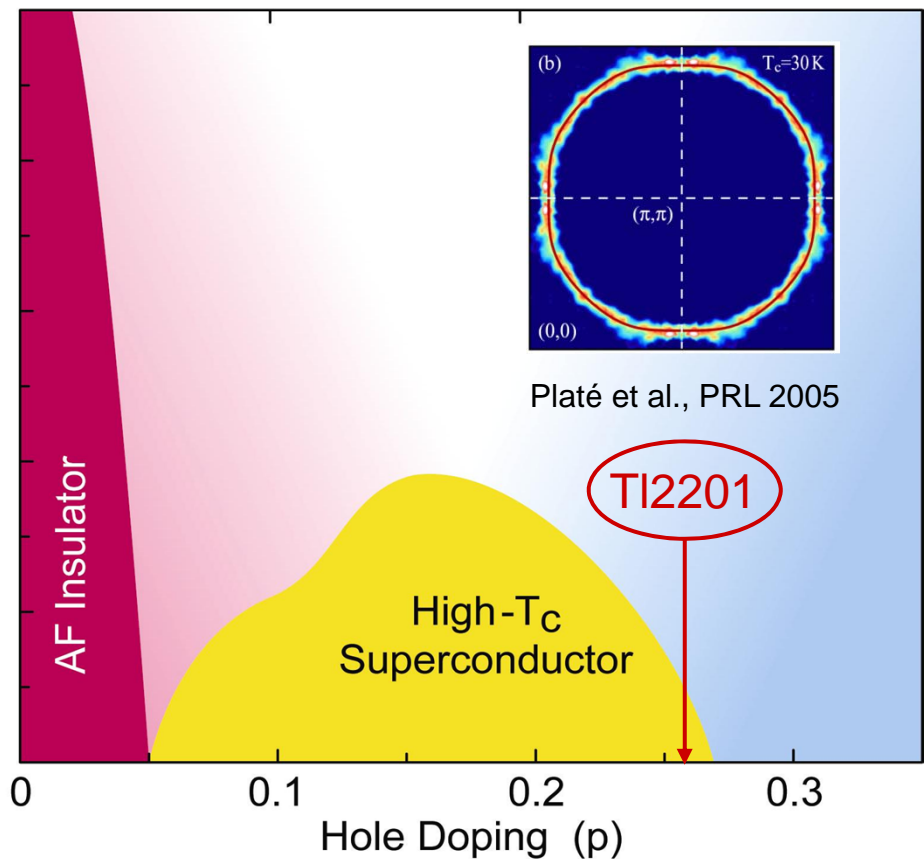
From Fermi Liquid to Mott Insulator

Correlations suppress Z_k



$$Z \simeq 2p/(p+1)$$

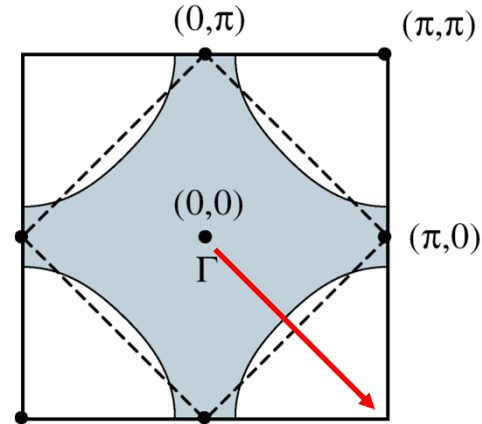
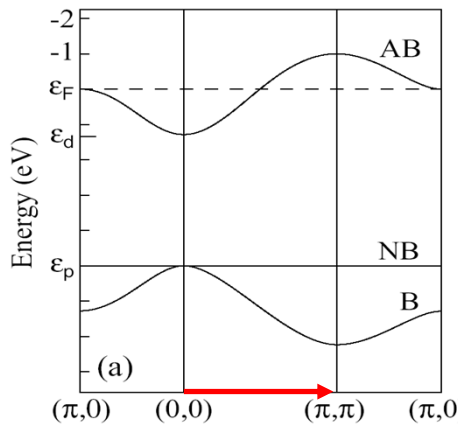
Sawatzky, Anderson, Randeria,
Paramekanti, Yang, Rice, et al.



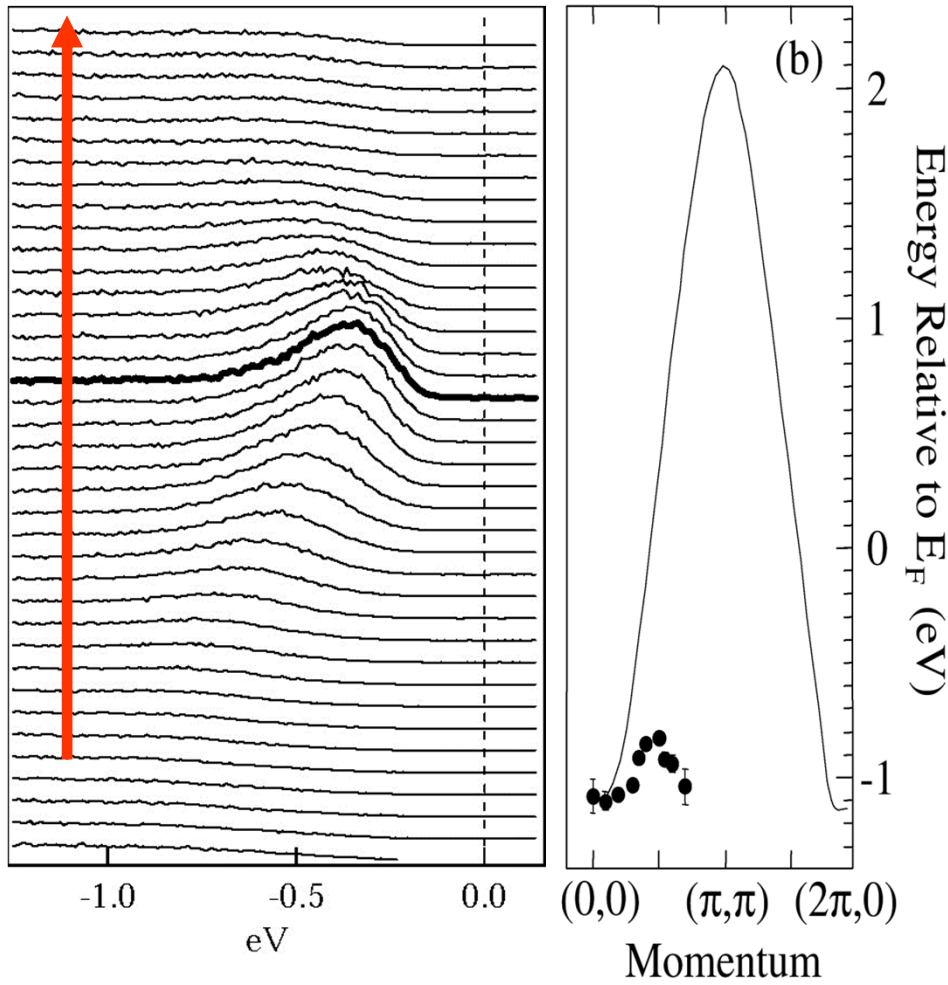
Normal state properties

HTSCs: Charge Transfer Insulators

$\frac{1}{2}$ Filled Metal

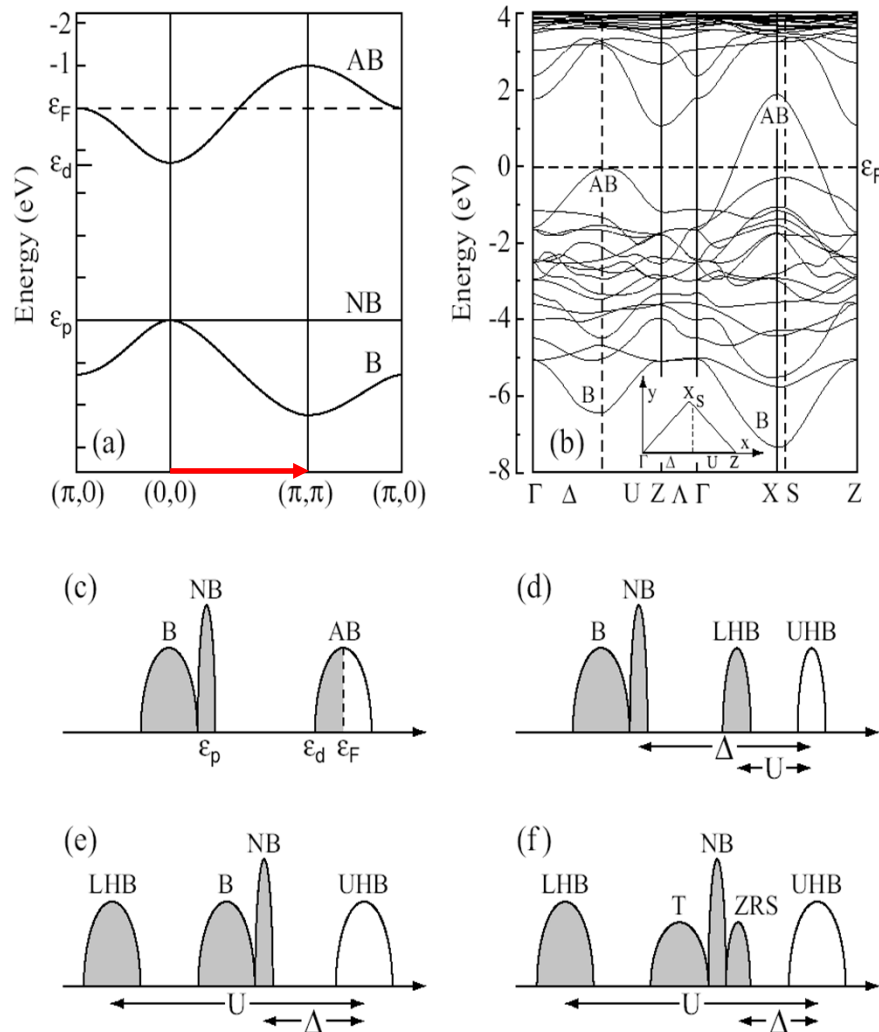
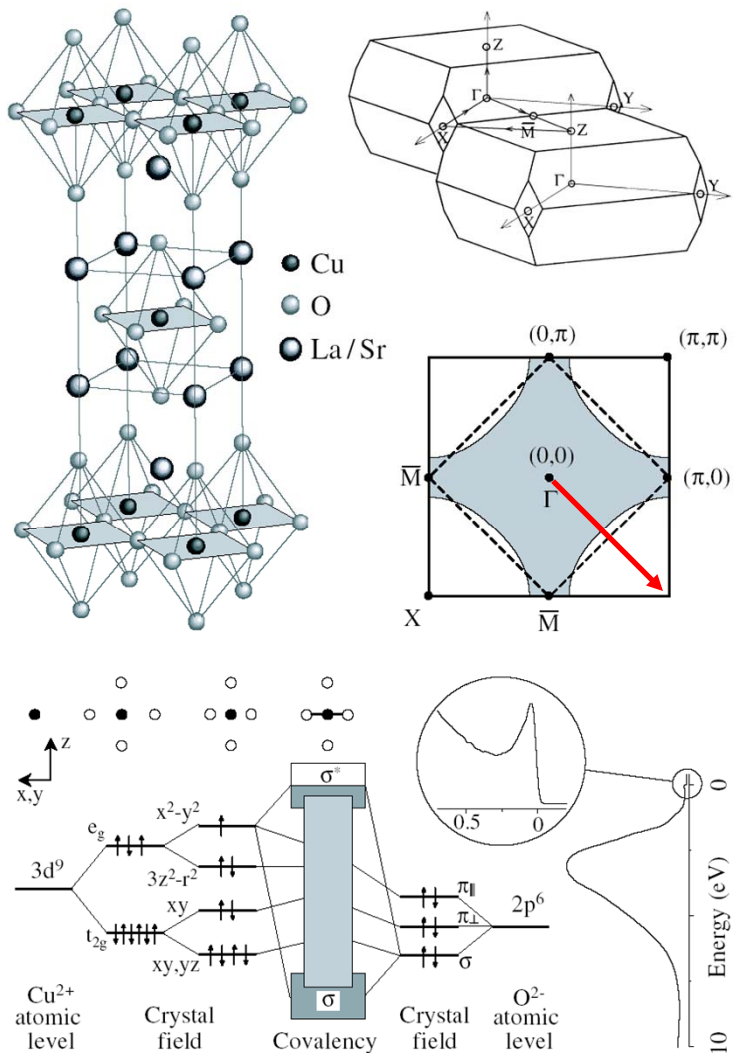


ARPES Spectra of Insulating
 $\text{Ca}_2\text{CuO}_2\text{Cl}_2$ along $(0,0) - (\pi, \pi)$

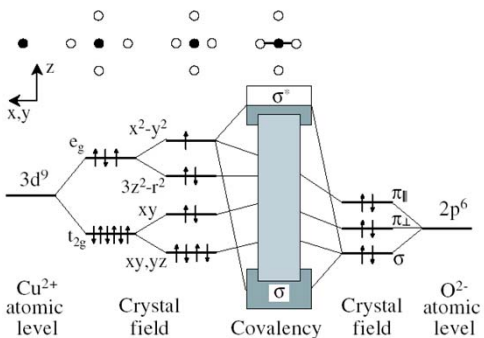


The dispersion instead of being the 2D tight-binding $8t$ ($t \sim 350\text{meV}$) is $2.2J$ ($J \sim 125\text{meV}$)

HTSCs: Charge Transfer Insulators



High-T_c Superconductors: A Minimal Model



Density functional theory
5d Cu orbitals and 3 O orbitals
8-band model

1987 Anderson: the essential physics of the cuprates is captured by the 1-band Hubbard model

$$H = -t \sum_{\langle ij \rangle, \sigma} (c_{i\sigma}^\dagger c_{j\sigma} + \text{H.c.}) + U \sum_i n_{i\uparrow} n_{i\downarrow}$$

3-band model

Cu 3d_{x²-y²} O 2p_x and 2p_y

1987 Emery: since the HTSCs are charge transfer insulators, both O and Cu have to be accounted for

1988 Zhang & Rice: projecting out double occupancy, Cu-O hybridization leads to an effective 1-band model

$$H = -t \sum_{\langle ij \rangle, \sigma} (\tilde{c}_{i\sigma}^\dagger \tilde{c}_{j\sigma} + \text{H.c.}) + J \sum_{\langle ij \rangle} \left(\mathbf{S}_i \cdot \mathbf{S}_j - \frac{n_i n_j}{4} \right)$$

Doping a Mott Insulator: Spectral Weight Transfer

PHYSICAL REVIEW B

VOLUME 48, NUMBER 6

1 AUGUST 1993-II

Spectral-weight transfer: Breakdown of low-energy-scale sum rules in correlated systems

M. B. J. Meinders

Materials Science Centre, Department of Solid State and Applied Physics, University of Groningen, Nijenborgh 4, 9747 AG Groningen, The Netherlands

H. Eskes

Max-Planck-Institut für Festkörperforschung, Heisenbergstrasse 1, D-7000 Stuttgart 80, Federal Republic of Germany

G. A. Sawatzky

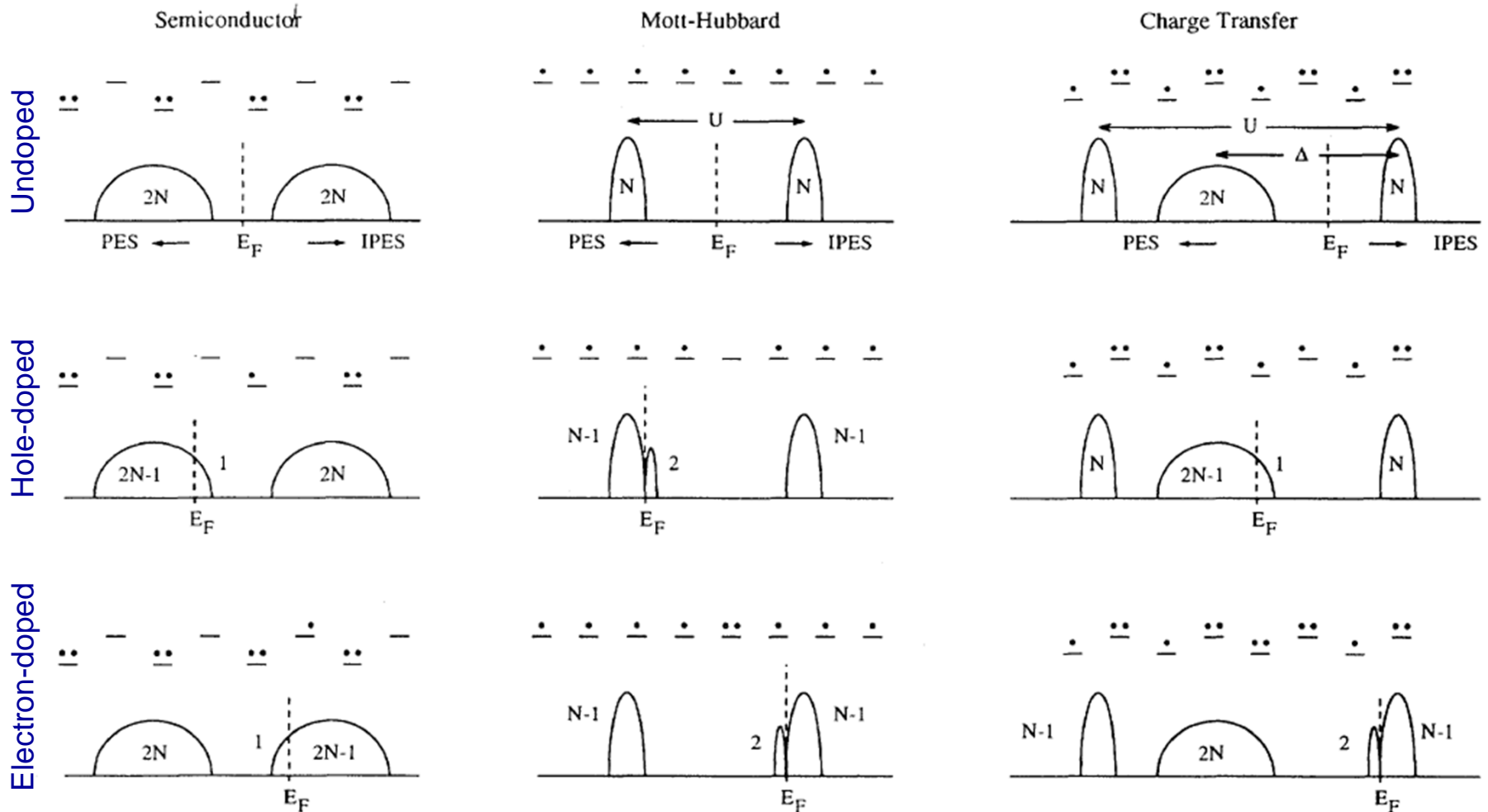
Materials Science Centre, Department of Solid State and Applied Physics, University of Groningen, Nijenborgh 4, 9747 AG Groningen, The Netherlands

(Received 4 March 1993)

In this paper we study the spectral-weight transfer from the high- to the low-energy scale by means of exact diagonalization of finite clusters for the Mott-Hubbard and charge-transfer model. We find that the spectral-weight transfer is very sensitive to the hybridization strength as well as to the amount of doping. This implies that the effective number of low-energy degrees of freedom is a function of the hybridization and therefore of the volume and temperature. In this sense it is not possible to define a Hamiltonian which describes the low-energy-scale physics unless one accepts an effective nonparticle conservation.

It is the connection between low and high energy scales that distinguishes the Mott gap from a more conventional gap (i.e., semiconductor, CDW, etc.)

Doping a Mott Insulator: Spectral Weight Transfer



It is the connection between low and high energy scales that distinguishes the Mott gap from a more conventional gap (i.e., semiconductor, CDW, etc.)

Doping a Mott Insulator: Spectral Weight Transfer

Meinders, Eskes, Sawatzky , PRB 48, 3916 (1993)

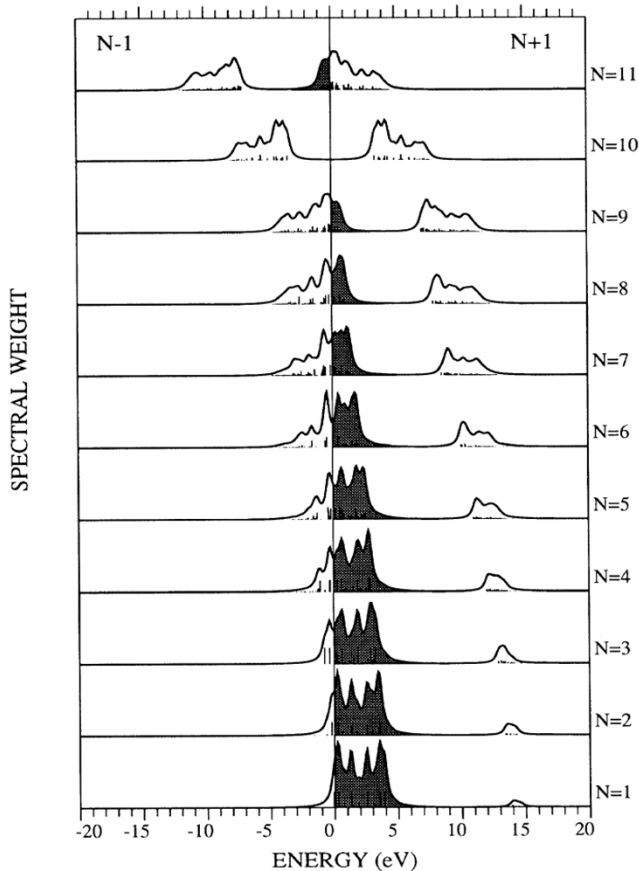


FIG. 2. One-particle Green's function for a one-dimensional Hubbard-ring of $N = 10$ sites for $U = 10$ eV and $t = 1$ eV. The number of electrons in the ground state N are indicated. The low-energy electron-addition spectral weight is obtained by integration over the shaded area.

C.T. Chen et al., PRL 66, 104 (1991)

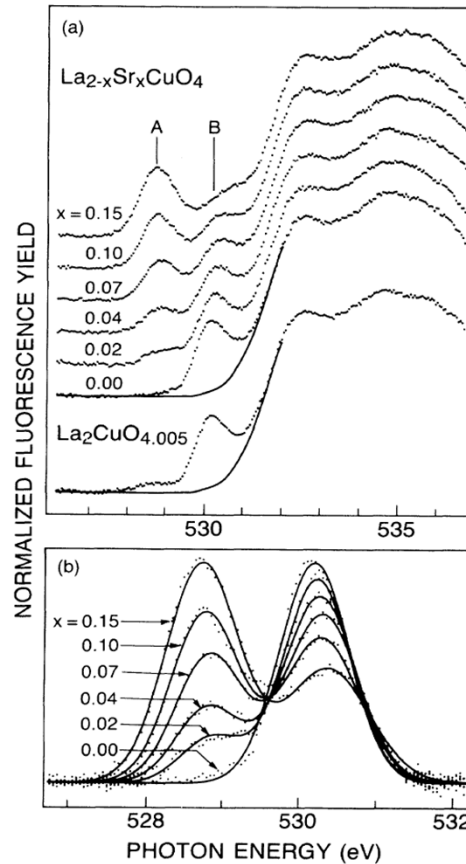
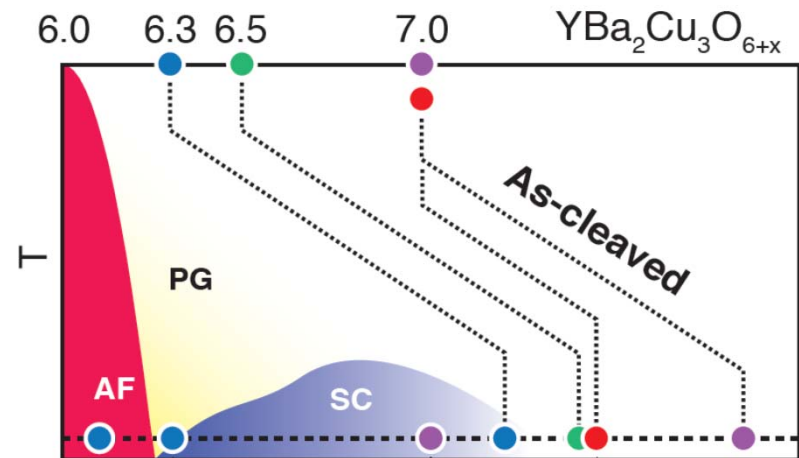
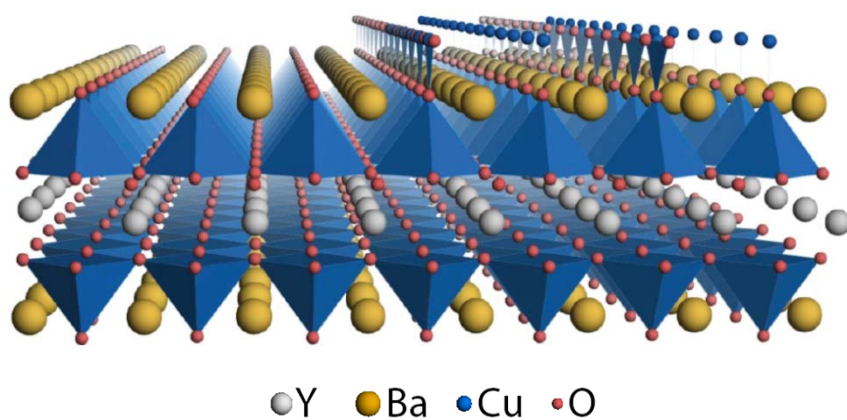


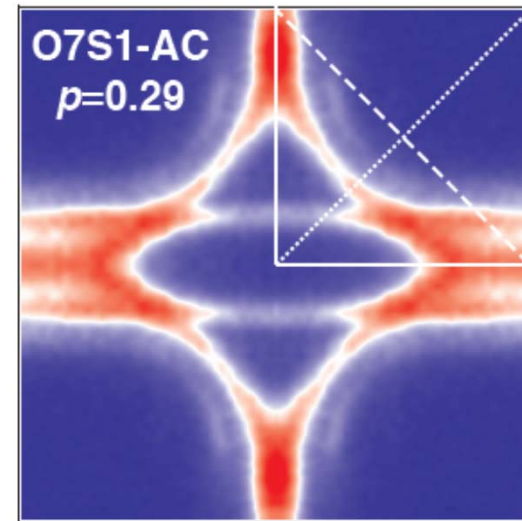
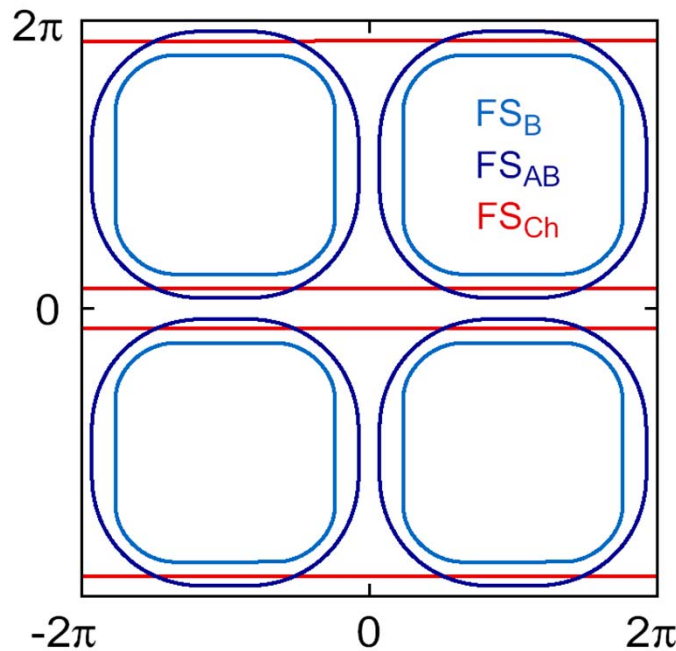
FIG. 1. (a) Normalized fluorescence yield at the O K edge of $\text{La}_{2-x}\text{Sr}_x\text{CuO}_{4+\delta}$. The solid curves are the common background described in the text. (b) The difference between the data of $\text{La}_{2-x}\text{Sr}_x\text{CuO}_4$ and the common background. The solid lines are the fitted curves using two Gaussian line shapes.

It is the connection between low and high energy scales that distinguishes the Mott gap from a more conventional gap (i.e., semiconductor, CDW, etc.)

Fermiology of Underdoped YBCO



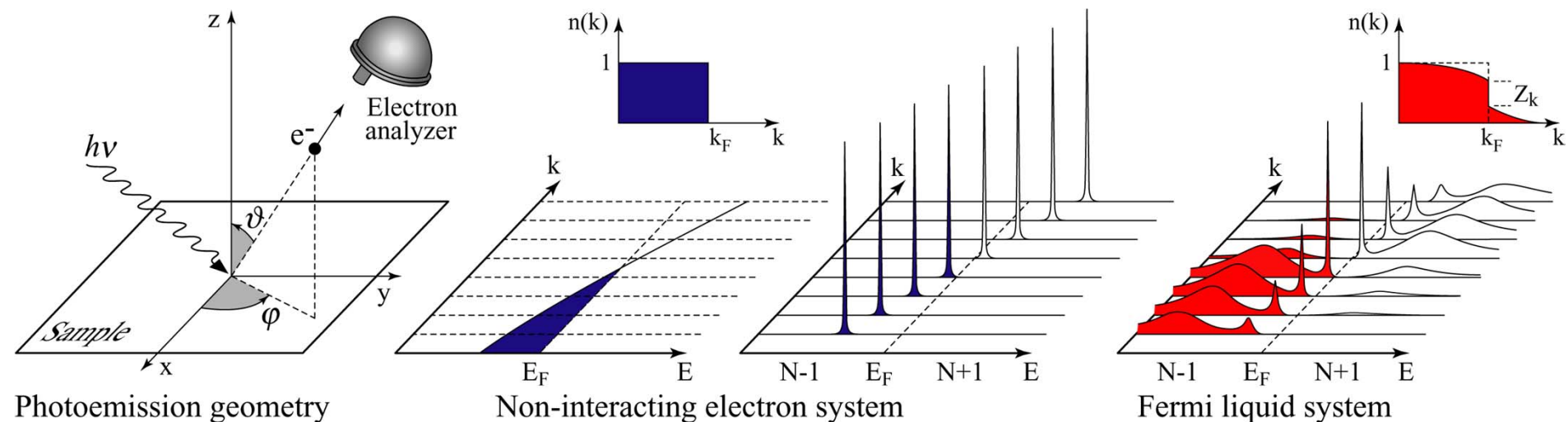
Elfimov, Sawatzky, Damascelli PRB **77**, 060504 (2008)



D. Fournier et al., Nature Physics **6**, 905 (2010)

ARPES: The One-Particle Spectral Function

A. Damascelli, Z. Hussain, Z.-X Shen, Rev. Mod. Phys. **75**, 473 (2003)



Photoemission intensity: $I(k, \omega) = I_0 / M(k, \omega)^2 f(\omega) A(k, \omega)$

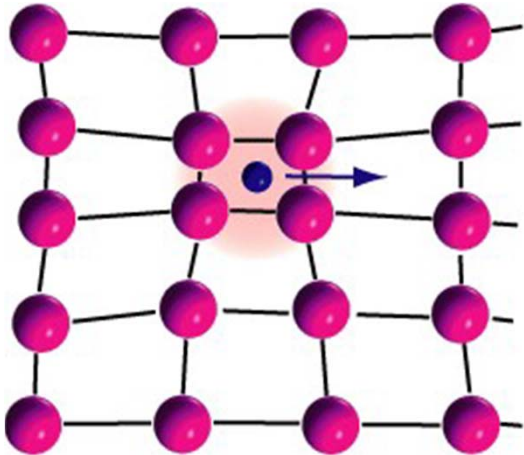
Single-particle spectral function

$$A(\mathbf{k}, \omega) = -\frac{1}{\pi} \frac{\Sigma''(\mathbf{k}, \omega)}{[\omega - \epsilon_{\mathbf{k}} - \Sigma'(\mathbf{k}, \omega)]^2 + [\Sigma''(\mathbf{k}, \omega)]^2}$$

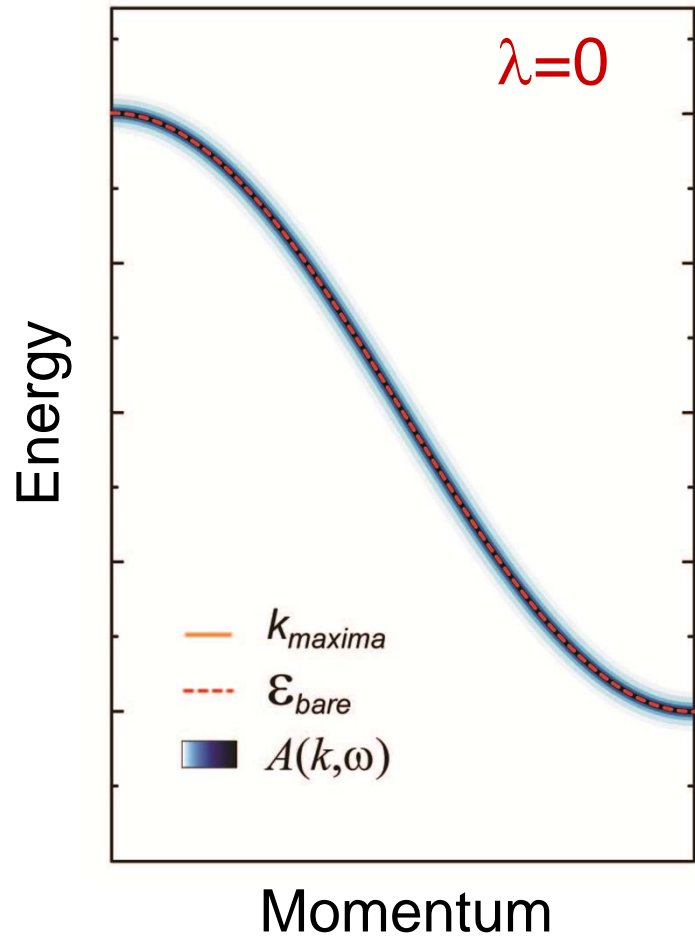
$\Sigma(\mathbf{k}, \omega)$: the “self-energy” captures the effects of interactions

Renormalization of Polaronic Quasiparticles

$$\mathcal{H} = \sum_k \varepsilon_k^b c_k^\dagger c_k + \Omega \sum_Q b_Q^\dagger b_Q + \frac{g}{\sqrt{N}} \sum_{k,Q} c_{k-Q}^\dagger c_k (b_Q^\dagger + b_{-Q})$$

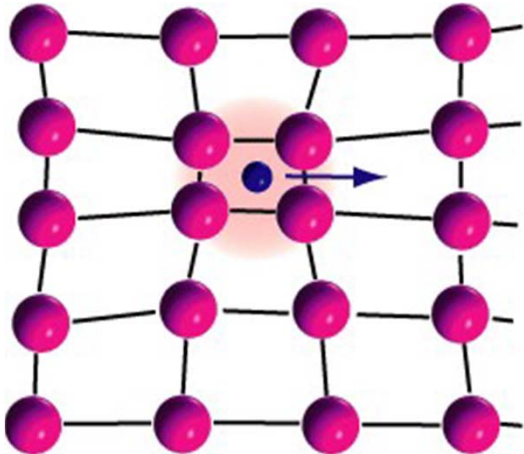


$$A(\mathbf{k}, \omega) = Z_{\mathbf{k}} \frac{\Gamma_{\mathbf{k}}/\pi}{(\omega - \varepsilon_{\mathbf{k}})^2 + \Gamma_{\mathbf{k}}^2} + A_{inc}$$
$$m^* > m \quad |\varepsilon_{\mathbf{k}}| < |\epsilon_{\mathbf{k}}|$$
$$\tau_{\mathbf{k}} = 1/\Gamma_{\mathbf{k}}$$

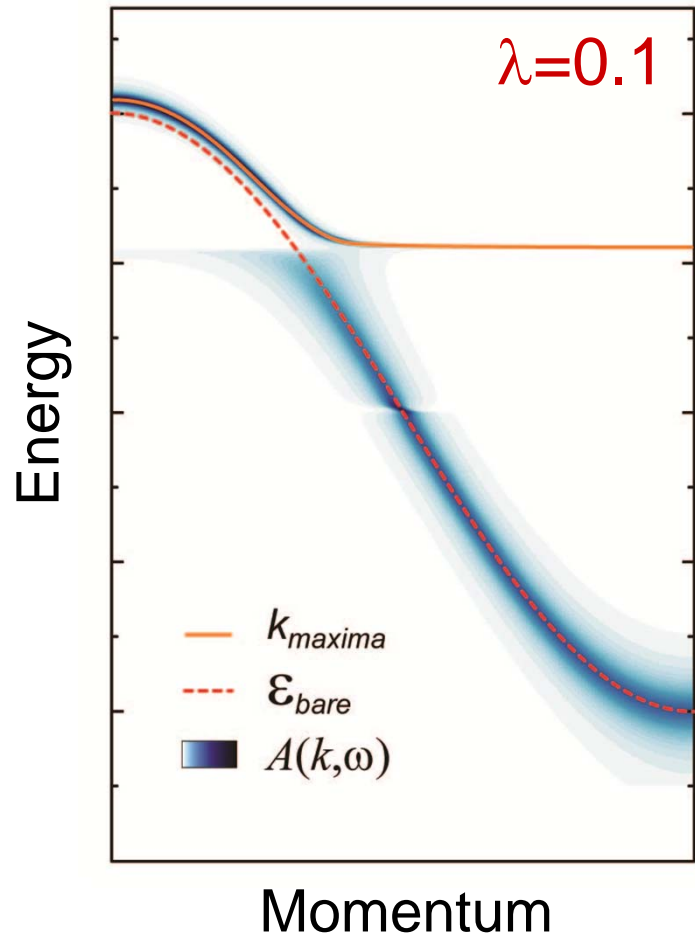


Renormalization of Polaronic Quasiparticles

$$\mathcal{H} = \sum_k \varepsilon_k^b c_k^\dagger c_k + \Omega \sum_Q b_Q^\dagger b_Q + \frac{g}{\sqrt{N}} \sum_{k,Q} c_{k-Q}^\dagger c_k (b_Q^\dagger + b_{-Q})$$

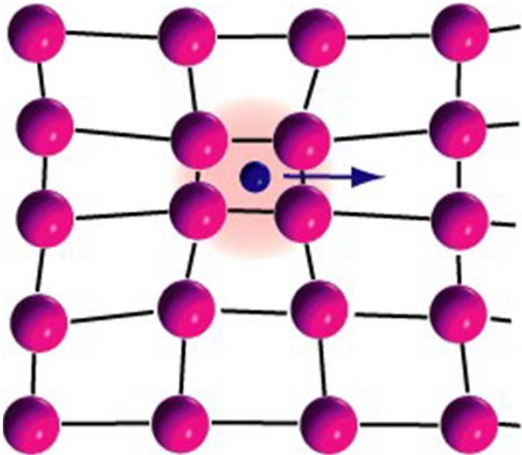


$$A(\mathbf{k}, \omega) = Z_{\mathbf{k}} \frac{\Gamma_{\mathbf{k}}/\pi}{(\omega - \varepsilon_{\mathbf{k}})^2 + \Gamma_{\mathbf{k}}^2} + A_{inc}$$
$$m^* > m \quad |\varepsilon_{\mathbf{k}}| < |\epsilon_{\mathbf{k}}|$$
$$\tau_{\mathbf{k}} = 1/\Gamma_{\mathbf{k}}$$

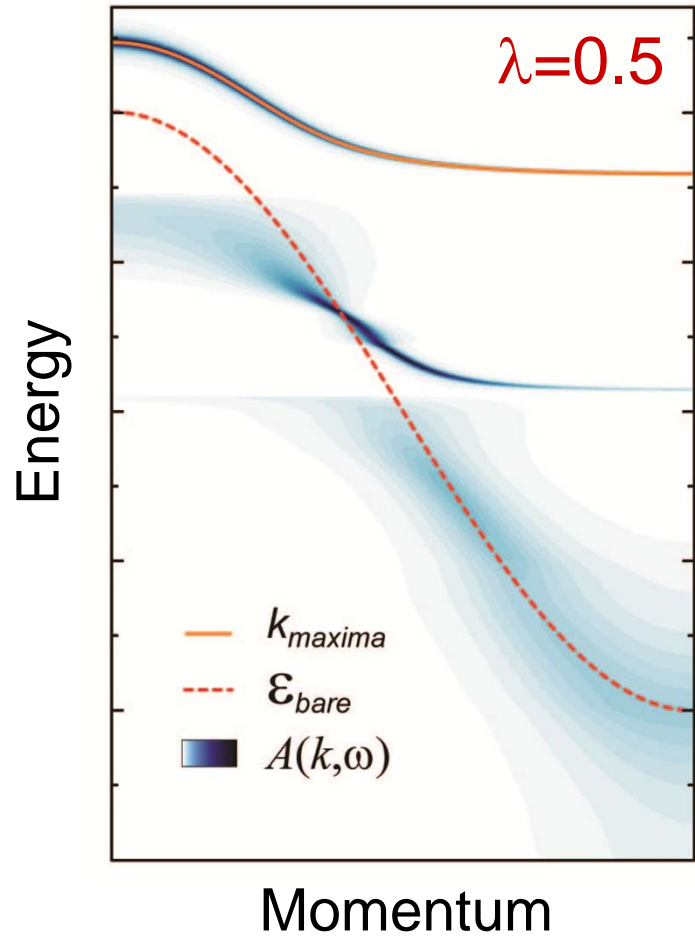


Renormalization of Polaronic Quasiparticles

$$\mathcal{H} = \sum_k \varepsilon_k^b c_k^\dagger c_k + \Omega \sum_Q b_Q^\dagger b_Q + \frac{g}{\sqrt{N}} \sum_{k,Q} c_{k-Q}^\dagger c_k (b_Q^\dagger + b_{-Q})$$

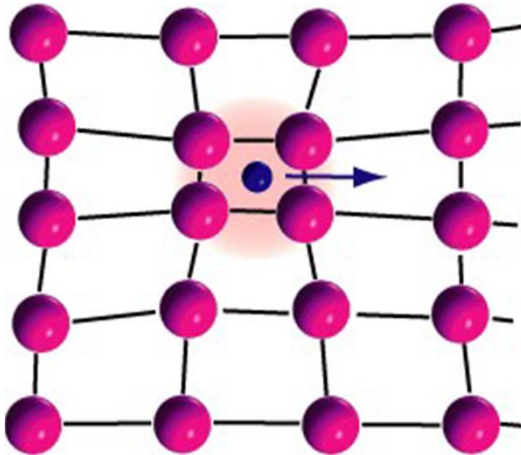


$$A(\mathbf{k}, \omega) = Z_{\mathbf{k}} \frac{\Gamma_{\mathbf{k}}/\pi}{(\omega - \varepsilon_{\mathbf{k}})^2 + \Gamma_{\mathbf{k}}^2} + A_{inc}$$
$$m^* > m \quad |\varepsilon_{\mathbf{k}}| < |\epsilon_{\mathbf{k}}|$$
$$\tau_{\mathbf{k}} = 1/\Gamma_{\mathbf{k}}$$

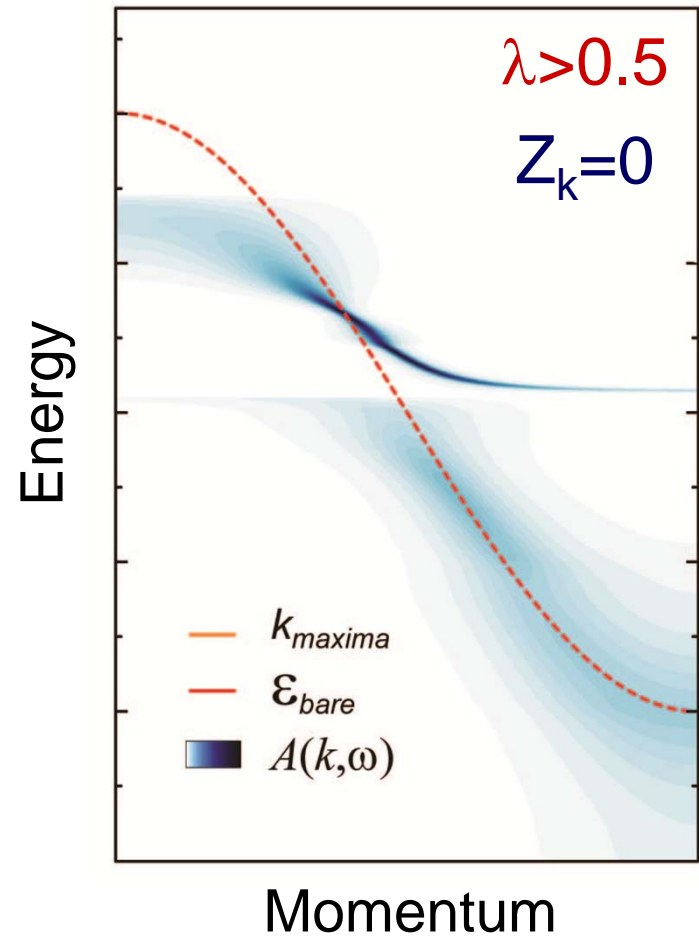


Renormalization of Polaronic Quasiparticles

$$\mathcal{H} = \sum_k \varepsilon_k^b c_k^\dagger c_k + \Omega \sum_Q b_Q^\dagger b_Q + \frac{g}{\sqrt{N}} \sum_{k,Q} c_{k-Q}^\dagger c_k (b_Q^\dagger + b_{-Q})$$

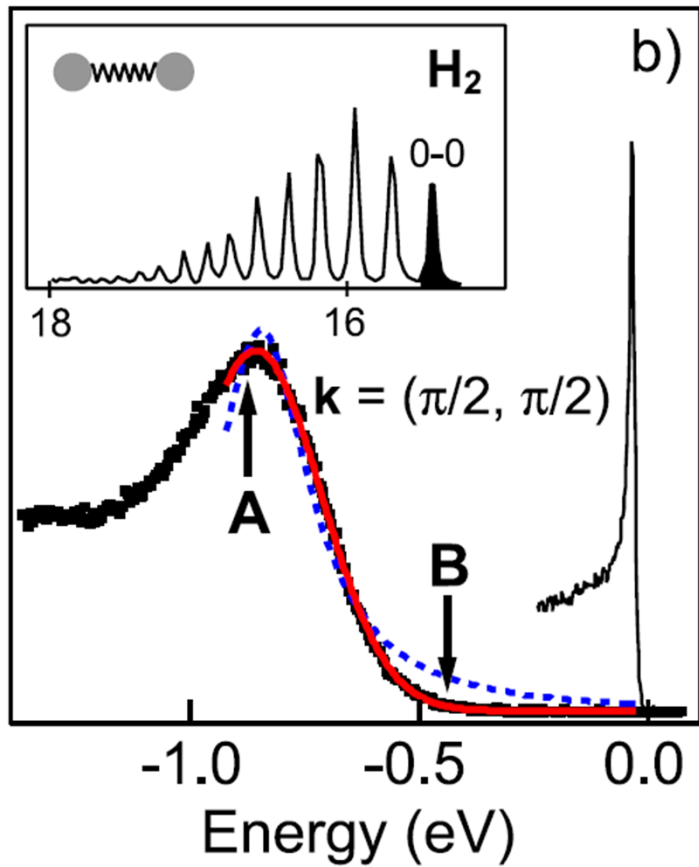


$$A(\mathbf{k}, \omega) = Z_\mathbf{k} \frac{\Gamma_\mathbf{k}/\pi}{(\omega - \varepsilon_\mathbf{k})^2 + \Gamma_\mathbf{k}^2} + A_{inc}$$
$$m^* > m \quad |\varepsilon_\mathbf{k}| < |\epsilon_\mathbf{k}|$$
$$\tau_\mathbf{k} = 1/\Gamma_\mathbf{k}$$

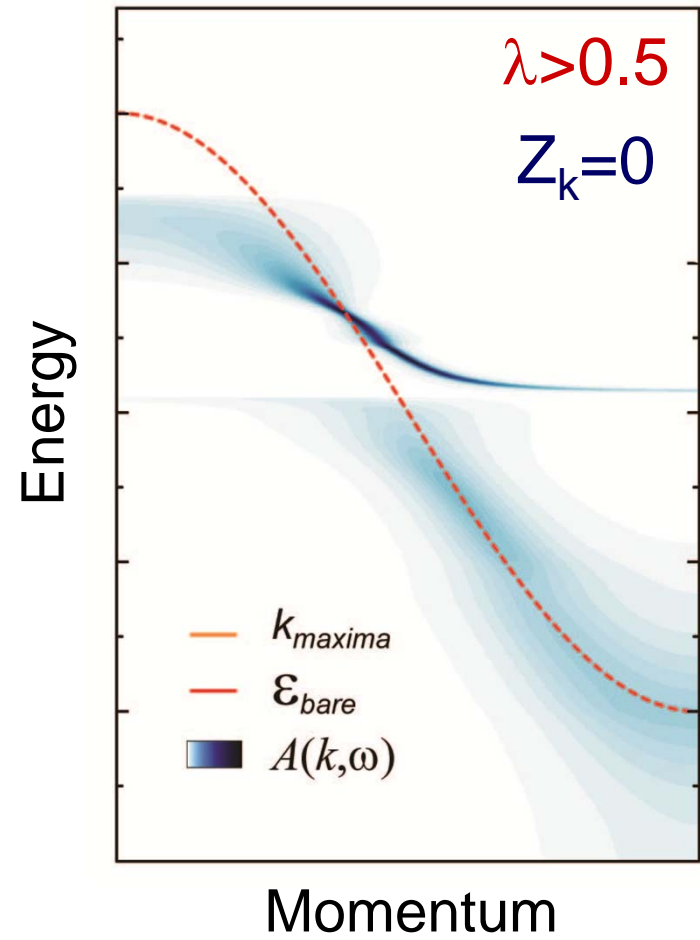


Renormalization of Polaronic Quasiparticles

$$\mathcal{H} = \sum_k \varepsilon_k^b c_k^\dagger c_k + \Omega \sum_Q b_Q^\dagger b_Q + \frac{g}{\sqrt{N}} \sum_{k,Q} c_{k-Q}^\dagger c_k (b_Q^\dagger + b_{-Q})$$

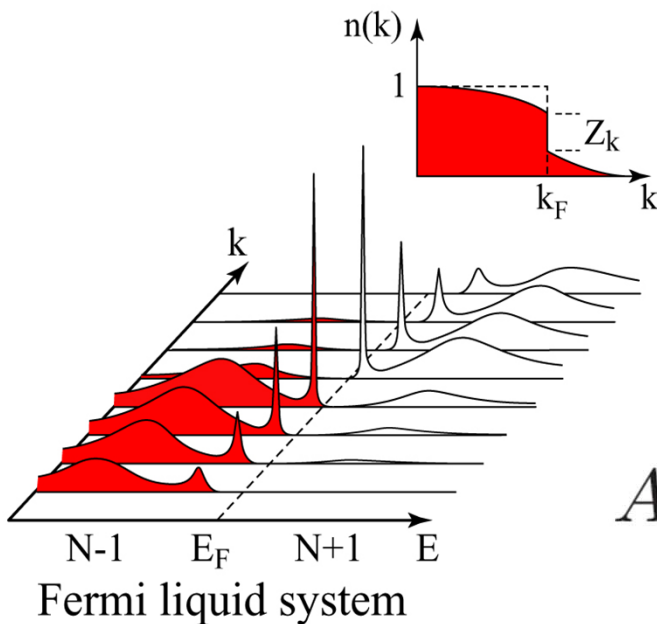


K.M. Shen et al., PRL 93, 267002 (2004)



Veenstra, Goodvin, Berciu, Damascelli, PRB 82, 012504 (2010)

Quasiparticle Coherence across the Phase Diagram



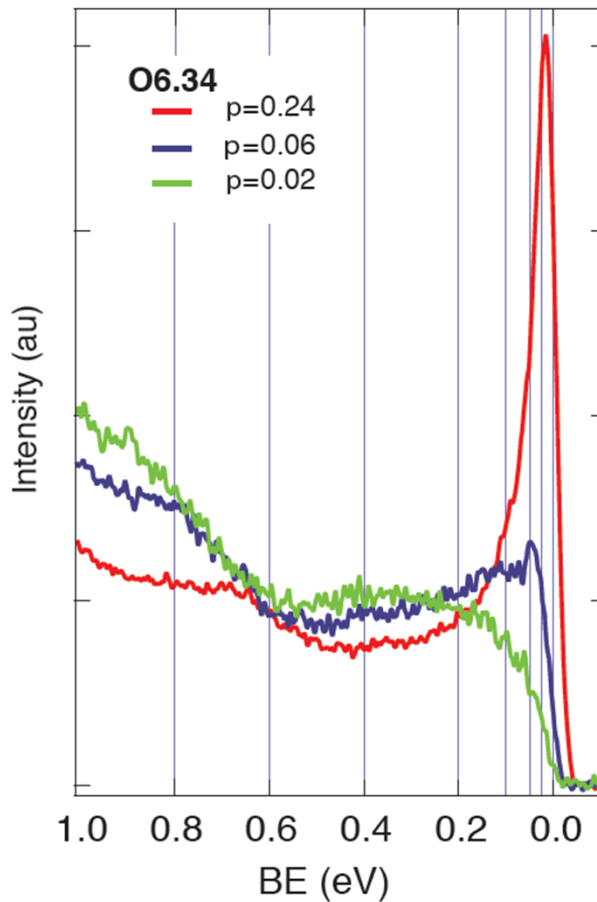
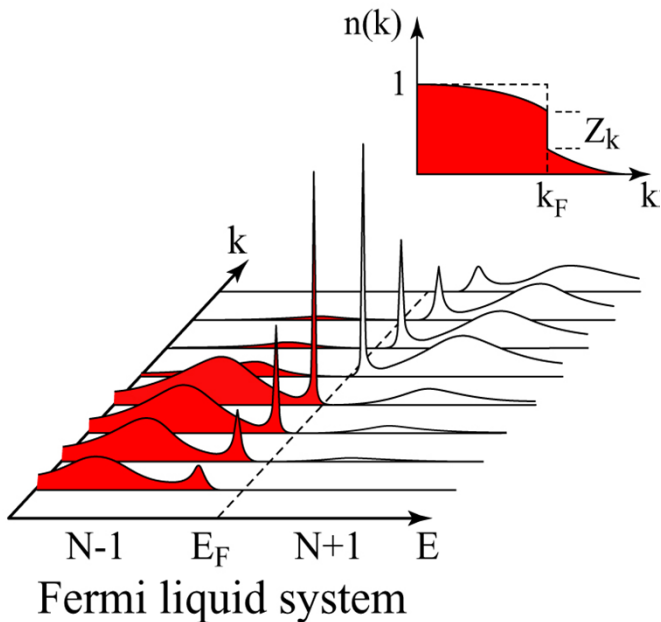
$$Z_k = \int A_{coh}(k, \omega) d\omega$$

$$I(k, \omega) = I_0(k) f(\omega) A(k, \omega)$$

$$A(k, \omega) \equiv A_{coh}(k, \omega) + A_{incoh}(k, \omega)$$

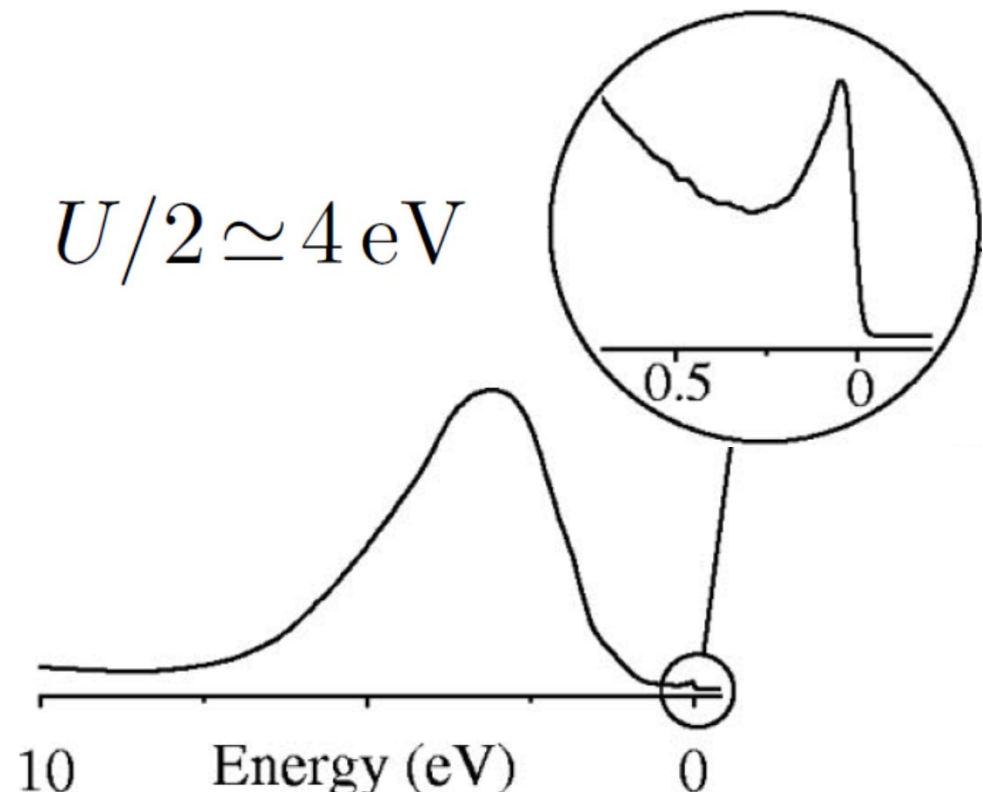
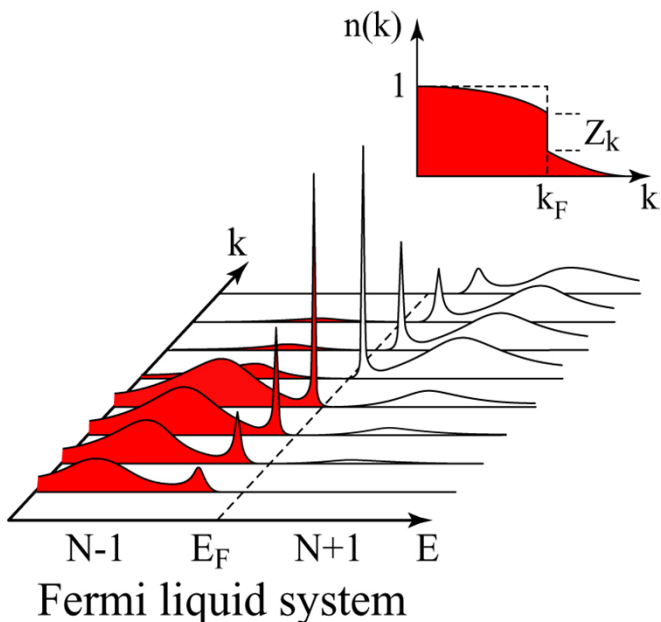
$$Z_k = \int I_{coh}(k, \omega) d\omega / \int I(k, \omega) d\omega$$

Quasiparticle Coherence across the Phase Diagram



$$Z_k = \int I_{coh}(k, \omega) d\omega / \int I(k, \omega) d\omega$$

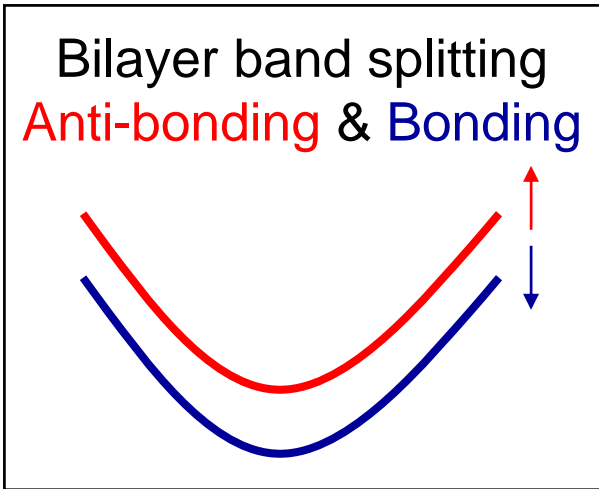
Quasiparticle Coherence across the Phase Diagram



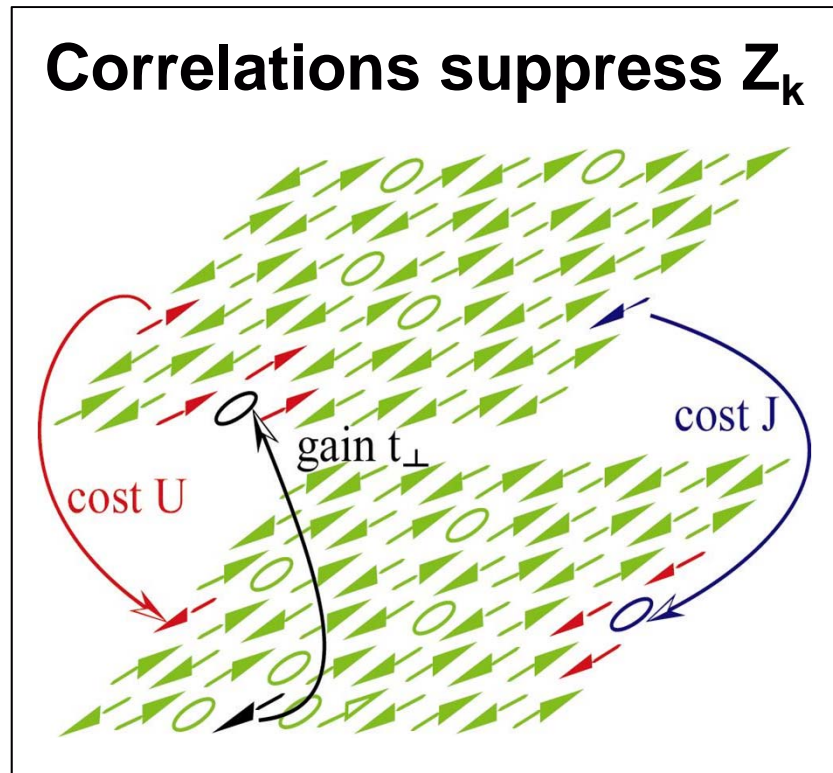
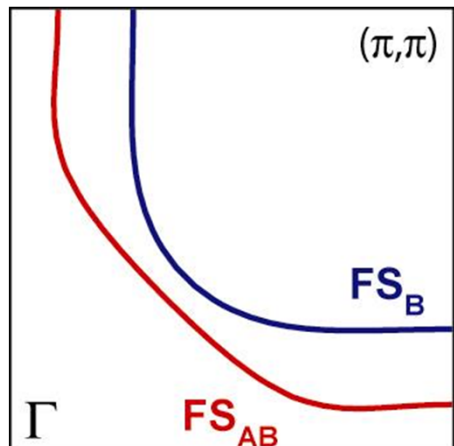
$$Z_k = \int I_{coh}(k, \omega) d\omega / \int I(k, \omega) d\omega$$

Bilayer Band Splitting and Quasiparticle Integrity

$$\epsilon^{B,AB}(k) = \epsilon(k) \mp t_{\perp}^{eff}(k) = \epsilon(k) \mp Z_k t_{\perp}^{LDA}(k)$$



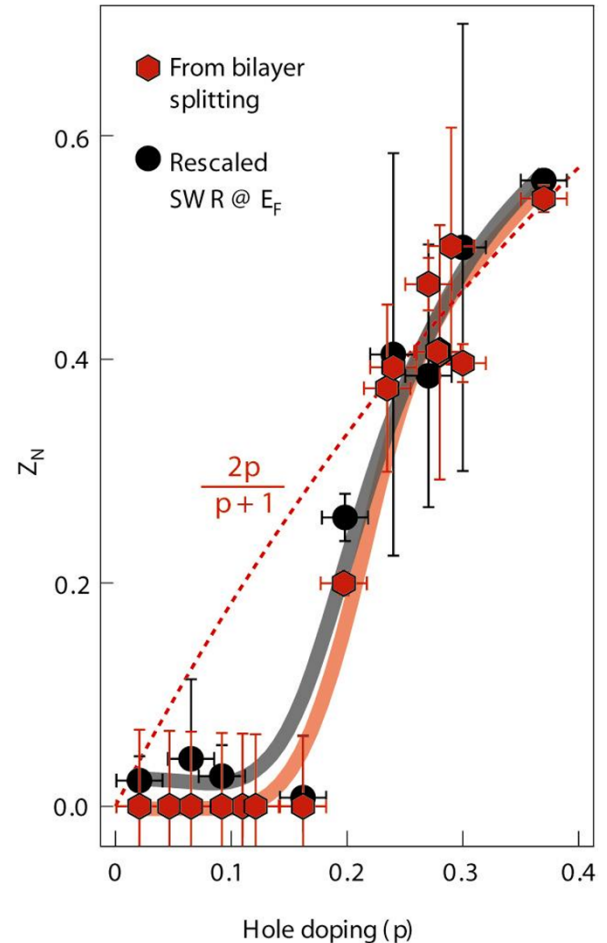
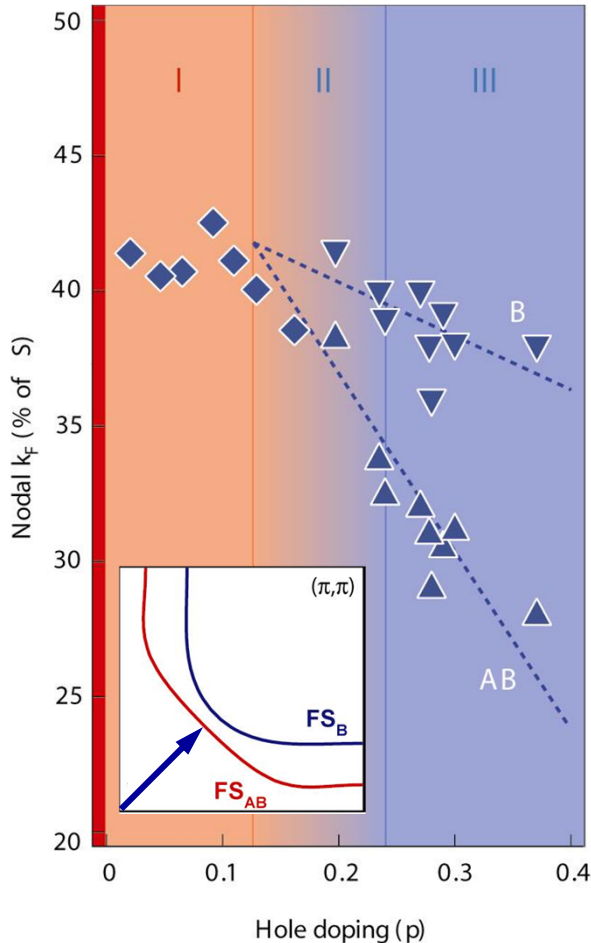
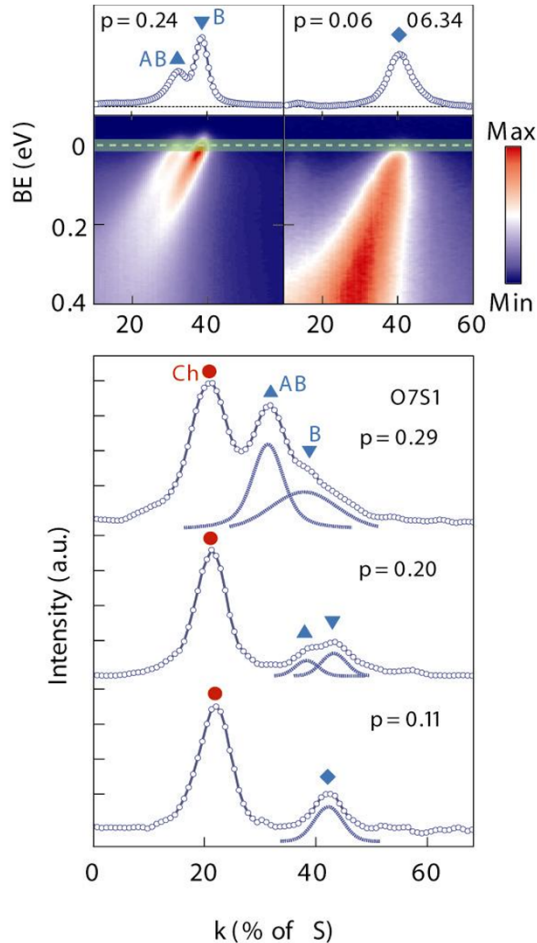
FS with bilayer splitting



$$Z \simeq 2p/(p+1)$$

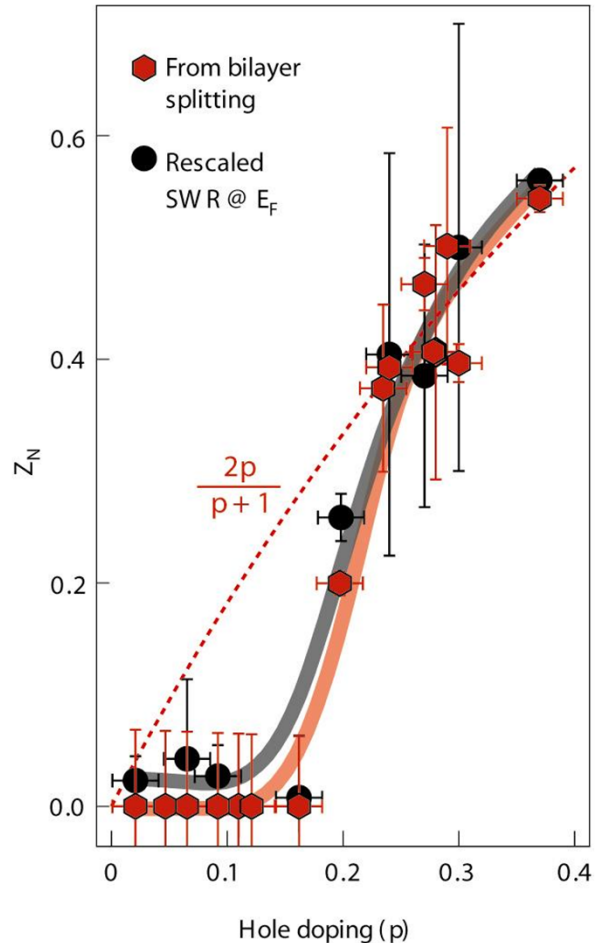
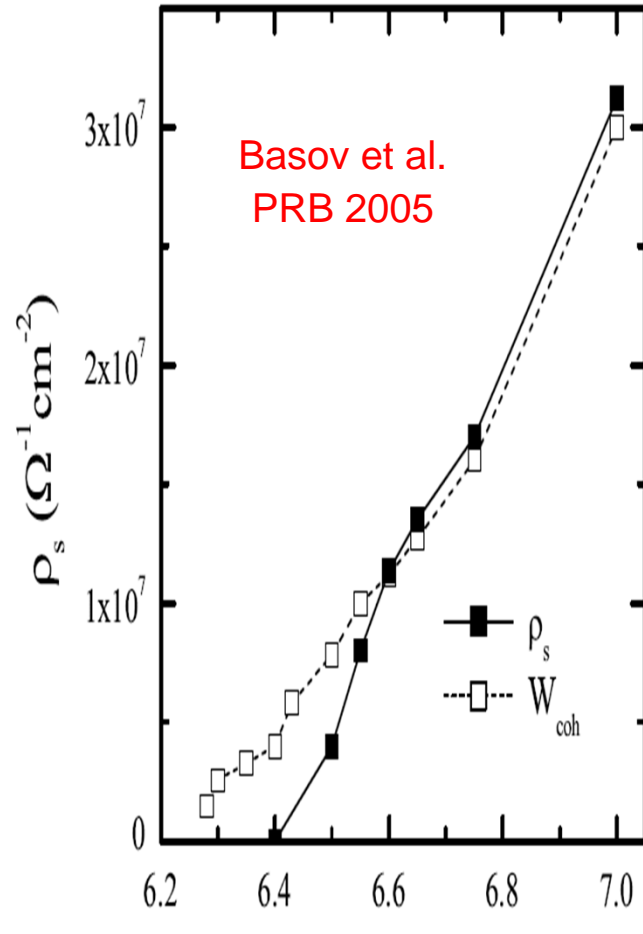
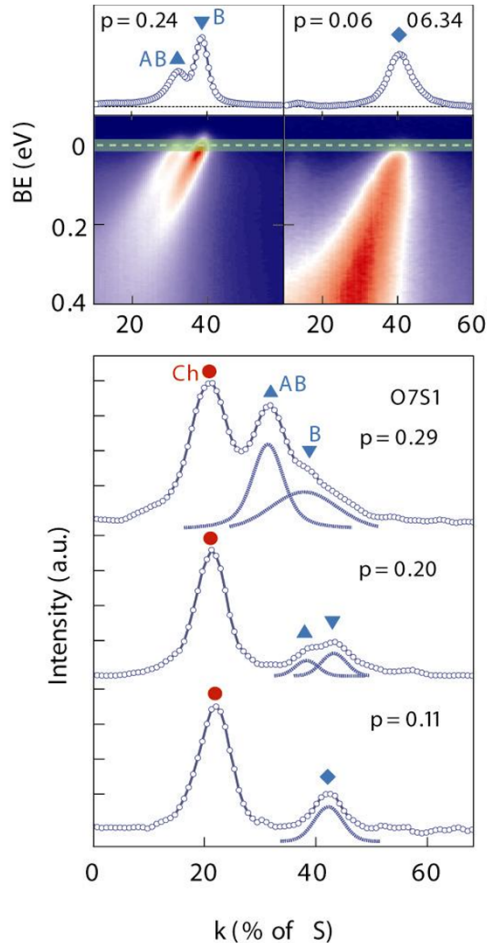
Bilayer band splitting and quasiparticle coherence

$$Z_N = \Delta\epsilon_N^{B,AB} / 2t_{\perp}^{LDA}(N)$$



Bilayer band splitting and quasiparticle coherence

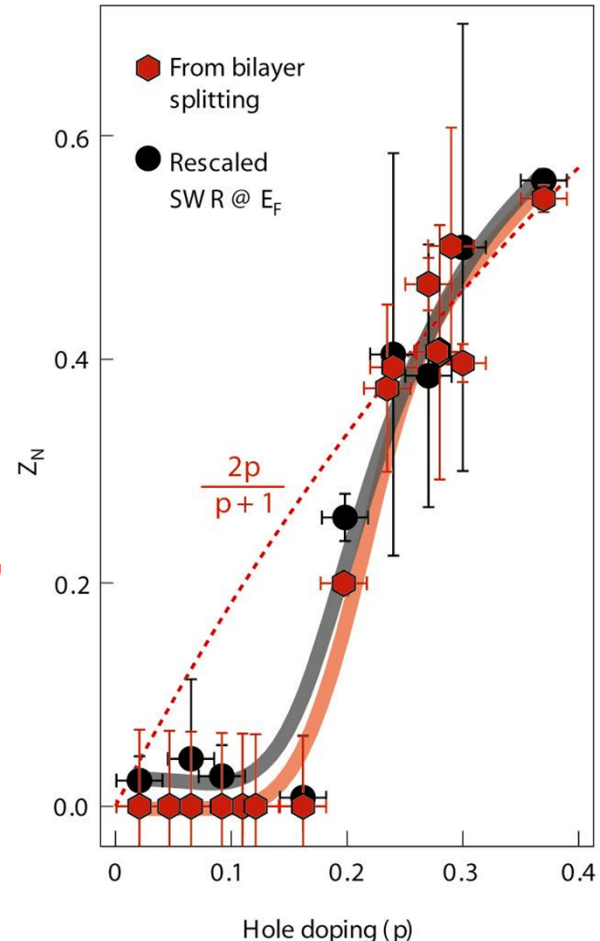
$$Z_N = \Delta \epsilon_N^{B,AB} / 2t_{\perp}^{LDA}(N)$$



Bilayer band splitting and quasiparticle coherence

$$Z_N = \Delta\epsilon_N^{B,AB} / 2t_{\perp}^{LDA}(N)$$

- Quantitative estimate of Z
- Agreement with $2p/(p+1)$ for $x > 0.23$
- Isotropic $Z_N \sim 0.54$ and $Z_{AN} \sim 0.50$
- Vanishing Z_N below 15-10%
- $t_{\perp} \sim 10$ meV consistent with QO
- Z even smaller for pockets' "other side"
- Pseudogap? Loss of coherent SW
- Fermi surface? Luttinger's counting?





UNIVERSITY OF BRITISH COLUMBIA



Andrea Damascelli

UBC-MPI Quantum Matter Institute

Thank you!

CUSO Lecture – Lausanne 02/2011